Disentangling the multiple drivers of ecological adaptation in a microorganism

Andrea Perna[1,2,†], Enrico S. Rivoli[2], and Daniel M. Perkins[2‡]

[1]IMT School for Advanced Studies, Lucca, Italy
[2]Life Sciences, University of Roehampton, London, UK
[†] ORCID: 0000-0001-8985-3920
[‡] ORCID: 0000-0003-0866-4816

Abstract

The survival and reproduction of living organisms depend on their ability to achieve an adequate balance between energy intake and energy expenditure. Multiple quantities contribute to this energetic balance, such as the feeding rate, and the allocation of available energy to growth, maintenance, movement and reproduction. Given that many of these quantities scale in a predictable way with the size of the organism and with environmental parameters, it should be possible to predict how organisms may adapt to novel environmental conditions in terms of adjusting their morphology, physiology, and behaviour. In a series of experiments, we adapted axenic experimental populations of the ciliate *Tetrahymena pyriformis* to different environmental conditions of temperature (15°C, 20°C and 25°C) and resource levels (50%, 100%, and 200% of a standard protein solution). We measured population growth, metabolic rate (from respiration), cell size, and movement speed (from video-tracking). On a very short time scale, movement speed and metabolic rate increased with environmental temperature in a way that can be predicted from simple physical scaling relations such as the Boltzmann-Arrhenius equation and the 'viscous drag' impacting movement. However, soon after the introduction of *Tetrahymena* into a novel environment, all the measured quantities were further modulated in a direction that likely provided better biological fitness in the new environment. Changes in cell size

played a central role in mediating these adaptations: in small organisms with short generation times, cell size regulations can be a fast and effective way to mediate environmental adaptation by simultaneously affecting multiple phenotypic traits, such as metabolic rate and the energetic costs of movement.

1 Introduction

Living organisms can vary hugely in size, morphology, and functional or behavioural traits, indicating that variation along such phenotypic axes is weakly constrained by evolution: organisms large and small, slow-moving and fast, can coexist on the same planet for millions of years, all having similar fitness.

However, when variables such as metabolic rate, body size, generation time, and movement speed are plotted one against the other, different organisms all cluster together along relatively narrow curves [1, 2]. These narrow 'inhabitable regions' of the phenotypic space likely reflect boundaries between regions that are physically unattainable (for example because either diffusion or transport of molecules imposes an upper limit on biological rates) and regions that are physically possible but biologically inefficient.

When the physical parameters of the environment change, for example if temperature increases or nutrient resources are depleted, these boundaries shift, and empirical evidence across a range of species suggests that organisms respond with consistent changes in their development [3, 4, 5], in their metabolism [6, 7], and in their movement or behaviour [8].

Unicellular organisms are particularly well-suited as a model for understanding environmental adaptation over time scales ranging from one to several generations because of their small size and relatively short generation time, which make them suitable candidates for controlled laboratory microcosm studies [9]. Microcosm studies have allowed identification of some of the elements that mediate the adaptation of microorganisms to their environment. There is evidence – for example – that unicellular organisms change their phenotypic traits rapidly – traits like cell size and shape [10, 11], or the metabolic rate of individual cells [12] – in response to environmental conditions, and over ecological time scales. In turn, these changes affect ecological quantities, such as population growth rate [12], carrying capacity[13], or predation risk [11]. Movement speed is also a temperature-dependent phe-

notypic trait with the potential to also affect – at least in theory – ecological variables such as the stability of predator-prey systems [14].

By testing cell populations across a wide range of different environments, microcosm studies have also pointed to possible explanations of why phenotypic changes occur at the individual level. For example, Padfield et al.[15] studied the adaptation of unicellular algae to different temperature conditions. In the absence of adaptation, with increasing temperature respiration increased faster than photosynthesis (the activation energy for respiration was larger than for photosynthesis). This difference caused a mismatch between energy acquisition and energy expenditure in warm environments. However, by selectively down-regulating respiration relative to photosynthesis, these organisms were able to increase their growth rate in high-temperature conditions that would have otherwise been limiting. All this happened over relatively short time scales of about 100 generations.

These and other similar studies have contributed to an increase in our phenomenological understanding of the phenotypic changes triggered by different environmental conditions. However, there is increasing recognition that the adaptation of organisms to environmental conditions is a multifaceted process, not only because phenotypic changes produced at the individual level in turn also affect ecological interactions (e.g.[16]) and impact population- and ecosystem-level variables, but also because multiple environmental parameters interact with each other in driving adaptation. For example, the temperature that maximizes the growth rate of organisms is not independent of the concentration of available nutrients in the environment [17, 18].

The complex relations between environmental parameters (such as temperature and available resources), the phenotypic changes induced by those parameters, and fitness, [19] imply that a detailed mechanistic understanding of these relations is necessary if we want to make generalisable predictions on the effects of environmental changes.

To address this gap, we performed an extensive study in which experimental axenic populations of a microorganism –the ciliate *Tetrahymena pyriformis* – were experimentally adapted over ecological time scales to a range of different environmental conditions characterised by different temperature and concentration of nutrients. We measure how the adaptation process affects reproduction rate, metabolic rate (respiration), movement speed, and organism size (cell volume). We interpret our results on the basis of the idea that the physical parameters of the environment affect the organisms directly (for example, through the effect of temperature on metabolic rate) and they

alter the costs and benefits of behaviour (for example, water viscosity affects the cost of movement, and the availability of nutrients determines the energetic return of foraging). We can then try to understand the phenotypic changes of cell size, movement speed, etc. that happen over longer time scales as adaptations that improve the balance between energy acquisition and expenditure in the new environment, eventually contributing to increase the biomass production of *Tetrahymena* in the new environment.

2 Methods

2.1 Cell cultures

Axenic cultures of *Tetrahymena pyriformis* strain 1630/1W were obtained from CCAP (`http://www.ccap.ac.uk`) and cultured at 20 °C in a Proteose peptone - yeast extract medium (20 g Proteose peptone + 2.5 g yeast extract in 1 L deionised water). In the following of this paper, we will refer to this "standard" medium composition as the 100% concentration, to distinguish it from a 50% medium (with half the concentration of Proteose peptone and yeast extract) and a 200% medium with double concentration.

2.2 Experiment design

Cells were maintained in exponential growth phase at 20°C and 100% medium concentration for about 50 days (constant temperature, no light) in two replicates. Subsequently, cultures were split across 9 different treatments (3 temperature conditions x 3 medium concentrations) and adapted to the new conditions for at least three weeks (corresponding to a minimum of 20 generations), in four replicates for each condition (see fig. 1 for a schematic diagram of the experiment). Throughout the entire duration of the adaptation period, cultures were kept in relatively constant growing conditions by adopting a serial transfer regime, subculturing repeatedly into fresh growth medium. At the end of the adaptation period, cultures were further split across a wide range of temperature conditions (keeping the same medium concentration at which they were adapted) to characterise thermal response curves for different biological quantities (respiration, movement speed, and population growth rate). Specifically, we measured acute thermal responses for respiration and movement speed (from 1.5 to 3 minutes after cells were moved to the

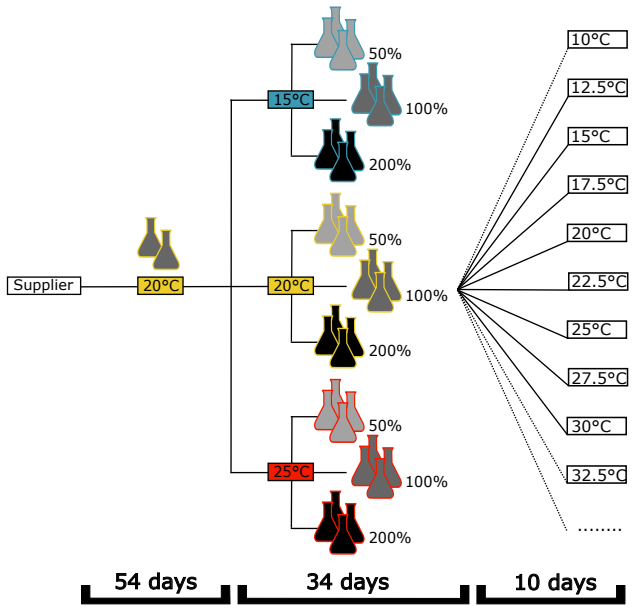

Figure 1: Schematic diagram of the main adaptation experiment. After an initial adaptation at 20°C and 100% culture medium in two replicates, cells were split across combinations of medium concentration and temperature, in four replicates. At the end of an adaptation period of at least three weeks, cultures were further split across different temperatures to assess thermal response curves for various measures of performance (for a variable duration depending on the treatment).

new temperature for speed recordings, and from approximately 30 minutes to three hours for respiration), and we measured long-term responses over a few days (2 to 6 generations, or 3.5 days on average, with differences depending on incubation temperature) for population growth, long-term movement speed, and cell volume changes.

2.3 Population growth

Assuming exponential growth throughout the experiment, the growth rate, expressed in number of generations per day was calculated as $\log_2(N(t)/N(0))/d$ where $N(0)$ is the density at the beginning of a subculture, $N(t)$ is the final density of the subculture, and d is the length of the subculture period in number of days.

2.4 Respiration

Oxygen consumption was measured using a 24-channel PreSens Sensor Dish Reader and 2 ml oxygen sensor vials from PreSens (`https://www.presens.de/`) inside thermal cabinets at the desired temperature (see SI sec. 1.3.A for details of the experimental procedure). Population-level respiration rate was then converted to rate of energy consumption per individual cell by accounting for population density in the vial, and assuming an equivalence $1\,\mathrm{mol}\ O_2 = 478576\,\mathrm{J}$.

2.5 Imaging

Tetrahymena cultures were imaged under the microscope in cell-counting slides (BVS100 FastRead), which provide a constant depth of 100 μm (details of the procedure in SI section 1.3). A microscope camera (Lumenera Infinity 3-3UR `https://www.lumenera.com/infinity3-3ur.html`) was used to record videos at 30 fps. Temperature while imaging under the microscope stage was controlled using a temperature-controlled stage (Linkam PE120 Peltier System).

2.6 Video tracking

We used a custom-made software (available at `https://github.com/pernafrost/Tetrahymena`) written in python and based on the opencv, traktor, and scikit-image libraries to extract trajectories and measurements of cell size and morphology directly from the videos. The software returns measurements for each 'tracked particle', where a particle generally corresponds to one individual cell. However, there isn't a perfect one-to-one correspondence between *Tetrahymena* cells and particles: a cell moving in and out of the field of view of the microscope camera would be labelled as a different particle, and occasionally the identity of two cells swimming close to each other and overlapping in the images were swapped. Given the very large number of individual measurements both across and within experimental conditions, we ignored this small intrinsic potential for pseudo-replication in our analyses.

2.7 Movement analysis

The instantaneous movement speed of each tracked particle was measured from the trajectories as the displacement per unit time of the centre of mass of the particle, measured over a time scale of 1/10 of a second (3 frames). We took the median of all the instantaneous speed values along the trajectory as the individual speed of the particle. We excluded from the analysis particles that did not move and cells with an unnaturally small size that might have been incorrectly detected in the image. Unless otherwise specified, in the analyses and in the figures presented here we focus on the top 20% faster moving cells within each tested experimental condition. This is because fastest moving cells are more likely to be representative of the intrinsic limits of *Tetrahymena* swimming, while slowly moving cells might be stuck temporarily against the microscope slide or they might be moving at slow speed for reasons independent of their ability to move faster. (Details of movement analysis in SI section 1.3)

2.8 Estimation of cell volume

The video-tracking software fits an ellipse around each segmented *Tetrahymena* cell. Cell volume V was estimated based on the major and minor axes of the best fitting ellipse (respectively l and w) using the formula $V = 4/3\pi l w^2/8$.

2.9 Feeding rate

Feeding rate is one of the variables that we consider in interpreting our results. However, we do not measure the feeding rate of *Tetrahymena* directly in our experiments. Instead, we model it based on movement speed, which determines the 'attack rate', and metabolic rate, which determines the digestion time. Details are provided in the SI section 3.1 and 3.3, and some empirical support for the way how we model feeding rate is provided in SI section 2.8.

2.10 Statistical analyses

We used linear mixed-effects (LME) modeling [20, 21] to test for the effects of temperature and medium concentration (fitted as fixed categorical factors)

on population growth rate and individual cell volume using the lme4 package in R v.3.0.2 [22]. Culture line was added as a random effect to account for the the multi-level structure of our data (e.g. the variance for each culture is nested within that of the whole dataset) and its unbalanced nature (e.g. there is variation in the number of measurements made for different culture lines) [20, 21]. Significance of fixed factors (temperature and medium concentration) and their interactions were determined using Satterthwaite's method for approximating degrees of freedom for the t and F tests from the lmerTest package in R. Model assumptions were checked using the Performance package in R.

2.11 Fitting thermal response curves

Respiration, movement speed, and population growth were analysed by fitting a slightly modified version of the Sharpe-Schoolfield model for thermal response [23, 24] implemented in the rTCP R package ([25]). The model assumes that the rate $R(T)$ of the process at a given temperature increases following an Arrhenius-type relation with temperature, but also accounting for the plateauing and typically fast decrease of biological rates at very high temperature (See SI section 3.1 for the full details of the Sharpe-Schoolfield model in its rTPC implementation). In the analyses that we report here, we focus on this Arrhenius part of the curve, which can be summarized as

$$R(T) = R_0 e^{-\frac{E}{k_B}\left(\frac{1}{T}-\frac{1}{T_0}\right)} \tag{1}$$

and is described by two parameters: a value of activation energy E, which describes how fast the rate increases with increasing temperature, and a reference rate R_0, which is the rate of the process at the reference temperature T_0. Throughout all our analyses we set $T_0 = 20\,^\circ\mathrm{C}$ (293.15 K). k_B is the Boltzmann constant.

3 Results

3.1 Population growth and individual cell size

Throughout the initial adaptation period at 20 °C, we observed a stable or slightly increasing *per capita* growth rate over time (fig. 2a). When cells

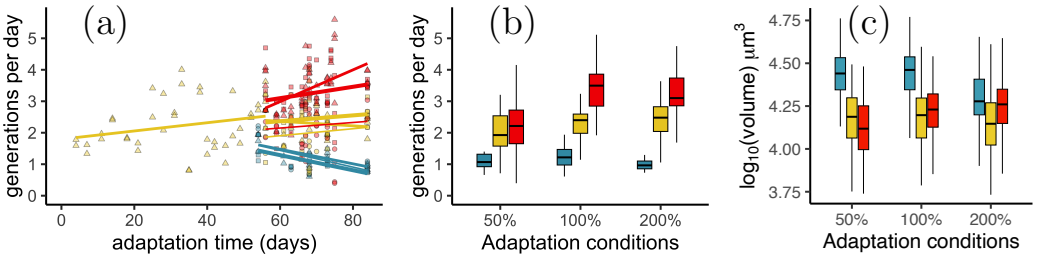

Figure 2: Adaptation to novel environmental conditions in *Tetrahymena* populations. (a) Population growth rate of the mother culture (20 °C and 100% medium concentration, yellow line, before day 56) and of subcultures (starting from day 54). Growth rate is expressed in number of generations per day. Blue, yellow and red colours refer to temperature treatments (15, 20, and 25 °C, respectively); thicker lines represent cultures with higher medium concentration. Population growth rates increase through time (excluding at 15 °C) indicating adaptation and improved performance. (b) Growth rate during the subculture period (temporal data are combined together). Growth rate is higher at higher temperatures and largely unaffected by nutrient concentration, except at high temperature and low nutrients. (c) Volume of individual cells in each treatment at the end of the subculture period. Individual body size increases with decreasing temperature, particularly at 15 °C.In all the boxplots that we present, horizontal lines are medians, boxes extend from the 25th to the 75th percentiles, whiskers extend to 1.5 times the interquartile range. SI section 2.2 presents additional measurements of cell size and shape across experimental conditions.

were moved to the various experimental conditions with different adaptation temperatures and medium concentrations, the growth rate shifted to different baselines (some environments can support faster growth), and then it remained stable or increased slightly over time, compatible with the idea that *Tetrahymena* improved their performance throughout the adaptation to the new environments (where 'performance' is measured through the quantities that we can measure such as the *per capita* growth rate, or the rate of biomass production, and which we consider proxies for biological fitness). One exception were cell populations growing at low temperature (15 °C), which exhibited a slight decrease in growth rate over time. However, the rate of biomass production might be increasing over time in this treatment as well if we consider that cells adapted at low temperature were simultaneously becoming larger in volume during this same adaptation period, as illustrated by their final volume (fig. 2c), or if we exclude some possible transient effect associated with the change of temperature (see SI section 2.1 for details). These changes in cell volume across different adaptation conditions are particularly marked if we consider that cells must approximately double in volume during each generation before they reproduce by fission (this corresponds to a span of $\log_{10}(2) \simeq 0.3$ units in the logarithmic y-axis scale of the boxplot in fig. 2(c), and imposes a minimum spread of data in each box), yet, in some nutrient conditions, recently divided cells at 15 °C are as large as cells cultured at 20 or 25 °C and which are near the end of their cell cycle, as indicated by the fact that the difference between distributions is of the same order as the $\simeq 0.3$ logarithmic units that correspond to the growth span of a single cell..

Temperature was a strong predictor of *per capita* growth rate (LME: $F_{[2,249]} = 124.4$, $P < 0.0001$; fig.2b), with growth rate generally increasing with temperature. The concentration of available nutrients was also a strong predictor of *per capita* growth rate (LME: $F_{[2,249]} = 11.72$, $P < 0.0001$; fig.2b), but the relative effect on *per capita* growth rates was small compared to temperature (fig.2b). There was also very strong evidence of an interaction between temperature and concentration (LME: $F_{[4,249]} = 6.6$, $P < 0.0001$; fig.2b): at low nutrient concentrations *per capita* growth rate increased by 86% from 15 °C to 25 °C; at intermediate nutrient concentrations this increased to 169%, whereas at high nutrients a 204% increase in *per capita* growth rate was observed over the same temperature range, consistent with the idea that when nutrients are in excess of a certain value, the *per capita* growth rate becomes asymptotically unaffected by any further increase in the

concentration of the growth medium (detailed in SI, section 2.9).

Temperature was also a very strong predictor of cell volume (LME: $F_{[2,679]} = 444.5$, $P < 0.0001$; fig.2c), as was the concentration of available nutrients (LME: $F_{[2,1196]} = 29.2$, $P < 0.0001$; fig.2c). There was also very strong evidence of an interaction between temperature and concentration (LME: $F_{[4,2089]} = 54.6$, $P < 0.0001$; fig.2c): at low nutrient concentrations cell size decreased by 7.4% from 15 °C to 25 °C; at intermediate nutrient concentrations this decline fell to 5.2%, whereas at high nutrients only a 1.6% decline in cell volume was observed over the same temperature range.

The energy that individual cells can invest into fuelling population growth and biomass production can be thought as the result of a balance between energy intake from feeding F, and energy spent for basal metabolism (maintenance) B, and movement (propulsion) P:

$$\frac{1}{N}\frac{dN}{dt} = \frac{1}{C_t}\Big(F - B - P\Big), \tag{2}$$

where N is the population size (number of cells), F, B, and P have units of power (nanoWatts) and C_t can be thought as the energy amount required to form a new cell. In order to better understand the way how *Tetrahymena* adapts to different environmental conditions, in the following sections we consider how these individual components of the *Tetrahymena*'s energy budget are each affected by temperature and resources.

3.2 Respiration and movement

It is well known that the metabolic rate of ectotherms increases with environmental temperature over a wide range of temperature conditions. In our data, the metabolic rate of *Tetrahymena* –measured from oxygen consumption– showed a clear increase with temperature, with values of activation energy E measured from respiration (top-left panel of fig. 3 and SI table S2.1) broadly in the range of commonly reported values for a variety of organisms (0.6 - 0.7 eV [7]). We can't detect any clear differences in activation energy across adaptation treatments with different temperature or medium concentration, as indicated by the overlapping error bars in figure 3 with the exception between 200% concentration at 25 °C and 100% concentration at 20 °C). We do, however, see a difference in the respiration rate at the reference temperature: cells adapted at 15 °C proportionally consumed more oxygen (fig. 3 left, second row), most likely reflecting the larger size of these cells (fig. 2c).

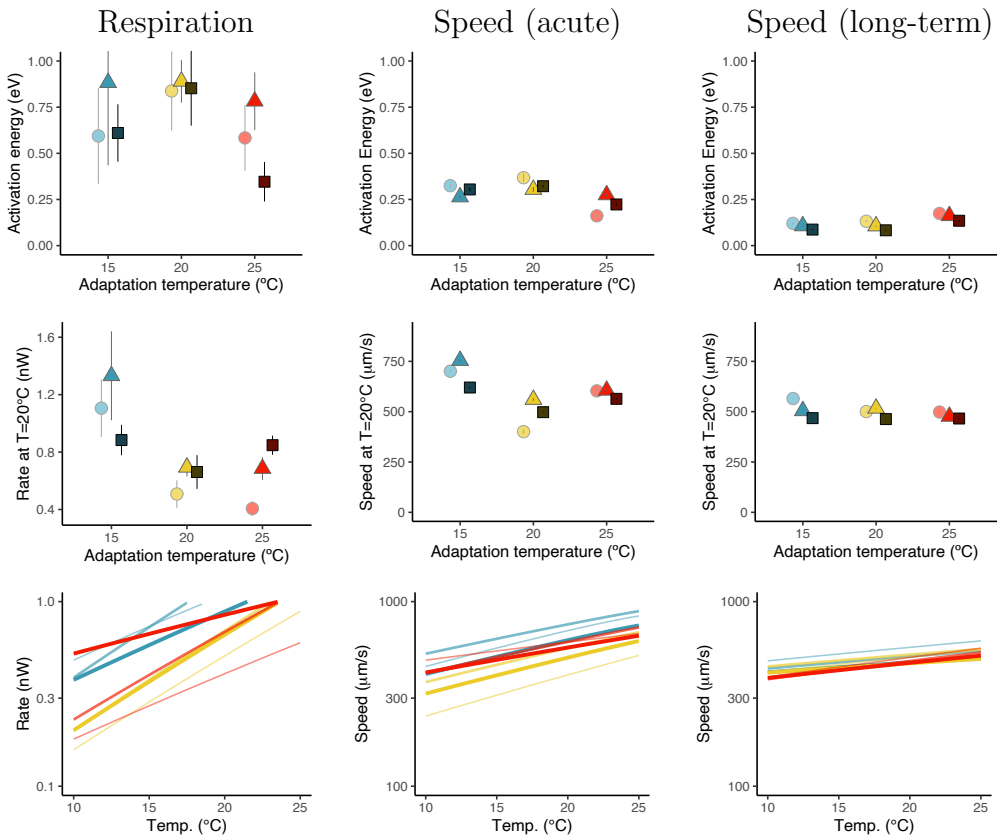

Figure 3: Thermal response curves for respiration and movement speed. Movement speed is further subdivided into an 'acute' response, where speed was recorded a few minutes after cells were moved to the new temperature, and a long-term response, a few days after cells were moved to the new temperature. Different color hues correspond to different temperature conditions (blue = 15 °C, yellow = 20 °C, red = 25 °C; bright colours correspond to low nutrient concentration: 50% medium, dark colours correspond to high nutrients: 200%). Error bars represent ±1 standard deviation, estimated from a bootstrap with 'residual' resampling in the rTPC package. Additional plots of these data and detailed thermal response curves for each condition are available as SI.

If – as a guiding hypothesis – a fixed proportion of metabolic energy is allocated to movement, the increase of metabolic rate with environmental temperature should be paralleled by a similar increase of movement speed. However, in general, we expect speed to increase with a lower activation energy than respiration because, in the low Reynolds number regime associated with *Tetrahymena* swimming, the power P dissipated for moving in water at speed U increases proportionally to the square of speed ($P \propto U^2$, see SI sec. 3.1), meaning that a 4-fold increase in the metabolic power invested into movement would lead only to a two-fold increase of swimming speed. This non-linear relation between power consumption and movement speed would lead to a predicted activation energy for speed about 50% the activation energy for respiration (or, indeed, slightly higher, because water viscosity also decreases with temperature, detailed in SI sec. **??**). In practice, however, the exact scaling between power consumption and speed is difficult to predict because most energy is dissipated within the ciliary layer with complex hydrodynamics [26, 27]. Our results (fig. 3 - central column) broadly confirm the prediction that movement speed would increase with temperature during a short-term, acute, exposure, and that the activation energy measured for speed would be lower than the activation energy for respiration; the empirical values are slightly lower than the predicted ones, with activation energies for speed being 42% on average of the activation energies for respiration (SI tables 2.1 and 2.2). Possibly, this discrepancy could reflect a slightly decreasing energy transduction efficiency of the mitochondria with increasing temperature (see e.g. [28, 29]); alternatively – already on this short time scale – cells could allocate proportionally less metabolic energy to movement when temperature increases. The most notable effect of the adaptation process was that cold-adapted cells (at 15 °C) were comparatively faster than warm-adapted cells when tested at the same temperature, (avg. intercept of thermal performance curve for speed of cells adapted at 15 °C = 692 μm/s; speed of cells in the other conditions = 538 μm/s, fig. 3-middle column/middle panel), a difference in speed that could entirely be explained by the larger size of these cold-adapted cells, which became capable of providing more metabolic power (if metabolic rate scales with cell volume) relative to drag (assumed to scale with the linear dimension; see SI section 2.12 for quantitative arguments and empirical data in support of this point).

The short-term thermal response curves for respiration and movement described above are likely to reflect simple chemio-physical changes in the rate

of metabolic reactions, but they might not correspond to efficient energy allocation strategies for an individual. For example, an increase of movement speed at high temperature, and the associated increase of metabolic power P allocated to movement (as in eq. 2) are only beneficial if they are also matched by a corresponding increase in energy intake from feeding F. However, this is unlikely to be the case for a number of reasons: first of all, the volume searched for food increases linearly with speed but, as we have seen above, the energy cost of movement (power consumption) increases with the square of speed (see e.g. [30, 31], SI section 3.2). In addition, the actual capture of nutrient molecules partly depends on the diffusion of the nutrients themselves, meaning that an increase of speed potentially only leads to a less than proportional increase in the actual amount of food collected [32]. Finally, digestion time also limits the amount of nutrients that can be consumed, independently of the rate at which they are encountered. In relation to this, our respiration data indicate that, after adaptation, *Tetrahymena* all have relatively similar metabolic rate each when measured each at their own adaptation temperature (as can be seen comparing the curves at the bottom-left in fig. 3 and is illustrated in the SI, fig. S2.5). This means that the rate at which they digest food is likely also similar. Supplementary section 3.3 expands on these arguments. But, in short, the increase in movement speed with temperature observed under short-term exposure (fig. 3 - central column) is unlikely to be sustainable in the long term.

In order to test directly this prediction, we also measured movement speed of cells that were transferred to a different temperature condition for a longer period of a few days (average 3.5 days). Under these conditions, speed varied very little across different treatments, with only a slight increase of speed with increasing temperature (activation energies in the range 0.083-0.174 eV) and a small reduction of speed at high nutrient concentrations (fig. 3 - right column, SI figure S2.8 and SI table S2.3).

3.3 Piecing together the puzzle

What can then explain a faster *per capita* growth rate at higher temperature, in spite of relatively limited variation in *per capita* energy intake and energy consumption $(F - B - P) \simeq$ constant? Imagine an extreme situation in which, through rapid adaptation, cells were able to completely compensate all the effects of temperature to the point that cells across the entire temperature range all have exactly the same metabolic rate, they individually consume

exactly the same amount of food, they breathe the same amount of oxygen, and spend the same amount of energy as they move around (this example is of course an oversimplification of what we observe empirically in our data, but we brought things to the extreme for the sake of simplicity of illustration). These cells that all eat the same and consume the same energy should have exactly the same population growth rates irrespective of temperature, isn't it? The answer is no, and the explanation lies in the remaining term of equation 2: $\frac{1}{C_t}$, the reciprocal of the energetic content of one cell.

One important way individual cells managed to contrast the effects of temperature on metabolic rate and movement was by changing their size. This ensured that metabolic rate and movement speed are now similar across cells growing in different conditions. However, if the energetic content of biomass is similar for large and small cells, then it takes more energy to produce a larger cell, and -everything else being equal- it takes more time. In other words, even in the most extreme hypothetical situation in which cells are able to completely compensate for the effects of temperature, shifting their size in order to always restore a constant value of *per capita* metabolic rate and energy intake irrespective of temperature, we would still expect the thermal response curves of *per capita* growth rate to be modulated by temperature, matching the thermal response curves for the reciprocal of cell volume (whenever cell volume becomes smaller, the growth rate should become larger in inverse proportion, and vice-versa).

Figure 4 reports thermal response curves for population growth and for the reciprocal of cell volume (which we assume proportional to $\frac{1}{C_t}$) in cells from each adaptation condition that were transferred to new values of temperature for a period of the order of a few days. All cell populations reproduced faster and developed smaller sizes when tested at high temperature than at low temperature (positive activation energies for population growth and for the reciprocal of volume in fig. 4-top row). These graphs show that cells started changing their size rapidly in response to changing temperature (the curves for 1/volume show similar values of activation energy and similar values at reference temperature, irrespective of the original adaptation temperature of the cultures; details on the time scale of volume change in SI section 2.11). Curves for population growth also additionally suggest that cold-adapted populations may be unable to start growing rapidly when they are exposed to higher temperatures (evidenced by their lower activation energy and lower growth at reference temperature).

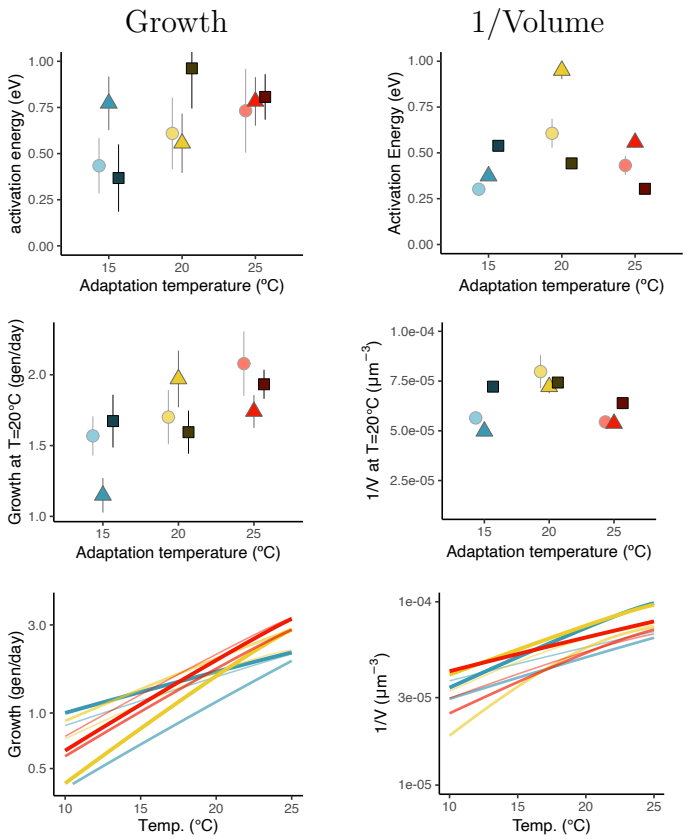

Figure 4: Adaptation of population growth rate and the reciprocal of cell volume. Top row: activation energies for population growth and for the reciprocal of volume are both positive and of comparable magnitude (cells grow faster and develop smaller sizes as temperature increases). Middle row: growth rate (left) and reciprocal of volume (right) at the reference temperature of 20 °C. Colour scale and markers as in figure 3. The values of cell volume reported here combine measurements of cells recorded over the entire population growth experiment (approximately 2 to 6 generations). Plots breaking down the measurements of cell volume on each day are presented in the SI section 2.11.A.

4 Discussion

Changes in environmental conditions, and particularly in environmental temperature, had very different effects on our studied organisms depending on the time scale considered. On a short time scale, both respiration rate and movement speed increased sharply with increasing temperature, in line with expectations from metabolic scaling theory [7]. But these changes were short-lasting, and many of the short-term changes of metabolic rate and movement speed induced by the exposure to a new temperature condition were significantly attenuated over time scales of just a few days.

Acute thermal response curves measured from respiration (a proxy for energy consumption), and those measured from swimming speed showed similarities but also important differences. Cells that were cold-adapted, and larger, had both higher respiration rates and higher movement speed, indicating that measurements of speed and respiration rates provide comparable information about the consequences of adaptation, and potentially the two measures could be used interchangeably. Importantly, however, the values of activation energy measured from respiration (0.35-0.89 eV) and those measured from movement speed (0.16-0.37 eV) were different, and lower for speed than for respiration: when environmental temperature increased, respiration increased disproportionately more than swimming speed. Previous studies have also found relatively low values of activation energy for acute movement-speed responses in ciliates. For example, Glaser [33] reported speed values for paramecia that correspond to an activation energy of approximately 0.37 eV, slightly higher, but similar to our results.

Mechanistically, we can understand the mismatch of activation energies for respiration and for movement as a physical consequence of the quadratic scaling of movement speed with power consumption for swimmers in a viscous medium. This led us to formulate the prediction of an activation energy for movement about half the activation energy for respiration (or slightly higher if we also account for the reduction of water viscosity at high temperature (SI section 3.2), but we remark that our values of activation energy for speed are slightly lower than this prediction, at 41% on average of the activation energy for respiration. Many factors can contribute to this discrepancy, ranging from noise in the data, to increasing inefficiency of energy conversion into movement at high temperature, or possibly to a fast-modulation of energy allocation to movement. We indeed call for further studies to establish a more precise relation between activation energy for speed and for

respiration across more species of unicellular swimmers, and across different experimental conditions.

Functionally, the activation energy for acute movement speed response, which is 0.2 - 0.4 eV lower than the activation energy for respiration, is likely responsible for introducing a mismatch between energy supply and energy demand, because prey encounter rate and prey capture (which depend on movement) would not keep up with the increase of metabolic energy requirements at increasing temperature. This 'mismatch requiring adaptation' process has a parallel in what is observed in the temperature response of autotrophs, where it is also the case that the energy acquisition process – which in this case is photosynthesis – has a lower activation energy than the energy expenditure process (respiration), and this mismatch imposes adaptation strategies based on the up- or down-regulation of the two processes (see e.g. [15]). It is interesting to note that – albeit for completely different reasons – similar temperature dependencies describe the energy intake and energy consumption of both primary producers and of ciliate consumers. This means that phenotypic responses that compensate for the mismatch between energy supply and demand (such as changing body size [34] or regulating the concentration of organelle such as mitochondria inside the cell [35]) are predicted to be similar across both autotrophs and eterotrophs, in spite of the fact that the mechanistic explanation might be completely different (i.e. the temperature-dependence of movement vs. the activation energy of photosynthesis).

While previous studies have already emphasized some of the possible ecological implications of the temperature dependence of animal movement (see e.g. [8]), our study indicates that complex adaptations of thermal responses –which depend on the time scale and on the phenotypic trait considered– can be observed also in axenic populations of one single organism. In future studies, our approach could be generalized to study the multiple drivers of phenotypic adaptation in multi-species microcosms.

Adaptation was incredibly rapid in our experiments, with cells changing their movement speed over just a few days in our 'long-term' temperature response data (SI section 2.11.B). Changes in cell volume also took place over a timescale that was possibly comparable to a single *Tetrahymena* generation (SI section 2.11.A). The reduction of cell size with increasing temperature is a well-described phenomenon, also observed in protists [36], for which various possible explanations have been put forward, ranging from temperature-induced limitations in oxygen supply relative to oxygen demand [37, 38] or

relative to other metabolic costs (such as the increasing costs of maintaining membrane gradients in smaller cells [39, 40, 41]), to developmental changes in the allocation of metabolic resources directed to maintenance and growth [42, 43], to cell size optimization in relation to the available resources at a given temperature [44] (summarized in [10]). In our experiments we found that cell size variation accounted for most, albeit not for all, of the variation observed also in the other phenotypic traits of respiration rate and movement speed (SI section 2.12). The fact that large cells also require more energy (and so proportionally also more time) to grow to a larger size, likely also contributed to explain some of the differences in the *per capita* growth rates of different adapted *Tetrahymena* populations (sec. 3.3). Temperature-size relations in *Tetrahymena* match to a good extent the changes of metabolic activity with temperature, with a thermal response curve characterised by both an activation and a deactivation part; conversely, oxygen availability did not seem to play a direct role limiting cell-volume growth in our experiments. This was probably due to a combination of the small size of *Tetrahymena*, and the fact that we worked with cultures in the exponential growth phase, before high cell densities could likely deplete oxygen and nutrients (see SI sections 2.10 and 3.4 for additional arguments about this).

Adaptation to different nutrient concentrations did not have a major effect on cell size, respiration, or movement speed in our experiments. Possibly, however, this was simply a consequence of having relatively limited variation in nutrient concentration (variation only spanning a factor of 4 from 50% to 200% medium concentration), combined with otherwise non-limiting growing conditions (i.e. exponential growth phase throughout). Previous studies [18, 17] have suggested that nutrient concentrations become a limiting factor for population growth when the metabolic requirements of organisms are high (e.g. at high temperature) and nutrient concentrations are low. Our results show some agreement with these predictions, for instance in figure 2(b), where cells adapted at 25 °C and 50% medium concentration show a reduced growth rate (see also SI section 2.9).

Our study highlights the multiple changes associated with the adaptation of microorganisms to their environment. Short-term, acute responses to changes in the environment are characterised by rapid and marked changes in metabolic activity and movement speed. These short-term changes mainly reflect simple physico-chemical processes, such as the effects of temperature on the rates of metabolic reactions [7, 45] and the temperature dependence of water viscosity [46]. Yet, movement and respiration are not affected in

the same way by changes of temperature. This likely introduces a mismatch between energy intake and energy expenditure that imposes behavioural and physiological adjustments. In our experiments the long-term exposure to a new environment resulted in the mitigation of acute responses, with both metabolic rate and movement speed converging towards similar values, independently of the environment in which cells were cultured. These adjustments were largely, but not entirely, mediated by changes in cell size. In a small organism with a short generation time like *Tetrahymena*, changes in cell size have a potential to play a major role in mediating rapid phenotypic adaptations because they can take place rapidly (due to the short generation times of less than one day) and because changes in cell volume affect simultaneously and in a consistent direction both the metabolic rate and the movement speed of individual cells.

We have proposed a preliminary theoretical framework, based on writing explicitly the energetic balance of individual cells (eq. 3.1 and SI section 3), to understand these phenotypic changes. Future research could aim to refine our methods to develop a fully quantitative model of phenotypic changes, by obtaining empirical estimations of parameters that we did not measure directly in our experiments, such as digestion times and the interplay between cell morphology and the mechanics of ciliary propulsion. Perhaps then, it will be possible to refine the approach that we have introduced here – which focuses on the interplay between physical constraints and the energetic costs and benefits of different phenotypic responses – to derive fully quantitative predictions about how individual organisms' and ecological communities' will adapted to future, and possibly unprecedented, changes in their environment.

5 Data availability

The data and analysis code used for this work are all publicly available at `https://github.com/pernafrost/Tetrahymena`. A snapshot of the analysis code at the time of manuscript submission has been submitted to Dryad. Doi: 10.5061/dryad.2v6wwpzvv.

This work was supported by the Royal Society Research Grant RG170282 to Andrea Perna.

References

[1] Brown JH, Hall CAS, Sibly RM. 2018 Equal fitness paradigm explained by a trade-off between generation time and energy production rate. *Nature Ecology & Evolution* **2**, 262–268. (10.1038/s41559-017-0430-1)

[2] Gazzola M, Argentina M, Mahadevan L. 2014 Scaling macroscopic aquatic locomotion. *Nature Physics* **10**, 758–761.

[3] Atkinson D, Sibly RM. 1997 Why are organisms usually bigger in colder environments? Making sense of a life history puzzle. *Trends in Ecology & Evolution* **12**, 235–239.

[4] Angilletta Jr MJ, Steury TD, Sears MW. 2004 Temperature, growth rate, and body size in ectotherms: fitting pieces of a life-history puzzle. *Integrative and Comparative Biology* **44**, 498–509.

[5] Walters RJ, Hassall M. 2006 The temperature-size rule in ectotherms: may a general explanation exist after all?. *The American Naturalist* **167**, 510–523.

[6] Gillooly JF, Brown JH, West GB, Savage VM, Charnov EL. 2001 Effects of size and temperature on metabolic rate. *Science* **293**, 2248–2251.

[7] Brown JH, Gillooly JF, Allen AP, Savage VM, West GB. 2004 Toward a metabolic theory of ecology. *Ecology* **85**, 1771–1789.

[8] Gibert JP, Chelini MC, Rosenthal MF, DeLong JP. 2016 Crossing regimes of temperature dependence in animal movement. *Global Change Biology* **22**, 1722–1736.

[9] Altermatt F, Fronhofer EA, Garnier A, Giometto A, Hammes F, Klecka J, Legrand D, Mächler E, Massie TM, Pennekamp F, Plebani M, Pontarp M, Schtickzelle N, Thuillier V, Petchey OL. 2015 Big answers from small worlds: a user's guide for protist microcosms as a model system in ecology and evolution. *Methods in Ecology and Evolution* **6**, 218–231. (https://doi.org/10.1111/2041-210X.12312)

[10] Weber de Melo V, Lowe R, Hurd PJ, Petchey OL. 2020 Phenotypic responses to temperature in the ciliate Tetrahymena thermophila. *Ecology and Evolution* **10**, 7616–7626.

[11] Gibert JP, Allen RL, Hruska III RJ, DeLong JP. 2017 The ecological consequences of environmentally induced phenotypic changes. *Ecology Letters* **20**, 997–1003.

[12] DeLong JP, Hanson DT. 2009 Metabolic rate links density to demography in *Tetrahymena pyriformis*. *The ISME Journal* **3**, 1396–1401.

[13] Bernhardt JR, Sunday JM, O'Connor MI. 2018 Metabolic theory and the temperature-size rule explain the temperature dependence of population carrying capacity. *The American Naturalist* **192**, 687–697.

[14] Dell AI, Pawar S, Savage VM. 2014 Temperature dependence of trophic interactions are driven by asymmetry of species responses and foraging strategy. *Journal of Animal Ecology* **83**, 70–84. (https://doi.org/10.1111/1365-2656.12081)

[15] Padfield D, Yvon-Durocher G, Buckling A, Jennings S, Yvon-Durocher G. 2016 Rapid evolution of metabolic traits explains thermal adaptation in phytoplankton. *Ecology Letters* **19**, 133–142.

[16] Hairston Jr NG, Ellner SP, Geber MA, Yoshida T, Fox JA. 2005 Rapid evolution and the convergence of ecological and evolutionary time. *Ecology letters* **8**, 1114–1127.

[17] Bestion E, Schaum CE, Yvon-Durocher G. 2018 Nutrient limitation constrains thermal tolerance in freshwater phytoplankton. *Limnology and Oceanography Letters* **3**, 436–443.

[18] Thomas MK, Aranguren-Gassis M, Kremer CT, Gould MR, Anderson K, Klausmeier CA, Litchman E. 2017 Temperature–nutrient interactions exacerbate sensitivity to warming in phytoplankton. *Global change biology* **23**, 3269–3280.

[19] Sinclair BJ, Marshall KE, Sewell MA, Levesque DL, Willett CS, Slotsbo S, Dong Y, Harley CD, Marshall DJ, Helmuth BS et al.. 2016 Can we predict ectotherm responses to climate change using thermal performance curves and body temperatures?. *Ecology Letters* **19**, 1372–1385.

[20] Bolker BM, Brooks ME, Clark CJ, Geange SW, Poulsen JR, Stevens MHH, White JSS. 2009 Generalized linear mixed models: a practical

guide for ecology and evolution. *Trends in ecology & evolution* **24**, 127–135.

[21] Zuur AF, Ieno EN, Walker NJ, Saveliev AA, Smith GM et al.. 2009 *Mixed effects models and extensions in ecology with R* vol. 574. Springer.

[22] R Core Team. 2022 *R: A Language and Environment for Statistical Computing*. R Foundation for Statistical Computing Vienna, Austria.

[23] Sharpe PJ, DeMichele DW. 1977 Reaction kinetics of poikilotherm development. *Journal of Theoretical Biology* **64**, 649–670.

[24] Schoolfield RM, Sharpe P, Magnuson CE. 1981 Non-linear regression of biological temperature-dependent rate models based on absolute reaction-rate theory. *Journal of Theoretical Biology* **88**, 719–731.

[25] Padfield D, O'Sullivan H, Pawar S. 2021 rTPC and nls.multstart: A new pipeline to fit thermal performance curves in r. *Methods in Ecology and Evolution* **12**, 1138–1143. (10.1111/2041-210X.13585)

[26] Katsu-Kimura Y, Nakaya F, Baba SA, Mogami Y. 2009 Substantial energy expenditure for locomotion in ciliates verified by means of simultaneous measurement of oxygen consumption rate and swimming speed. *Journal of Experimental Biology* **212**, 1819–1824.

[27] Gueron S, Levit-Gurevich K. 1999 Energetic considerations of ciliary beating and the advantage of metachronal coordination. *Proceedings of the National Academy of Sciences* **96**, 12240–12245.

[28] Martinez E, Hendricks E, Menze MA, Torres JJ. 2016 Physiological performance of warm-adapted marine ectotherms: thermal limits of mitochondrial energy transduction efficiency. *Comparative Biochemistry and Physiology Part A: Molecular & Integrative Physiology* **191**, 216–225.

[29] Chung DJ, Schulte PM. 2020 Mitochondria and the thermal limits of ectotherms. *Journal of Experimental Biology* **223**, jeb227801.

[30] Visser AW. 2007 Motility of zooplankton: fitness, foraging and predation. *Journal of Plankton Research* **29**, 447–461.

[31] Visser AW. 2011 Small, Wet and Rational. *Dr. Techn. Dissertation. Technical University of Denmark, Copenhagen.*

[32] Karp-Boss L, Boss E, Jumars P et al.. 1996 Nutrient fluxes to planktonic osmotrophs in the presence of fluid motion. *Oceanography and Marine Biology* **34**, 71–108.

[33] Glaser O. 1924 Temperature and forward movement of *Paramecium*. *The Journal of General Physiology* **7**, 177–188.

[34] Deutsch C, Penn JL, Verberk WC, Inomura K, Endress MG, Payne JL. 2022 Impact of warming on aquatic body sizes explained by metabolic scaling from microbes to macrofauna. *Proceedings of the National Academy of Sciences* **119**, e2201345119.

[35] Hochachka PW, Somero GN. 2002 *Biochemical adaptation: mechanism and process in physiological evolution*. Oxford university press.

[36] Atkinson D, Ciotti BJ, Montagnes DJ. 2003 Protists decrease in size linearly with temperature: ca. 2.5% C- 1. *Proceedings of the Royal Society of London. Series B: Biological Sciences* **270**, 2605–2611.

[37] Verberk WC, Atkinson D, Hoefnagel KN, Hirst AG, Horne CR, Siepel H. 2021 Shrinking body sizes in response to warming: explanations for the temperature–size rule with special emphasis on the role of oxygen. *Biological Reviews* **96**, 247–268.

[38] Forster J, Hirst AG, Atkinson D. 2012 Warming-induced reductions in body size are greater in aquatic than terrestrial species. *Proceedings of the National Academy of Sciences* **109**, 19310–19314.

[39] Atkinson D, Morley SA, Hughes RN. 2006 From cells to colonies: at what levels of body organization does the 'temperature-size rule'apply?. *Evolution & development* **8**, 202–214.

[40] Czarnołeski M, Kozłowski J, Dumiot G, Bonnet JC, Mallard J, Dupont-Nivet M. 2008 Scaling of metabolism in Helix aspersa snails: changes through ontogeny and response to selection for increased size. *Journal of Experimental Biology* **211**, 391–400.

[41] Hermaniuk A, van de Pol IL, Verberk WC. 2021 Are acute and acclimated thermal effects on metabolic rate modulated by cell size? A comparison between diploid and triploid zebrafish larvae. *Journal of Experimental Biology* **224**, jeb227124.

[42] Von Bertalanffy L. 1957 Quantitative laws in metabolism and growth. *The Quarterly Review of Biology* **32**, 217–231.

[43] Zuo W, Moses ME, West GB, Hou C, Brown JH. 2012 A general model for effects of temperature on ectotherm ontogenetic growth and development. *Proceedings of the Royal Society B: Biological Sciences* **279**, 1840–1846.

[44] DeLong JP. 2012 Experimental demonstration of a 'rate–size'trade-off governing body size optimization. *Evolutionary Ecology Research* **14**, 343–352.

[45] Arroyo JI, Díez B, Kempes CP, West GB, Marquet PA. 2022 A general theory for temperature dependence in biology. *Proceedings of the National Academy of Sciences* **119**, e2119872119.

[46] Beveridge OS, Petchey OL, Humphries S. 2010 Mechanisms of temperature-dependent swimming: the importance of physics, physiology and body size in determining protist swimming speed. *Journal of Experimental Biology* **213**, 4223–4231.

Supplementary Information: Disentangling the multiple drivers of ecological adaptation in a microorganism

A. Perna[1,2], E.S. Rivoli[2], and D.M. Perkins[2]

[1] *Networks Unit, IMT School for Advanced Studies, Lucca, Italy*
[2] *Life Sciences, University of Roehampton, London, UK*

Contents

1 Supplementary methods **3**
1.1 Cell cultures . . . 3
1.2 Adaptation took place in exponential growth . . . 3
1.3 Experimental procedures . . . 5
1.3.A Measurements of respiration . . . 5
1.3.B Measurements of speed . . . 6
1.3.C The measured movement speed is not driven by transient effects . . . 7
1.4 Missing data points . . . 9

2 Supplementary results **10**
2.1 Growth rate changes with adaptation . . . 10
2.2 Additional measurements of cell size and shape . . . 12
2.3 Thermal response curves for respiration . . . 13
2.4 Thermal response curves for movement speed (short-term exposure) . . . 16
2.5 Thermal response curves for movement speed (long-term exposure) . . . 18
2.6 Thermal response curves for population growth . . . 19
2.7 Thermal response curves for cell volume (long-term exposure) . . . 21
2.8 Speed vs. medium concentration . . . 22
2.9 Effects of medium concentration on population growth . . . 23
2.10 Effects of oxygen concentration on cell size and shape . . . 25
2.11 Phenotypic plasticity or evolutionary change? . . . 25
2.11.A Changes of cell volume were very rapid . . . 28
2.11.B Speed changed rapidly after the transfer to the new temperature condition and remained stable afterwards . . . 31
2.11.C Effects of changes of temperature on population growth rates . . . 35
2.12 Impact of cell volume on metabolic rate and speed . . . 39

3 Some theoretical considerations **42**
3.1 The energetic balance of individual cells . . . 42
3.2 Predicted relationship between activation energies for respiration and movement speed 44
3.3 Optimisation of swimming speed . . . 46
3.4 Oxygen availability to *Tetrahymena* cells . . . 48
3.5 Diffusion around a sphere . . . 53
3.6 Temperature dependence of oxygen concentration in fully saturated water . . . 54
3.7 Diffusion of molecules in water . . . 55
3.8 Implications of cell shape for swimming . . . 56

Section 1

Supplementary methods

1.1 Cell cultures

Axenic cultures of *Tetrahymena pyriformis* strain 1630/1W were obtained from CCAP (`http://www.ccap.ac.uk`). We initially separated two culture lines, which we cultured for 53 days at 20 °C (constant temperature, no light) in a Proteose peptone - yeast extract medium (20 g Proteose peptone + 2.5 g yeast extract in 1 L deionised water – this is our '100% medium concentration'). During this time, population density and medium quality were maintained stable with a serial transfer regime, with repeated dilutions into fresh medium every 1-4 days. Throughout the experiment, the cell culture flasks were kept horizontal on a shaker plate to facilitate the exchange of gases between the culture medium and air. After 53 days we started the adaptation lines cultured at 15 °C and medium concentrations of 50%, 100% and 200%, in four replicates (two lines originating from each of the two initial adaptation lines), and after 55 days we also started the adaptation lines cultured at 20 °C and 25 °C, for all medium concentrations (in four replicates each). At this stage there were 9 experimental conditions (3 temperature conditions x 3 conditions of medium concentration), each in 4 replicates, for a total of 36 parallel cultures. Cultures were kept in these new conditions and maintained in exponential growth phase by frequently subculturing into fresh medium for an estimated number between 21 and 68 generations, before being measured for movement speed, respiration and cell size (this range of generations was due both to the differences in growth rate across experimental conditions, and to the time taken for some of the subsequent measurements, which typically required multiple days as each line had to be tested across a wide range of temperature conditions in order to fit a thermal response curve). After 33 days of adaptation; 35 days for the lines kept at 15 °C (38 to 112 generations), all cells were taken from their initial adaptation culture and split across multiple temperature conditions (between 12.5 and 30 °C), where they were further kept in culture (without further subcultures) to be measured over a time scale of 2-6 generations in terms of population growth, changes of cell size, and 'long-term' movement speed.

1.2 Adaptation took place in exponential growth

In our experiment, cells were maintained in exponential growth phase throughout the experiments by subculturing frequently into fresh culture medium (every 1 to 4 days, depending on the estimated

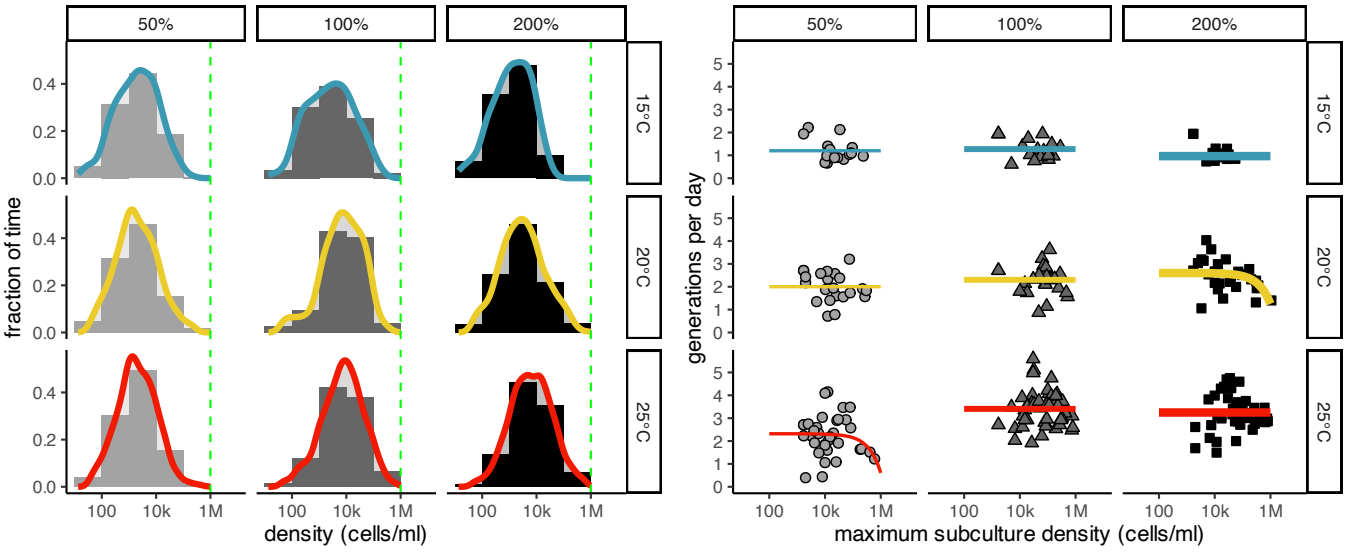

Figure S1.1: *Tetrahymena* growth happened in the exponential growth phase. **Left:** Estimated time spent by *Tetrahymena* cell cultures at each population density throughout the adaptation to each experimental condition. The dashed green vertical line is added to visually mark an approximate value of maximum density for *Tetrahymena*, at around 1 million cells/ml. **Right:** When the cultures approach the carrying capacity, we should expect to observe a decrease in the *per capita* growth rate for increasing population densities. The figure plots the measured growth rate of each subculture as a function of the maximum density of cells observed for the same subculture. Fitted lines are the best fitting model (i.e. the model with the minimum Akaike information criterion AIK) chosen among (1) a model in which the growth rate (expressed in number of generations per day) was constant and independently of culture density throughout the entire range of the data, and (2) a model in which the growth rate was $\propto (1 - N/K)$ (i.e. decreasing at high density).

cell density of the culture on the subculture days).

In preliminary experiments, we had observed that if we let *Tetrahymena* cultures grow without subculturing for extended periods (e.g. one week), we typically reached maximum densities of the order of 1,000,000 cells per ml. These values are similar to commonly reported values in the scientific literature for *Tetrahymena* species. For example, Hofmann and Cleffmann [*S1*] report maximum densities between 400,000 cells/ml and 1.7×10^6 cells/ml in *Tetrahymena thermophila*, depending on the culture medium used (also providing some evidence that *T. thermophila* population growth was not limited by oxygen availability, even at the highest densities). Reported densities for *T. pyriformis* are also in the order of 1 million cells/ml; for instance, Mogami et al. [*S2*] identify the late exponential - early stationary phase at $1.2 - 1.6 \times 10^6$ cells/ml. DeLong and Hanson [*S3*] report much lower maximum culture densities for *T. pyriformis*, at 8379 cells/ml, but we believe that there might be a typo or an error in their reporting of measurement units, because not only their maximum density is about two magnitude orders lower than the typical values reported in other studies, but also their reported respiration rates per individual cell are approximately two orders of magnitude higher than what we measure in our experiments.

In our culture conditions, the estimated median cell density was 4440 cells/ml (with a large

variation due to exponential population growth), and for this reason we believe that growth took place in the exponential phase. However, in order to get some insight on the issue whether cell growth rate was limited by density-dependent effects directly from our own data, in figure S1.1 on the left we report the estimated distribution of densities at hourly intervals throughout the entire adaptation period for each of the nine culture conditions (note that values in-between direct counts had to be interpolated with an exponential). On the right panel in the figure, we report the measured growth rate as a function of culture density. If, within the range of culture densities that we used, population growth was not limited by density, then the *per capita* growth rate should be constant independently of density $\frac{1}{N}\frac{dN}{dt} = r$, with r a constant. If, instead, within the same range of population densities the *per capita* growth rate was limited by population density, we should see this *per capita* growth rate decrease at high densities: $\frac{1}{N}\frac{dN}{dt} = r\left(1 - \frac{N}{K}\right)$, where K, also a constant, expresses the 'carrying capacity' of the growth environment (culture medium and temperature).

Selecting between these two alternative models (based on Akaike information criterion – AIK), we find that the model with constant number of generations per day was preferred in 7 culture conditions out of 9. In the condition with growth temperature T=25 °C, and medium concentration 50%, the model with density-limited growth was slightly preferred, but the AIK difference was negligible (ΔAIK = 0.132). Finally, in the growing condition with temperature T=20 °C and 200% medium, the density-limited model was preferred with a non-negligible ΔAIK = 3.702. However, also in this case the fitted value of carrying capacity was large (K = 1.9M cells/ml), and the number of subcultures affected by growth-limiting densities was small (i.e. the density independent model would become the preferred model again if we excluded only two of the 28 subcultures).

1.3 Experimental procedures

1.3.A Measurements of respiration

Oxygen consumption was measured by placing experimental populations of know density of *Tetrahymena* in 2 mL oxygen sensor vials, Sensor Dish Reader from PreSens (`https://www.presens.de/`). In order to control environmental temperature during the measurement, the vials were kept inside thermal cabinets (Lovibond TC 255 S, Tintometer GmbH, Germany) at the desired temperature.

Temperature affects the solubility of oxygen and can also affect the readings of the Sensor Dish Reader directly. Because of this, we had to take a series of precautions to minimize the changes of temperature during the measurements of respiration, in spite of the fact that, inevitably, there is a change of temperature associated with moving cells from their incubation temperature to the temperature at which they were tested for respiration.

In advance of any respiration measurement, we filled small disposable flasks each with approximately 5 ml of sterile culture medium at the desired concentration (50%, 100%, 200%) and stored them at the same temperature at which we would later measure respiration. This was done so that we had fresh culture medium already at the right temperature. We also placed the empty oxygen sensor vials into their holding wells in the Sensor Dish Reader, and we placed the whole kit in the incubator to acclimate at the desired temperature.

Just before the respiration measurement started, we took cells from their incubation temperature, we counted their density in cell-counting slides under the microscope and we transferred the

appropriate amount of cell suspension into the previously prepared small disposable flasks with culture medium at the testing temperature, so as to obtain a density of approximately 8000 cells/ml. We then mixed gently by swirling the flasks and we used this diluted suspension to fill the oxygen sensor vial. The vials prepared in this way were then placed back onto the Sensor Dish reader and in the thermal cabinet, leaving their lid open in order to allow temperature and oxygen to equilibrate. After 15 to 30 minutes, we sealed the vials with their lids, and we started the recording.

The density of 8000 cells/ml was chosen as it gave a good compromise between recording time and oxygen depletion across the range of temperature conditions that we tested. At lower densities, cells would only consume oxygen very slowly, leading to long recording times, potentially leading to some population growth during the recording itself, and leaving open the possibility that cells might start adapting to the new experimental conditions. Higher cell densities could lead to significant oxygen depletion during the recording, and consequently to short recording times, with the possibility of incomplete temperature stabilization during the recording.

The Sensor Dish Reader has an internal temperature measurement, and we only used the portion of recording for which temperature had stabilized to approximately 0.5°C around the set temperature and there was almost no change in recorded oxygen concentration within the vials used as a control. Control vials were prepared in a similar way as the experimental ones, but they did not contain any *Tetrahymena* cells.

The Sensor Dish Reader recorded the measured oxygen concentration ($[O_2]$ in units of μmol/L) at 15 s intervals throughout the experiment. Respiration rates were then calculated from the slope of a regression line fitted through the oxygen concentration data during the time interval for which temperature was stable and oxygen consumption was linear. The exact starting time and duration of this interval was variable depending on the recording temperature (oxygen consumption was reduced at low temperature), but as an indication it started approximately 20 minutes after the vials were sealed and ended approximately 1 to 4 hours later, when we stopped the recording or oxygen started to get depleted (recordings were typically longer at low temperature).

Population-level respiration rate was then converted to rate of energy consumption per individual cell by accounting for population density in the vial, and assuming an equivalence 1 mol O_2 = 478576 J.

After each usage, the oxygen sensor vials were cleaned with deionised water, rinsed with ethanol, and left to dry in the oven at 50 °C for approximately 48 hours.

1.3.B Measurements of speed

Tetrahymena movement speed was measured from videos taken under the microscope at the desired temperature. For each measurement, we placed a cell-counting slide (BVS100 FastRead) on the microscope stage to get to temperature; we then gently pipetted a drop of culture (20 μL) directly on the slide. After pipetting, we waited 90 seconds before starting the recording, to let temperature in the culture to fully equilibrate and to exclude transient effects on *Tetrahymena* behaviour associated with the pipetting and with the abrupt change of temperature (rather than with the value of temperature itself). Preliminary experiments in which we monitored *Tetrahymena* movement for up to 20 minutes after pipetting indicated that the movement patterns stabilized a few seconds after pipetting, and remained stable until the end of the 20 minutes period (see below, section 1.3.C).

Speed was measured under two different conditions: a 'short-term exposure' and a 'long-term

exposure' to temperature. In practice, the **speed data under short-term exposure** were collected by pipetting cells from one of the nine main adaptation cultures (3 temperature conditions crossed with 3 medium concentration values) directly on the microscope slide at a different temperature, ranging from 10 to 40 degrees. In order to reduce experimental time with these measurements, only two out of the four replicates were randomly used for these measurements. **Speed data under long-term exposure** were collected as part of the same experiment that we used to measure thermal response curves for population growth: each experimental replica from all conditions (9 conditions x 4 replicas each) was split into 8 different flasks, which were then transferred to temperatures ranging from 12.5 to 30 °C (12.5, 15, 17.5, 20, 22.5, 25, 27.5, 30). Speed was then measured at the same temperature at which each flask had been stored, after an incubation period corresponding approximately to two to six *Tetrahymena* generations.

1.3.C The measured movement speed is not driven by transient effects

In a preliminary series of experiments on a different population of the same strain of *Tetrahymena pyriformis* 1630/1W, we recorded cells under the microscope for long periods of 20 minutes, in order to monitor potential changes of speed over time (approximately 30 experimental cultures with different combinations of adaptation temperature and test temperature were recorded in this way). These preliminary experiments were justified by the theoretical possibility that, over short timescales, cells could change speed while the temperature of the suspension on the microscope slide was still equilibrating, or because of the stress of being transferred to the new environment; over long timescales, oxygen might get depleted from the very thin layer of suspension – 100 μm – between the microscope slide and its cover, also affecting their movement. However, our preliminary experiments led us to exclude the presence of transient changes of movement speed associated with the transfer of *Tetrahymena* cells onto the microscope slide. As an illustrative example, figure S1.2 presents data for cells adapted at 20 °C and 100% culture medium, and tested across a range of temperature conditions (data for cells adapted at 15 and 25 °C, and tested across the whole range of temperature conditions – not shown here – are also similar). These data indicate that speed did not consistently increase or decrease throughout the 20 minutes recording period, except at very high testing temperature of 37.5 and 40 °C (bottom plots shown as an example), where cells stopped moving soon after they were transferred onto the microscope slide (fewer cells are detected by the tracking software – which only detects moving objects – as time progresses, and the speed of cells that are detected decreases). From these data we concluded that the recording time-window used in the main experiment (highlighted in green in the figure) was representative of the acute movement speed of our *Tetrahymena pyriformis* cells also over longer timescales, while a shorter recording duration allowed us to limit considerably the amount of time required to run the experiments.

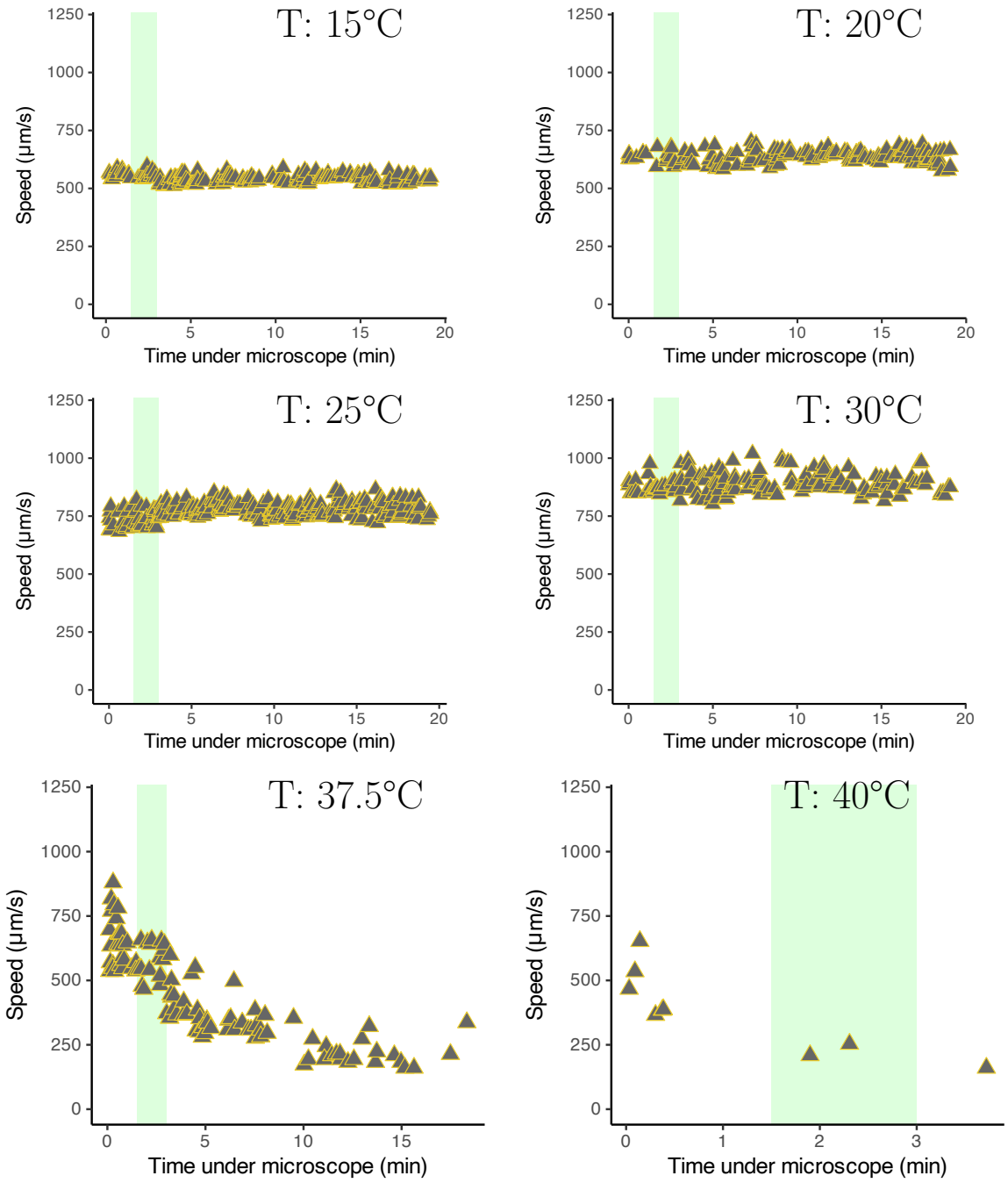

Figure S1.2: Movement speed over time. Examples of the distribution of *Tetrahymena* speed as a function of the time lapsed since they were transferred onto the slide. In all the panels shown, cells adapted to 20 °C and 100% culture medium were transferred onto the slide at a new temperature at time 0 on the x axis, and their speed was measured in the same way as for all the other analyses in our manuscript (the speed values shown in the figure were calculated on the 20% faster cells in each 1.5 minutes time interval and in each condition). The green shaded region corresponds to the time window that was used in the main experiment (1.5 – 3 minutes).

We should note that Dupont and collaborators [*S4*] have very recently reported of experiments on the related ciliate *Tetrahymena thermophila* in which the movement speed only equilibrated over a longer time-scale of over 30 minutes after the change of temperature. As these results are presented as an illustrative example in their paper, and the experimental methods are not described in full detail, we cannot interpret the differences between our respective studies in terms of different experimental methodologies, or perhaps of temperature itself not having fully converged to the new value in their experiment, but we remain confident that – at least in the conditions adopted in our own experiment – speed changes were almost instantaneous, consistent with our interpretation that the changes of short-term movement speed observed in our data are driven by the physics of the system (higher temperature induces faster chemical reactions and – consequently – a faster movement) rather than by phenotypic changes aimed at buffering the fitness costs of the changed environment, as reportedly would instead be the case in reference [*S4*].

1.4 Missing data points

Our study involves a large amount of data, with 9 treatments, each in 4 replicates, and where each replicate is then tested at 9 or more different temperature conditions for movement, respiration, population growth and cell size. The analysis was automated with custom made scripts in R and python, and no data points were selectively altered or excluded. However, for the short-term speed response curves, only two of the four replicates were used (randomly chosen) in order to cut experimenter and computing time by reducing the number of recorded videos from approximately 4 x 9 x 13 = 468 to approximately 2 x 9 x 13 = 234 for this specific measurement. Across the various measurements, a small number of combinations of conditions were not recorded because either (1) the density in the culture was too low or too high on the day when the recording was planned and we couldn't record on another day, or (2) the video file was corrupted, or (3) particularly for cells grown and tested at the same temperature (e.g. grown at 15 °C and tested at 15 °C), we initially preferred to omit some speed measurement because of logistic constraints with maintaining the culture in axenic conditions (speed measurements took place under the microscope *not* in axenic conditions).

In the measurements of respiration, we removed a single data point for the respiration rate of the culture adapted at 25 °C, 200% nutrient concentration, cell line B, tested at 25 °C. Cells in this culture were recorded as having a respiration rate of approximately 4 nW, much higher than for the other lines and nearby temperatures. We believe that we probably made an error with the dilution in preparation for the oxygen recording (that is, cell density was considerably higher than 8000 cells/ml)), but we cannot confirm this *a posteriori*.

Section 2

Supplementary results

2.1 Growth rate changes with adaptation

In this section we examine how the growth rate and biomass production of our *Tetrahymena* cultures changed over time.

We noted in the main text that during the initial adaptation of the mother culture, and during

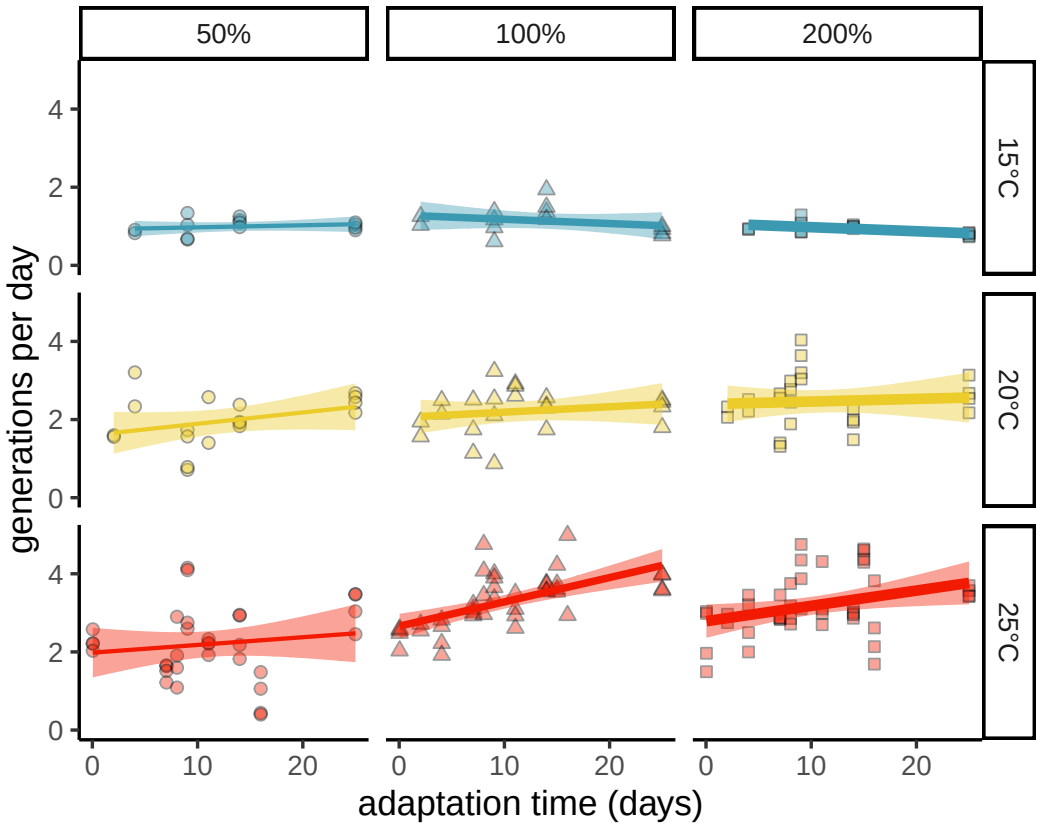

Figure S2.1: Population growth rate of *Tetrahymena* over the 25 last days of the experiment (starting approximately 9 days after cells were transferred to the new culture conditions).

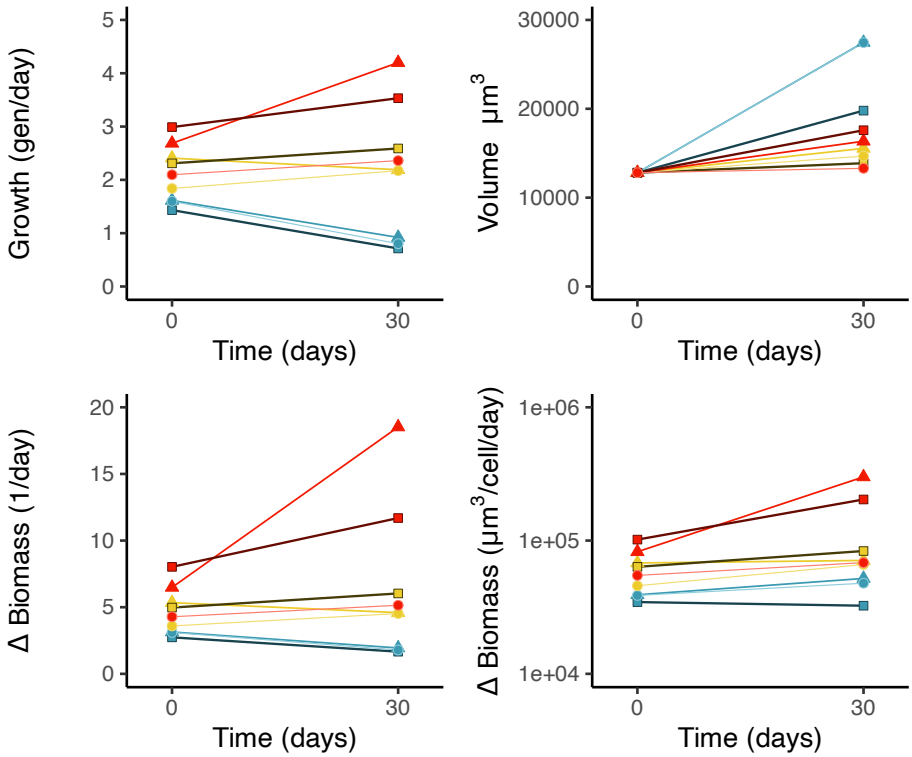

Figure S2.2: Changes in the growth rate and biomass production of *Tetrahymena* between the beginning of the subculture period (day 0), and approximately the end of the subculture period (day 30). **Top left**: growth rate over time, measured in cellular generations per day. **Top right**: estimated changes of cell volume over the time interval. **Bottom left**: Estimated biomass production rate (volume of biomass produced after one day for one initial unit of volume). **Bottom right**: Estimated biomass production rate per individual cell (volume of biomass produced by one cell in one day. Adaptation conditions: red=25 °C, yellow=20 °C, blue=15 °C, square=200% medium concentration, triangle=100%, circle=50%.

the adaptation of *Tetrahymena* to each growth culture, the growth rate remained stable or increased slightly over time, with the exception of cultures kept at 15 °C where we observed a slight decrease in population growth rate over time, which potentially could be explained by the changes in cell volume of these cultures. Here, we expand on these observations by providing additional details on the changes in growth rate and biomass production in each of the 9 culture conditions.

In figure 2(a) of the main document we can see that there is a discontinuity in the fitted curves for population growth rate at the time when the cultures are transferred to a different environment (i.e. to a different temperature or concentration of the culture medium). This likely reflects simple constraints of the different environments: high temperature and non-limiting food availability can support faster population growth. However, it might be interesting to explore whether, after these transient changes in our populations which are directly driven by the different physical parameters of the environment, cells further evolved to adapt to the conditions of their new environment, e.g. increasing their growth rate over time.

Figure S2.1 shows the population growth rate of each culture line over the last 25 days of the experiment (which also corresponds to the last 25 days of figure 2(a) of the main document,

starting approximately 9 days after the transfer to the new culture conditions). Over this period, the population growth rate increased over time in three culture conditions (T=25 °C with 100% and 200% medium concentration, and T=20 °C with 50% medium concentration), it decreased in one culture condition (T=15 °C, 200% concentration), and it remained statistically indistinguishable from constant in the other conditions (though with a positive trend, except at T=15 °C, 100% concentration).

Tetrahymena changed their cell volume depending on culture conditions (as shown in figure 2(c) of the main document). In particular, cells adapted at 15 °C exhibited the most pronounced changes in cell volume. Hence, there is a possibility that these cold-adapted cells were still increasing their biomass production rate over time spent in the new environment, in spite of the nearly constant or decreasing trend in population growth rate: simply, they would be increasing the volume of the offspring that they produce, rather than increasing the rate at which they produce it. Unfortunately, while we monitored the population growth rate over the entire duration of the adaptation experiment, we only measured cell volume at the beginning (in the mother culture), and near the end of the subculture period (when we imaged the cells to measure their size and movement speed). In spite of this limitation, we can still try to estimate how the rates of population growth and biomass production change between the two endpoints of the adaptation time interval. For example, figure S2.2 reports the population growth rates, change in the volume of individual cells, and estimated biomass production calculated by assuming that the log(volume) of cells changed linearly over the period of approximately 30 days in-between the time when cells were moved to the new environment and when their volume was measured. Biomass production can be expressed in units of biomass produced by one cell in one day (bottom-right panel), or in units of biomass produced by one unit of biomass in one day (bottom-left panel in the figure). Figure S2.2 supports the idea of a slight increase in both population growth rate and biomass production for most culture conditions, while the pattern remains slightly less clear for cells cultured at 15 °C, for which there was no clear increase of performance (where performance is intended as either an increase in population growth or of biomass production rate) over subculture time. We can speculate that this might be due to an inability of *Tetrahymena* to fully adapt to the cold-temperature conditions, possibly because the comparatively smaller number of generations of cultures kept at low temperature. Likely, however, some of the differences between *Tetrahymena* populations cultured at 15 °C and those cultures at the other temperatures could also be ascribed to an anomalous high initial estimate of population growth for the 15°C culture lines (cell densities were particularly low in the initial counts of these cultures, leading to larger estimation errors). The effect of this anomalous initial estimate of population growth would be reflected in the much more pronounced negative slope of the blue curves in figure S2.2, top-left panel (where the entire subculture period was considered) compared to figure S2.1, top row, where the first population growth measurement after the change of environment was excluded.

2.2 Additional measurements of cell size and shape

Figure S2.3 reports measurements of cell size and shape. The figure shows that when cells increased their volume at low temperature, the change was mainly driven by an increase in cell length (major axis length S2.3(a)), leading to a more elongated shape (S2.3(c)), while cell width (minor axis length S2.3(b)) changed proportionally less.

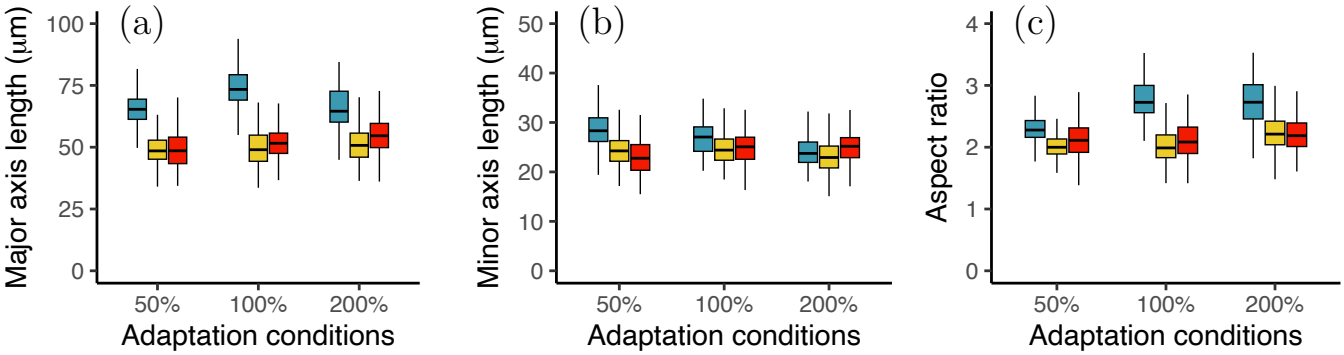

Figure S2.3: Cell size and shape in different adaptation conditions. (a) Major axis length (approximately equivalent to cell length). (b) Minor axis length (cell width). (c) Aspect ratio (ratio between length and width). All measurements are obtained by fitting an ellipse along the perimeter of the cell as imaged under the microscope and measuring the major and minor axis of the ellipse. The aspect ratio is calculated as the length of the major axis divided by the length of the minor axis.

We do not have an explanation for these changes of cell shape in terms of their putative adaptive value for swimming performance (see below, section S3.8), or for oxygen uptake (see below, section S3.4). We can speculate that these changes of shape may be related to other factors (e.g. intracellular structure), or that, possibly, a more elongated shape allows for more powerful (albeit less efficient) swimming by increasing the number of cilia oriented orthogonally to the swimming direction.

2.3 Thermal response curves for respiration

Figure S2.4 reports the thermal response curves for respiration under a short-term exposure (approximate range 20 minutes to 4 hours) to the new temperature.

The fitted parameters of the thermal response curves are also reported in table S2.1

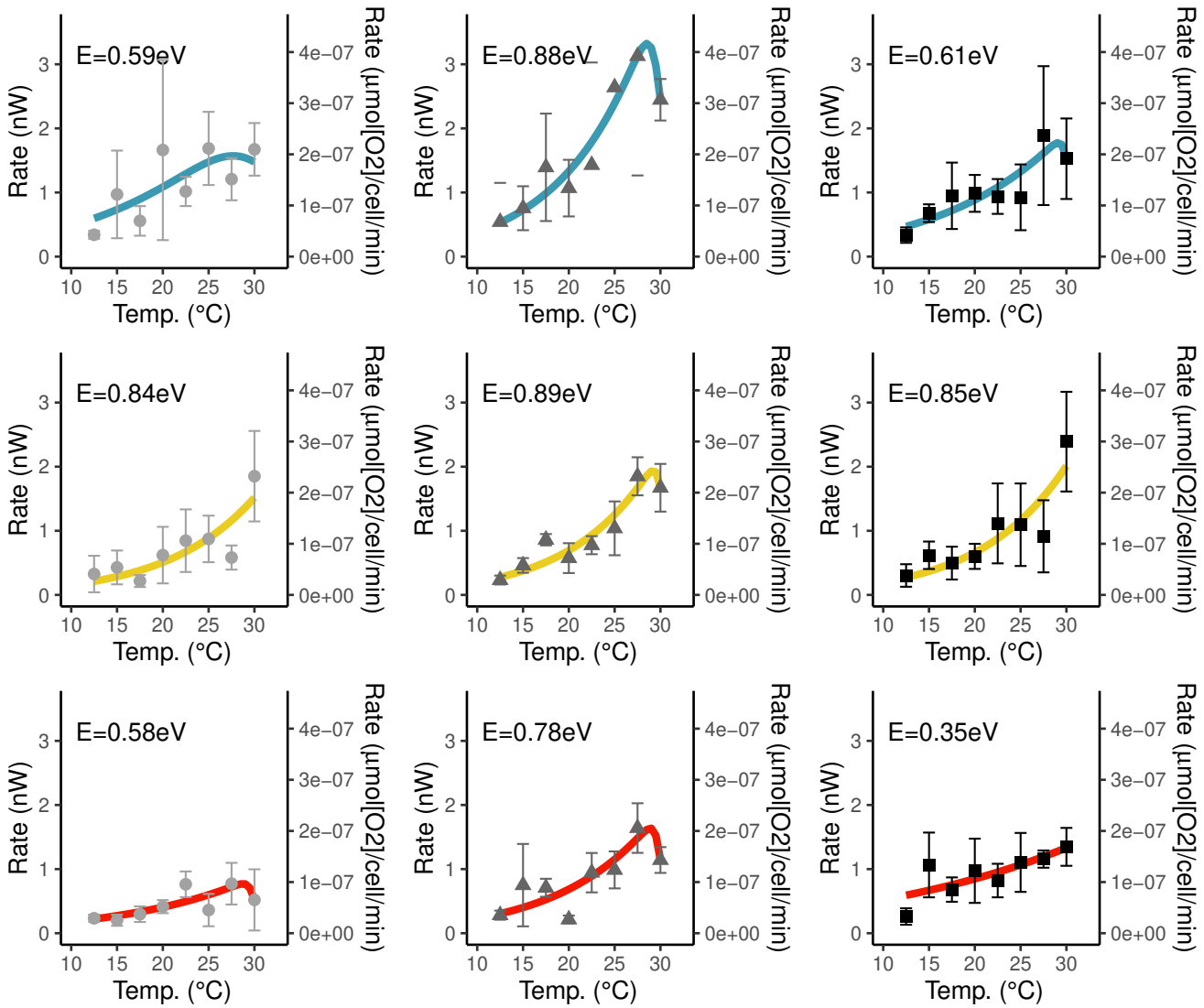

Figure S2.4: Thermal response curves for respiration. Each row corresponds to a different temperature condition (top = 15 °C, middle = 20 °C, bottom = 25 °C); each column corresponds to a different medium concentration (left = 50%, centre = 100%, right = 200%). Data points represent the mean across four replicates and error bars are ±1 standard deviation. Continuous lines represent fitted Sharpe-Schoolfield curves (rTPC package version). The text on each graph reports the value of activation energy E for the Arrhenius part of the curve.

Table S2.1: Measured parameters of the thermal response curves for respiration (short-term response)). Values in brackets indicate the 95% confidence intervals obtained from a bootstrap procedure with resampling of the residuals.

Adaptation temperature	Medium concentration	Activation energy (eV)	Oxygen consumption at reference temperature (nW/cell)
15°C	50%	0.594 [0.189 - 1.238]	1.106 [0.824 - 1.578]
	100%	0.883 [0.409 - 2.075]	1.331 [0.764 - 1.942]
	200%	0.610 [0.321 - 0.993]	0.884 [0.657 - 1.106]
20°C	50%	0.838 [0.543 - 1.448]	0.508 [0.335 - 0.696]
	100%	0.890 [0.680 - 1.132]	0.694 [0.576 - 0.820]
	200%	0.852 [0.575 - 1.337]	0.661 [0.444 - 0.893]
25°C	50%	0.584 [0.262 - 0.990]	0.407 [0.296 - 0.502]
	100%	0.782 [0.483 - 1.109]	0.685 [0.545 - 0.862]
	200%	0.346 [0.195 - 0.594]	0.848 [0.718 - 0.981]

While the respiration data in figure S2.4 are somewhat noisy, when the thermal responses curves are plotted together on the same graph - as in figure S2.5 - we can appreciate the fact that cells adapted at low temperature tend to have higher *per capita* respiration, most likely because of their larger volume (see main text, fig. 2). A consequence of this is that, at the end of the adaptation process, the metabolic rate of cells (measured in terms of oxygen consumption), is similar across

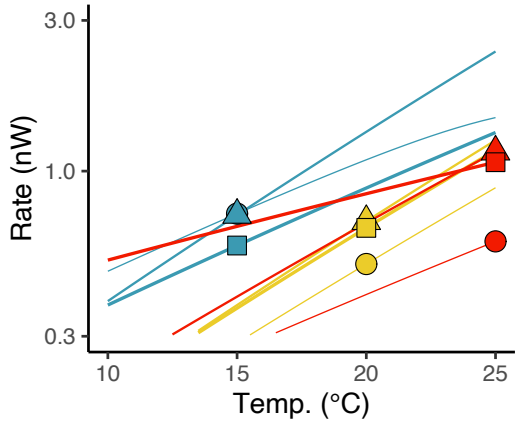

Figure S2.5: Thermal response curves for respiration rate across all the nine adaptation conditions. The markers indicate the value of the thermal response curve at the adaptation temperature. Different color hues correspond to different temperature conditions (blue = 15 °C, yellow = 20 °C, red = 25 °C; bright colours and narrow lines correspond to low nutrient concentration: 50% concentration of culture medium; dark colours and thick lines correspond to high nutrients: 200% medium). The markers highlight the values of the thermal response curves at the adaptation temperature: circle = 50% medium concentration, triangle = 100% medium concentration, square = 200% medium concentration.

cells measured each at their respective adaptation temperature.

2.4 Thermal response curves for movement speed (short-term exposure)

Figure S2.6 reports the thermal response curves for movement speed under a short-term (1.5 – 3 minutes) exposure to the new temperature. The fitted parameters of the thermal response curves

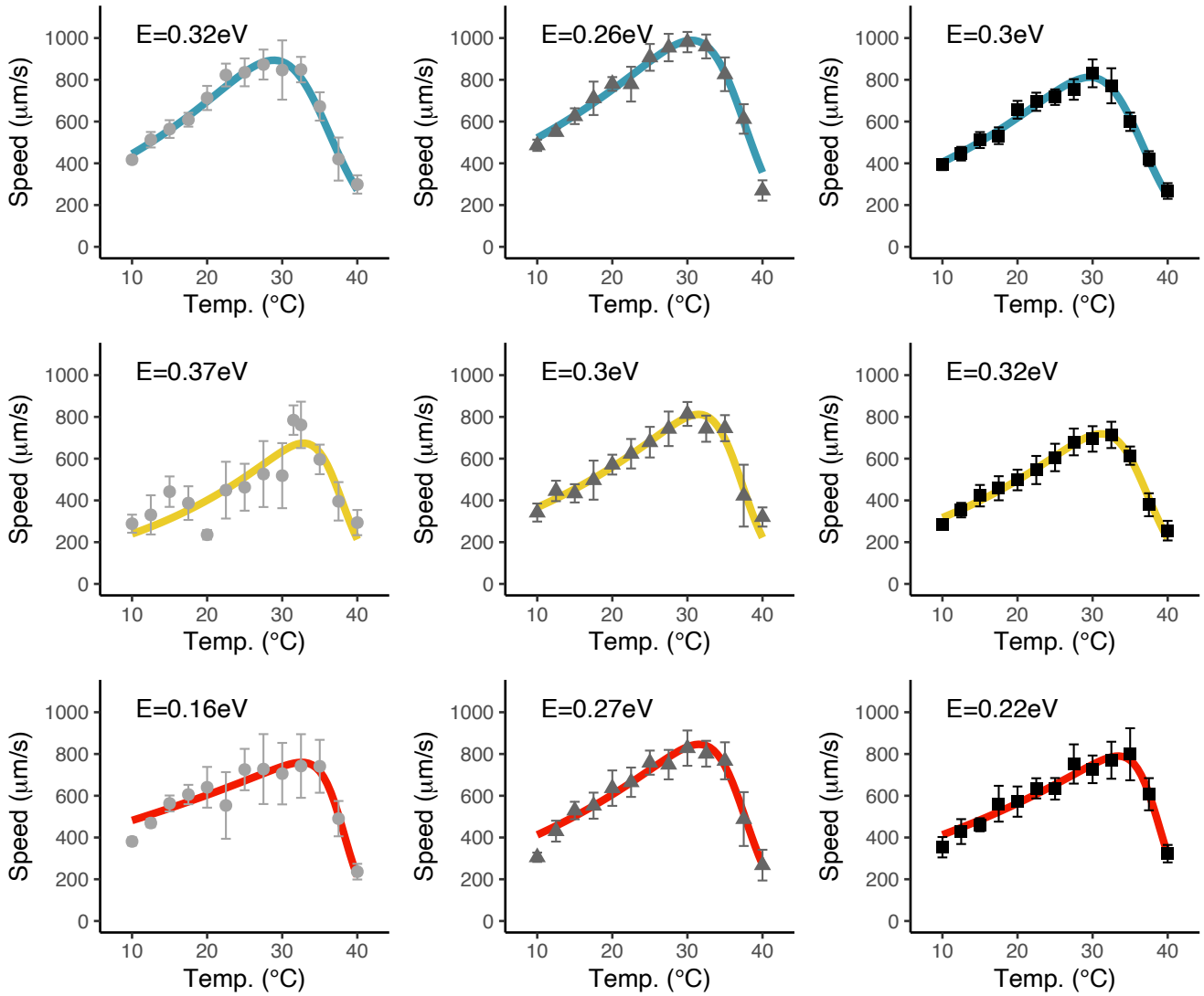

Figure S2.6: Thermal response curves for movement speed. The arrangement of panels and other details are the same as in figure S2.4. For each condition of adaptation temperature, medium concentration and tested temperature, we retain the 20% faster moving particles, and each marker in the figure represents the mean speed across all retained speed measurements for that condition (typically from two different replicates of the adaptation experiment). Error bars are ±1 standard deviation.

Table S2.2: Measured parameters of the thermal response curves for movement speed (short-term exposure). Values in brackets indicate the 95% confidence intervals obtained from a bootstrap procedure with resampling of the residuals.

Adaptation temperature	Medium concentration	Activation energy (eV)	Speed at reference temperature (μm/s)
15°C	50%	0.325 [0.309 - 0.342]	701 [693 - 709]
	100%	0.263 [0.248 - 0.278]	754 [745 - 762]
	200%	0.304 [0.286 - 0.324]	620 [614 - 627]
20°C	50%	0.368 [0.320 - 0.421]	401 [382 - 423]
	100%	0.304 [0.280 - 0.331]	560 [548 - 572]
	200%	0.322 [0.310 - 0.334]	498 [493 - 501]
25°C	50%	0.161 [0.136 - 0.187]	603 [589 - 618]
	100%	0.275 [0.260 - 0.291]	606 [597 - 612]
	200%	0.223 [0.210 - 0.236]	564 [557 - 570]

are also reported in table S2.2

Given that in these experiments we tested cells through a wide range of temperatures going up to 40 °C, we can also reliably estimate the optimal temperature for movement speed in each culture condition. This is shown in figure S2.7.

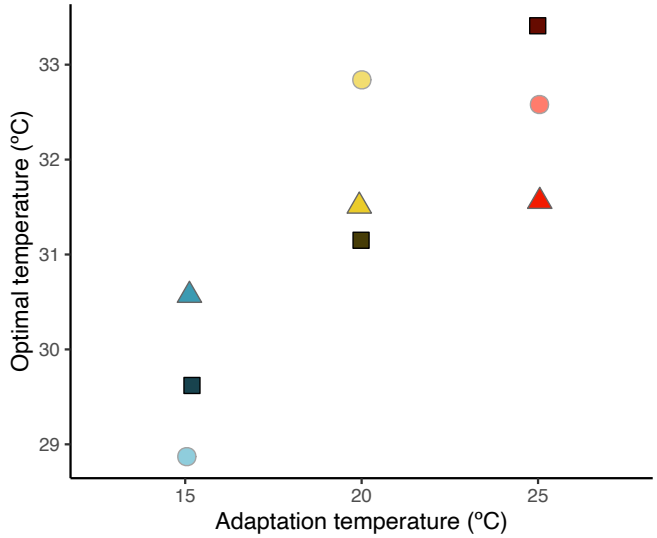

Figure S2.7: Optimal temperature for speed (temperature at which the movement speed reaches a maximum), as a function of the adaptation temperature. Circles: 50% medium, triangles: 100% medium, squares: 200% medium.

2.5 Thermal response curves for movement speed (long-term exposure)

Figure S2.8 reports the thermal response curves for movement speed under a long-term exposure (days) to the new temperature. In these conditions, an increased temperature only leads to a modest increase of movement speed.

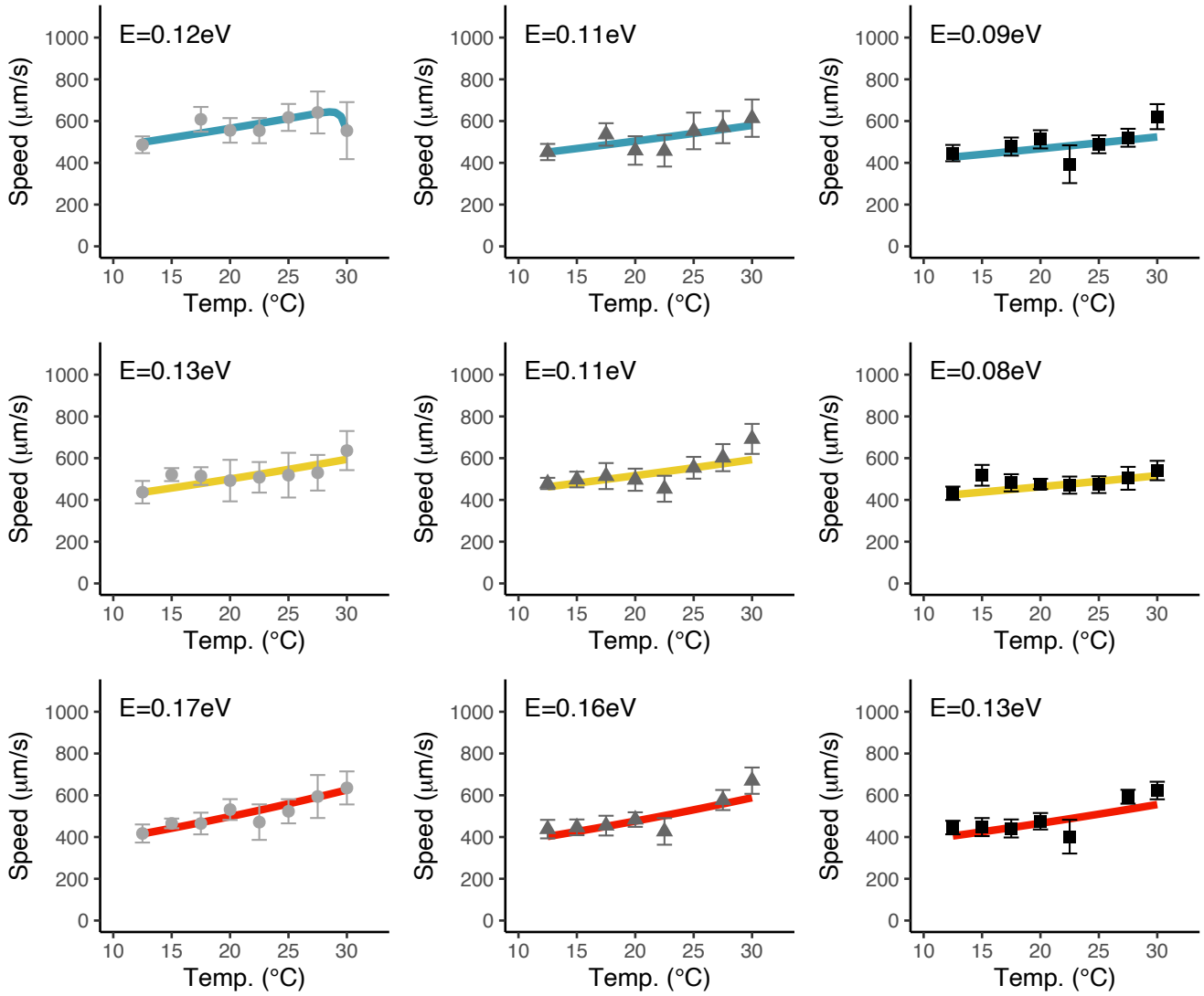

Figure S2.8: Thermal response curves for movement speed measured after a few generations of adaptation to the new temperature. Each panel corresponds to one adaptation condition. For each condition of adaptation temperature, medium concentration, and tested temperature, we retained the 20% faster moving particles. Markers represent the mean across all retained measurements of speed from all four replicates, and error bars are ± 1 standard deviation. Continuous lines represent fitted Sharpe-Schoolfield curves (rTPC package version). The text on each graph reports the value of activation energy E for the 'activation' part of the curve.

The fitted parameters of the thermal response curves are also reported in table S2.3, pointing to low values of activation energy (0.08 - 0.13 eV) and a slight decrease of movement speed with increasing medium concentration, at least at 15 and 25°C. Confidence intervals on the estimated parameters are small, but the effect size is also small (e.g. from 498 to 466 μm/s at 25°C), and for this reason we refrain from over-interpreting our results.

We also note here that a previous study on different ciliate species [*S5*] did not find a difference in activation energy for movement speed when measured in an 'acute response' or 'long-term response' for *Colpidium striatum*, and found an opposite effect (higher activation energy upon long-term exposure) on *Didinium nasutum*. Interestingly, their studied organisms did not change size with adaptation.

Table S2.3: Fitted parameters of the thermal response curves for movement speed measured after a few generations of adaptation to the new temperature. Values in brackets indicate the 95% confidence intervals obtained from a bootstrap procedure with resampling of the residuals.

Adaptation temperature	Medium concentration	Activation energy (eV)	Speed at reference temperature (μm/s)
15°C	50%	0.121 [0.113 - 0.128]	565 [562 - 568]
	100%	0.106 [0.103 - 0.111]	504 [503 - 506]
	200%	0.087 [0.082 - 0.093]	468 [466 - 470]
20°C	50%	0.132 [0.124 - 0.142]	500 [497 - 504]
	100%	0.106 [0.102 - 0.111]	516 [515 - 518]
	200%	0.083 [0.079 - 0.088]	463 [461 - 465]
25°C	50%	0.174 [0.168 - 0.183]	498 [495 - 501]
	100%	0.162 [0.157 - 0.167]	476 [475 - 479]
	200%	0.135 [0.128 - 0.143]	466 [464 - 469]

2.6 Thermal response curves for population growth

At the end of the adaptation process, each *Tetrahymena* culture was split into different flasks and transferred to temperatures ranging from 12.5 °C to 30 °C. Cells were then grown at the new temperature and *per capita* growth rates at the new temperature were measured by counting cells at 2 or 3 points in time and fitting an exponential growth function to the counted densities as a function of their respective times.

Figure S2.9 reports the thermal response curves for population growth measured in this way. The estimated values of activation energy for population growth ranged from 0.37 eV to 0.96 eV, and they did not show a clear pattern depending on the initial adaptation condition, except possibly for a slightly higher activation energy in cells that were originally adapted to high temperature. In practice, there was a relatively large variability in estimates of population growth, which is partly explained by concurrent adaptation of *Tetrahymena* to the growth conditions in which their thermal performance was measured. Measuring thermal response curves for population growth requires monitoring the growth of *Tetrahymena* cultures over multiple generations, a time span

over which cell had already started adapting to the new temperature conditions by changing, for instance, their movement speed (see fig. S2.8) and their cell volume (see below fig. S2.10). These adaptations likely meant that the population growth rate may also have changed throughout the measurement period. It is a known problem when studying thermal responses, particularly in small organisms with fast metabolic rate, that the studied organisms start acclimating or adapting to the growth conditions themselves in which they are being tested (as pointed out, for instance, in ref. [*S6*]).

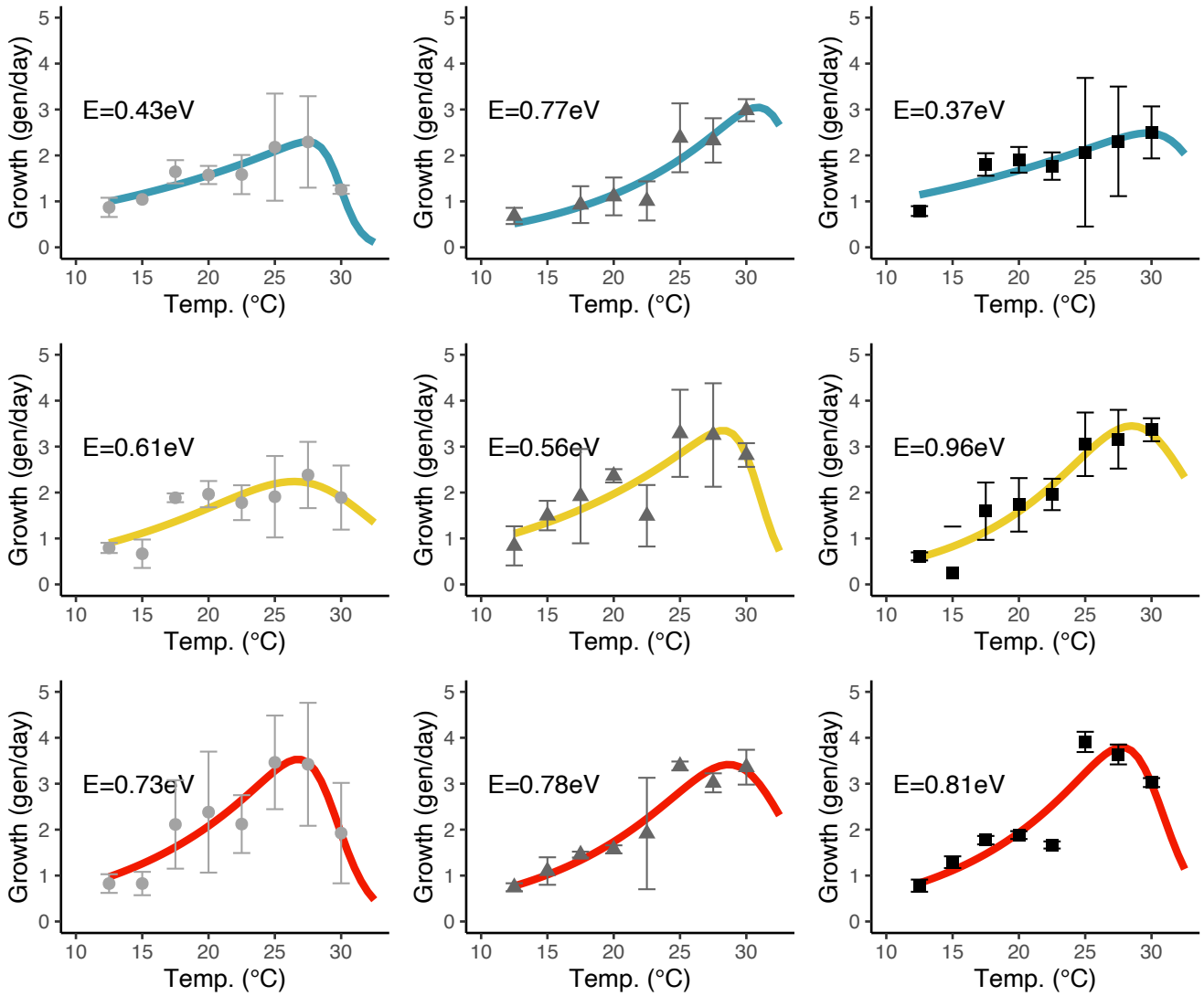

Figure S2.9: Thermal response curves for population growth measured after a few generations of adaptation to the new temperature. Each panel corresponds to one adaptation condition. Markers represent the mean across four replicates and error bars are ±1 standard deviation. Continuous lines represent fitted Sharpe-Schoolfield curves (rTPC package version). The text on each graph reports the value of activation energy E for the Arrhenius part of the curve.

2.7 Thermal response curves for cell volume (long-term exposure)

Cells moved to a different temperature started changing their volume relatively rapidly after they were moved to the new environment.

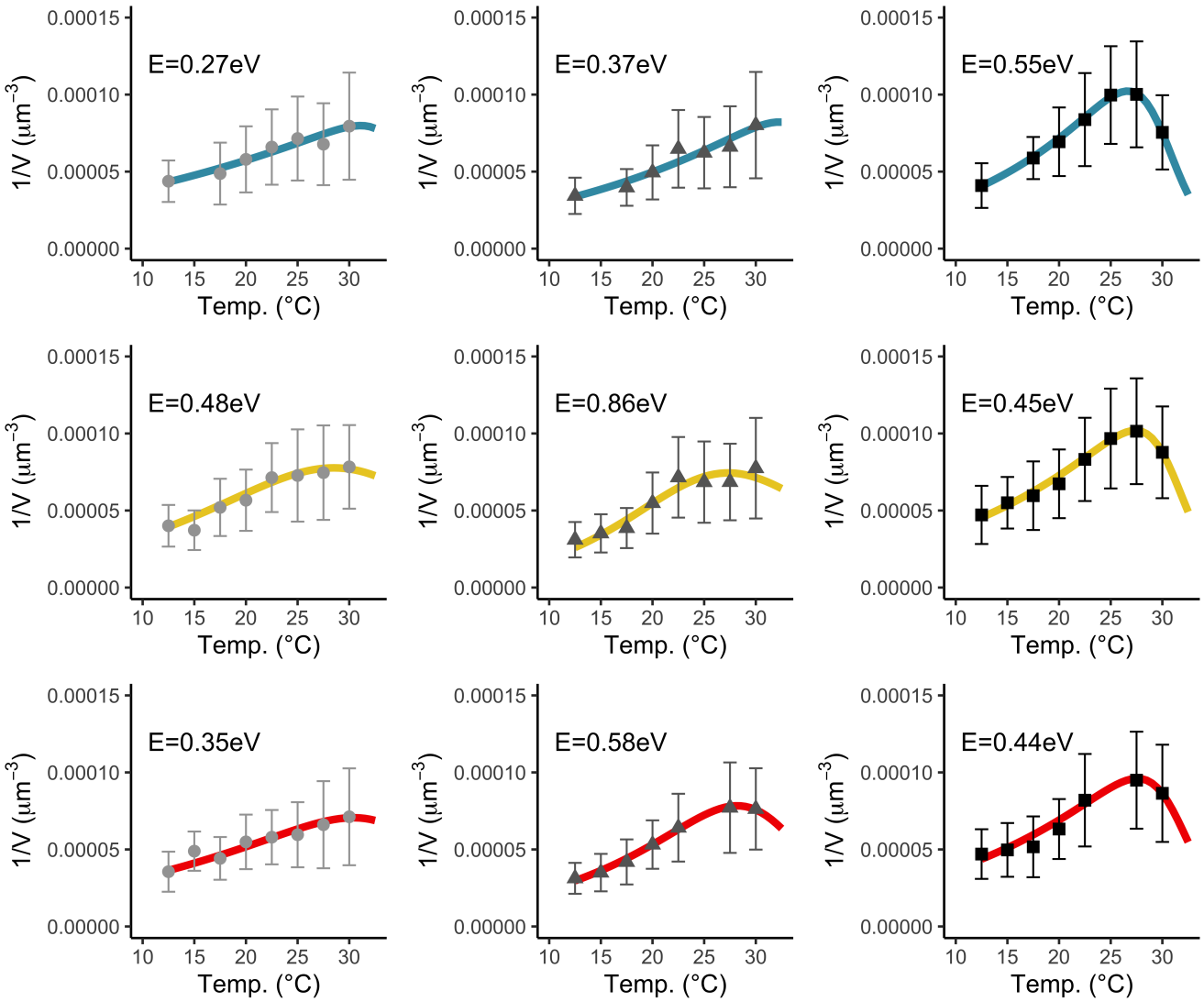

Figure S2.10: Thermal response curves for the reciprocal of cell volume. Each panel corresponds to one adaptation condition. Each data point in the figure represents the mean of $1/V$ (estimated by fitting ellipses on the 2D images of *Tetrahymena* and calculating the volume of the corresponding 3D spheroid) across all measured cells (where each cell is a "particle" in the video-tracking). Error bars are ± 1 standard deviation. Continuous lines represent fitted Sharpe-Schoolfield curves (rTPC package version). The text on each graph reports the value of activation energy E for the Arrhenius part of the curve.

These changes in volume are already well visible over the time scale used in the population growth experiments described above (sec. S2.6; see also below, sec. S2.11 for more details on the timescale of change).

Cell volume is affected by environmental temperature in the opposite way to how metabolic rate or movement speed change with temperature. In order to fit thermal performance curves to volume data in a similar way as for the other quantities, in figure S2.10 we report the thermal response curves for *the reciprocal* of cell volume ($1/V$).

2.8 Speed vs. medium concentration

While our experiments only focus on three possible values of growth medium concentration, we would like to report here also the results of two preliminary experiments aimed at testing how medium concentration modulated the movement speed, and population growth rate of *Tetrahymena*. These preliminary experiments were performed on different populations of the same strain of *Tetrahymena pyriformis* 1630/1W, obtained from the same supplier (CCAP).

In the first preliminary experiment we measured the movement speed of *Tetrahymena* adapted to a wide range of medium concentrations, including more diluted culture media than those used in our main experiment. Here we present the data, and in section S3.3 below, we will discuss these through some theoretical considerations. Figure S2.11 shows the movement speed of cells adapted to a new environment for a few days. Environments differed in temperature (15 °C, 20 °C, 25 °C) and in the concentration of culture medium, with a large number of concentrations used, ranging from 0% to 200%. The incubation period was different for each temperature to reach a similar number of cell generations: 1.9 days at 25 °C, 3 days at 20 °C and 7 days at 15 °C. The graphs show that, in all temperature conditions, speed was at a minimum when nutrients were almost absent from the culture medium, it reached a maximum for intermediate values of medium concentration, and then decreased slightly when the concentration of nutrients increased even further.

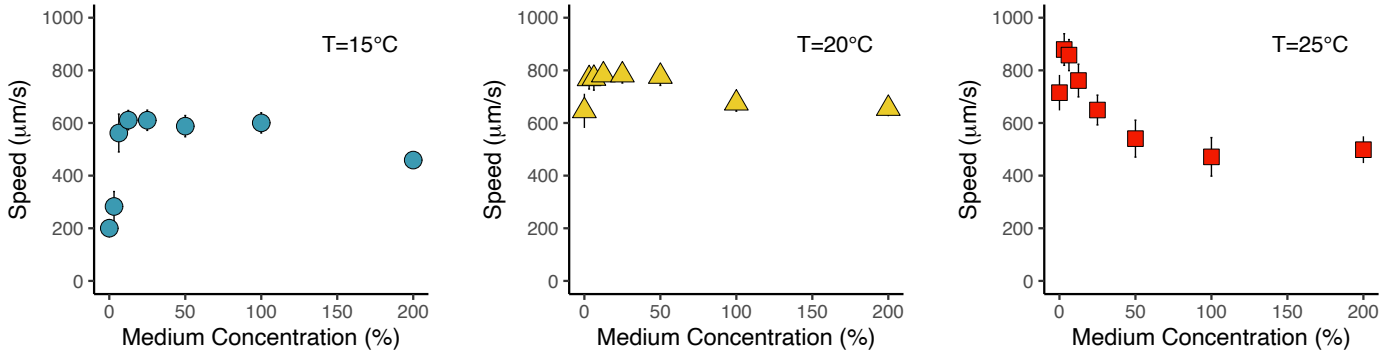

Figure S2.11: Results of a preliminary experiment looking at movement speed vs. the concentration of the culture medium. Each panel corresponds to one temperature condition. For each condition of medium concentration and tested temperature, we retain the 20% faster moving particles, and each data point in the figure represents the mean speed across all retained speed measurements for that condition. Markers represent the mean across all measured speed values from four replicates and error bars are ±1 standard deviation.

2.9 Effects of medium concentration on population growth

In a separate preliminary experiment, we tested how the concentration of the growth medium affected the population growth of *Tetrahymena*. To this end, an initial population of *Tetrahymena pyriformis*, strain 1630/1W, initially cultured at 20 °C and 100% culture medium (Proteose peptone - yeast extract) was split across a range of different culture conditions, with temperature ranging from 10 °C to 30 °C and culture medium concentration ranging from 0% (pure water) to 400% (4 times the density of standard growth medium). Cells were kept growing in the new condition, in three parallel replicate lines, for a variable number of days in order to approximately achieve a similar number of generations in each condition (ranging from 1.8 days at 30°C, to 7 days at 15°C and 8 days at 10°C); after this culture period, population densities were counted, and population growth rates were estimated.

Figure S2.12 reports the results of this experiment, showing that both temperature and growth medium concentration affect the growth rate of *Tetrahymena*. One possible way to model the effects of culture medium concentration on population growth is by fitting a Michaelis-Menten equation to the population growth data (inspired by ref. [*S7*]). Specifically, we modelled the *per capita* growth rate of *Tetrahymena* G as a function of medium concentration $[C]$ through the following equation:

$$G([C]) = \frac{v_{max}[C]}{K_m + [C]} - G_0, \tag{S1}$$

where v_{max} is the maximum growth rate, K_m is the concentration of growth medium at which *per capita* growth is $\frac{1}{2}v_{max}$, and G_0 is a mortality rate, introduced here to account for the expectation that, in the absence of nutrients, population growth should be negative.

This type of analysis confirms that temperature affects the maximum growth rate of *Tetrahymena* (with v_{max} being maximum at 25 °C), and that the growth rate of *Tetrahymena* is not strongly limited by the concentration of the growth medium in the range of concentrations used in our main experiment (values of K_m are small). The fact that *Tetrahymena* populations tested at 30 °C presented a negative value of parameter G_0 may seem puzzling upon first inspection (it is equivalent to saying that these populations experienced positive growth also in the limit of a complete absence of nutrients), but this observation is probably explained by the fact – also observed elsewhere in our study – that *Tetrahymena* cells undergo cellular divisions and reduce their cell volume when they are moved from a lower temperature (in this case the 20°C of the original culture) to a higher temperature (up to approximately 30°C). In other words, the negative value of G_0 probably describes a phenomenon of cell replication in the absence of additional *Tetrahymena* biomass production.

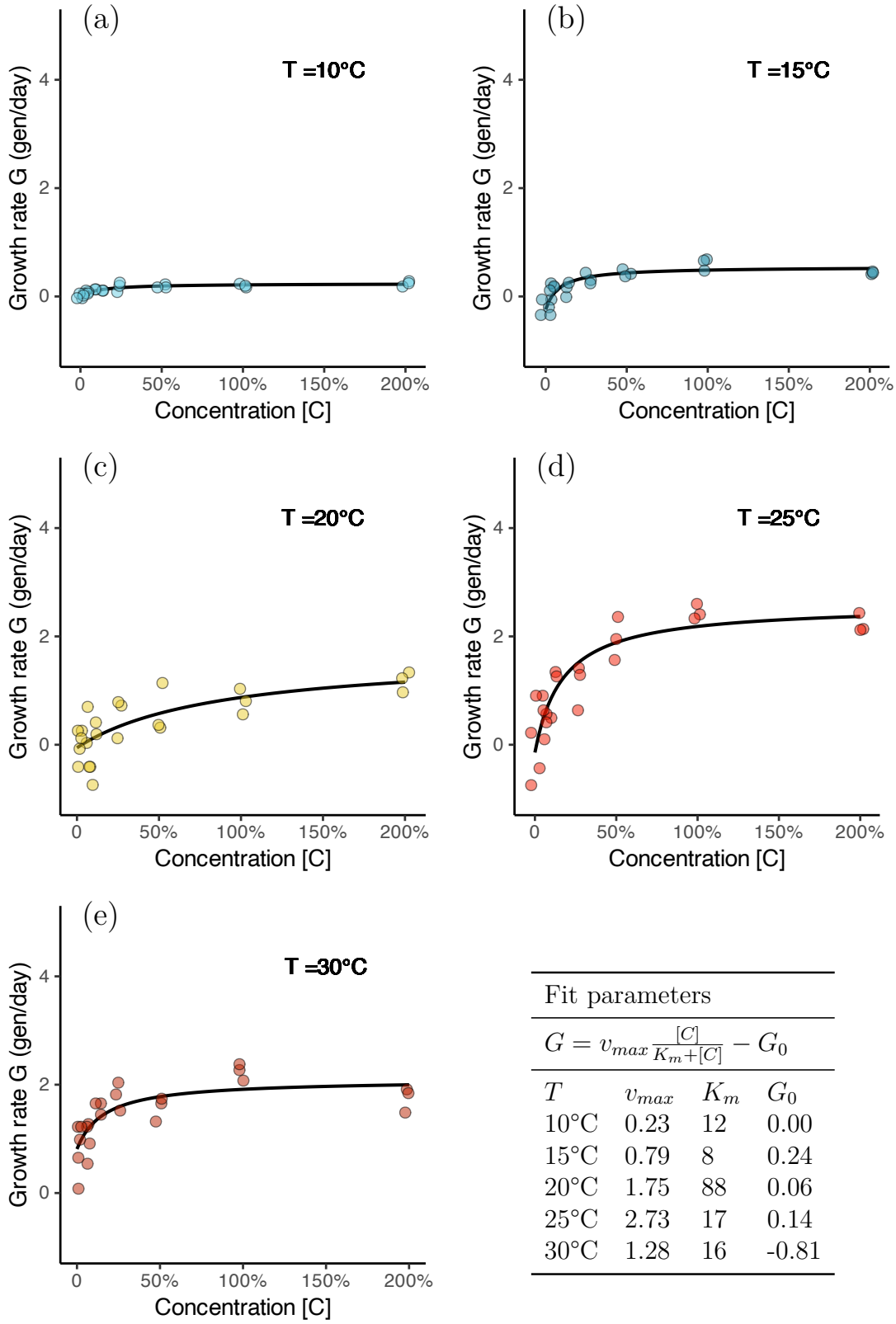

Fit parameters			
$G = v_{max}\frac{[C]}{K_m+[C]} - G_0$			
T	v_{max}	K_m	G_0
10°C	0.23	12	0.00
15°C	0.79	8	0.24
20°C	1.75	88	0.06
25°C	2.73	17	0.14
30°C	1.28	16	-0.81

Figure S2.12: Effect of medium concentration on population growth

2.10 Effects of oxygen concentration on cell size and shape

In our main experiment, we modulated the concentration of nutrients in the growth medium in order to study the adaptation of *Tetrahymena* to its environment. It is well known, however, that oxygen concentrations can play an important role in mediating the temperature-size rule of organisms (i.e. the variation in the typical body size of organisms which depends on the temperature of the environment in which they develop), as well as other adaptations (see e.g. [*S8*, *S9*, *S10*, *S11*, *S7*]).

Here, we report on a preliminary experiment in which we cultured axenic populations of the same strain of *Tetrahymena pyriformis* in an anoxic and in an hyperoxic environment for 15 days. Cells were cultured in standard 100% Proteose peptone – yeast extract medium in culture flasks as in other experiments that we describe. In this experiment, however, the flasks were stored in sealed boxes with an altered ratio of nitrogen and oxygen to reach approximately 50% of the standard oxygen concentration (in the anoxic treatment) or 200% (in the hyperoxic treatment). The boxes had to be opened every 2-3 days for subculturing *Tetrahymena* into fresh culture medium, and oxygen concentrations were rapidly restored after each subculture.

At the end of the adaptation treatment, we measured the size and shape of *Tetrahymena* cells from microscope images, obtaining the plots in figure S2.13. These plots confirm that cells cultured at low temperature were typically bigger than cells cultured at high temperature. In contrast, exposure to low or high oxygen concentration within the range 50% – 200% did not appear to have a strong effect on cell size and morphology.

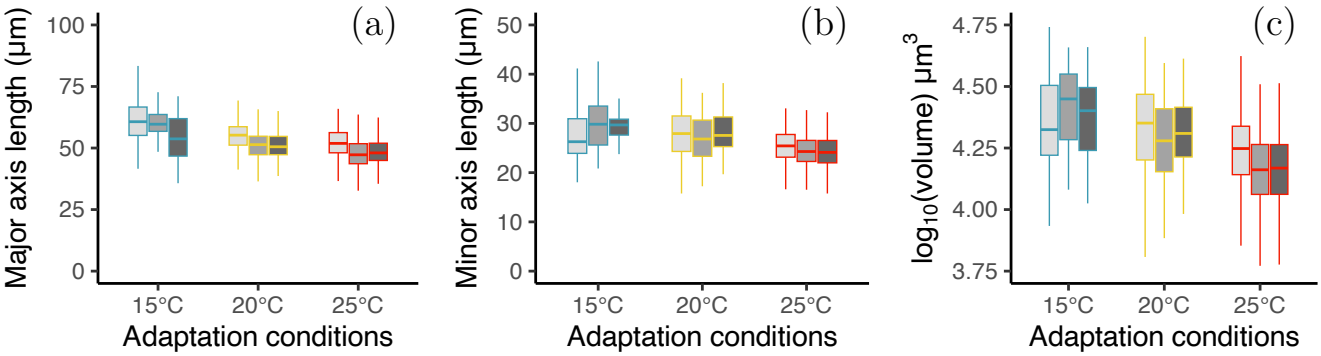

Figure S2.13: Effect of oxygen availability on cell size and shape. (a) Major axis length (approximately equivalent to cell length). (b) Minor axis length (cell width). (c) Cell volume. Light-shaded boxes indicate the anoxic treatment, middle boxes indicate normoxia, dark-shaded boxes indicate hyperoxia.

2.11 Phenotypic plasticity or evolutionary change?

Phenotypic plasticity and genetic change are the most important mechanisms that mediate how organisms adapt to a new environment. In this section, we first clarify our usage of relevant terms, and then we discuss the evidence from our experiment in support for each of the possible alternative mechanisms.

With the term *phenotypic plasticity* we refer to the ability of an organism to change its physiology, behaviour, or morphology in response to changes in the environment. In order to be considered phenotypic plasticity, these changes should happen within the scope of a same genotype (i.e. potentially they would be expressed also by clonally identical individuals). We further consider that the changes underlying phenotypic plasticity are produced as a result of the organism actively modulating its gene expression or its behaviour, rather than being passively affected by the physical properties of the environment.

In this respect, morphological or behavioural changes that are a *simple and direct consequence of the physical properties of the environment* are not considered to be examples of plasticity. For example, if the increased or decreased salinity of the aquatic medium affect the buoyancy of an organism, or if it changes the volume of the same organism through the action of osmotic pressure, we would not consider these changes to be indicative of phenotypic plasticity. Similarly, an aquatic microorganism whose swimming speed is reduced by an increase of viscosity of the medium in which it moves would not in itself denote plasticity. All these changes are driven by the physical properties of the environment and would happen also in simple non-living objects, such as floating or passively sinking sediment, semi-permeable membranes etc. Similarly, we do not consider to be the effect of phenotypic plasticity all the changes in metabolic rate and activity of organisms that are directly determined by changes of temperature through its effect on molecular diffusion and chemical reaction rates, as a plastic response by the organism only intervenes when the organism is able to actively modulate the value of activation energy and other parameters of its thermal response curves.

As a working hypothesis, the passive modulation of phenotypic traits by the environment could either increase or decrease the fitness of the organism, while phenotypic plasticity is – in general – expected to be adaptive (though see [*S4*] for a recent review covering also the adaptiveness of plastic responses), that is, to increase the fitness of the organism in the new environment. This is because active regulations of gene expression that have a negative effect on fitness are unlikely to be conserved through evolution (although – in practice – these effects on fitness may be difficult to measure directly).

Evolution is the change in the genetic composition of a population over time. Contemporary evolution, happening over ecologically relevant time scales of only a few generations is possible (reviewed in [*S12*]) and well-documented in empirical studies on *Tetrahymena* [*S13*]. Over such relatively short timescales, evolution is likely to be mediated by the selection of preexisting genetic variation rather than by *de novo* mutations, although new mutations are not excluded.

In ecological research, disentangling the effect of phenotypic plasticity from that of evolution can be challenging because both have similar effects and can happen concurrently. Plastic phenotypic changes can also be transmitted across generations through epigenetic mechanisms.

In relation specifically to our own study, we should also note that *Tetrahymena* is found across a very wide range of freshwater environments [*S14*] with variable amounts of nutrients, and with temperatures ranging from 4°C to 30°C (in fact, some natural populations likely experience on a seasonal basis temperature variations similar to those used in our study): for this reason, it is plausible that both the intrinsic genetic variation of *Tetrahymena* populations, and the regulatory patterns underlying phenotypic plasticity may be already aligned with the changes of environmental parameters that we impose in our experiments. As we did not sequence our cells, the main aspect that can give us an indication on the relative contribution of phenotypic plasticity and inherited variation (whether genetic or epigenetic) is the timescale over which the phenotypic changes that

we observe are produced. In particular, our measured thermal response curves for 'long-term' movement speed, for the changes in cell volume, and for population growth are likely to be the most informative. In these data – analogous to the way how genotype-specific reaction norms to the environment are usually quantified – cells from each of the nine conditions of adaptation (which would hence correspond to different adapted 'genotypes') are grown for a short period of time in a variety of different conditions (the 8 values of incubation temperature at which each adapted line was tested). After undergoing this treatment, when the cells are tested for the variables that we measure, if the thermal response curves from different adapted lines overlap, being identical to each other, we should conclude that the effect of genotypic differences between the different adapted conditions are negligible. Conversely, if all the curves are different for each adapted line, we can interpret this as the persistence of some genetic memory of the original adaptation condition that still continues after the environmental conditions have switched.

In our data, the measurements of long-term movement speed (figure 3, right column, in the main document, and SI figure S2.8 above) show very similar, overlapping, curves irrespective of the original adaptation condition (note that lines are adapted and tested at the same medium concentration, and so curves taken at different medium concentrations are not expected to overlap). This suggests that movement speed is adjusted rapidly, and could reflect phenotypic plasticity, rather than inherited differences between the adapted lines (the fact that these curves are almost flat, with values of activation energy in the range 0.08 to 0.17 eV, does not in itself exclude a role of plasticity because the null expectation here is that movement speed should increase with temperature, through the simple physical effect that temperature has on chemical metabolic reactions and on water viscosity, see also below section S3.2).

Measurements of cell volume (figure 4, right column, in the main document, and SI figure S2.10 above) also indicate a very strong modulation of cell size as a function of the temperature at which cells are tested: the thermal response curves are clearly not flat! (While here there isn't an expectation that temperature should affect cell volume through simple physical mechanisms, and cell volume remained stable – data not shown – when measured upon an acute exposure to various temperature conditions).In the case of cell volume, however, there isn't a complete overlap of the thermal response curves from different adaptation conditions. This could result simply from noisy data, or indicate persisting genetic differences between cells originating from the different adaptation conditions.

The data on population growth (figure 4, left column, in the main document, and SI figure S2.9 above) are perhaps the least informative about the relative contributions of phenotypic plasticity and evolution in shaping the adaptation of *Tetrahymena* in our experiment. This is because the measurement of population growth rates requires counting cell populations over at least two points in time (on two different days), meaning that fewer independent measurements are available, especially if we consider that the first measurement necessarily reflects the characteristics of the originally adapted population. These data point to some differences depending on the adaptation conditions (non-overlapping of thermal response curves), but for the issues that we just mentioned, we believe that the temporal component of how population growth changes over the few days following the change of environmental temperature cannot be neglected.

More generally, as all the data discussed here are integrated over a few days, we believe that it is instructive to look directly at the timescale of change for all the three variables considered: cell volume, movement speed, and population growth rate. This is what we do in the subsections below.

2.11.A Changes of cell volume were very rapid

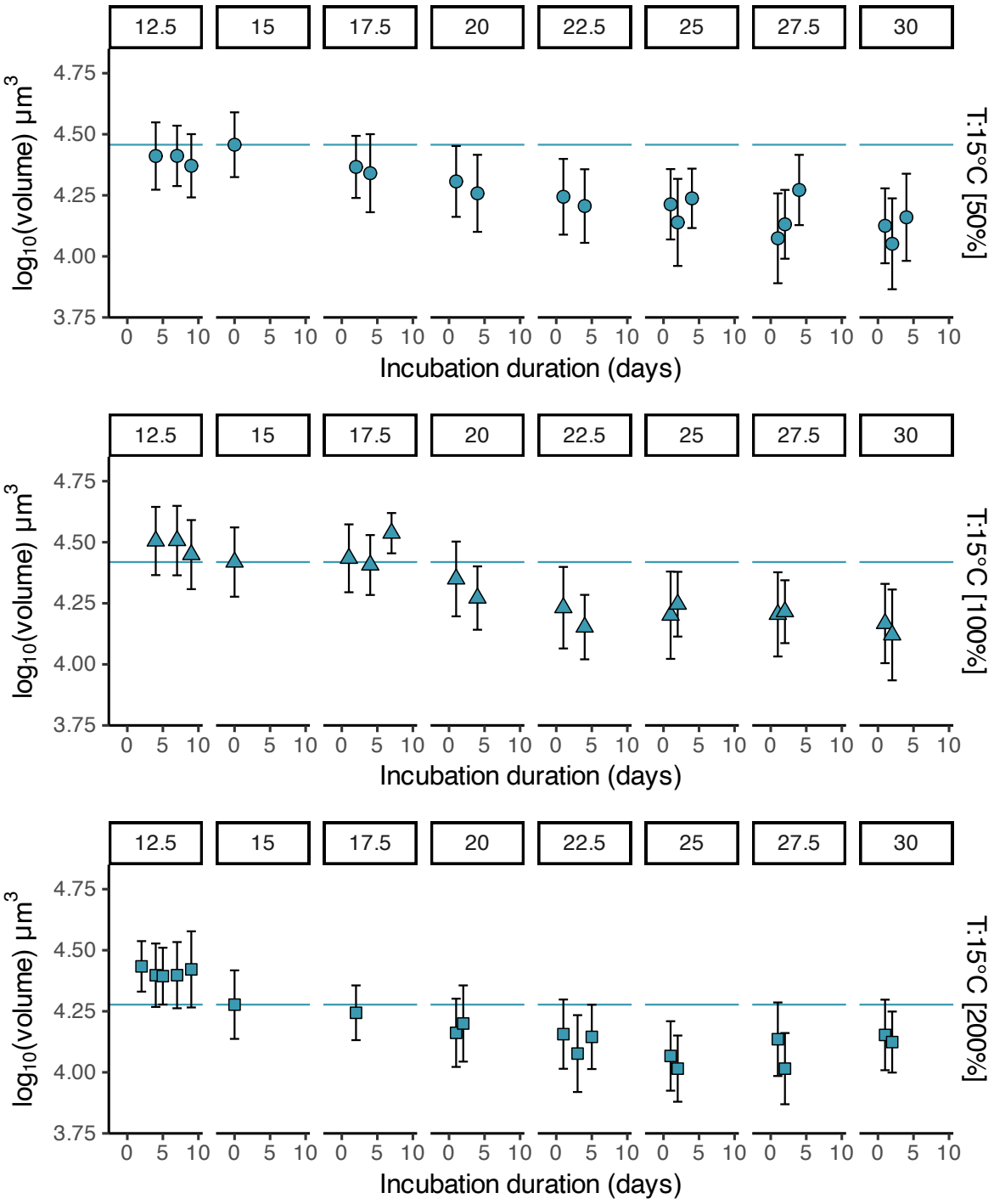

Figure S2.14: **Body size change over time – adaptation temperature 15 °C**. Rows correspond to different values of medium concentration; columns correspond to different test temperatures. Markers and errorbars indicate the mean ± standard deviation across all measurements on a given day of incubation; independent replicate lines were merged together. The blue lines indicate the mean volume of the original cell lines.

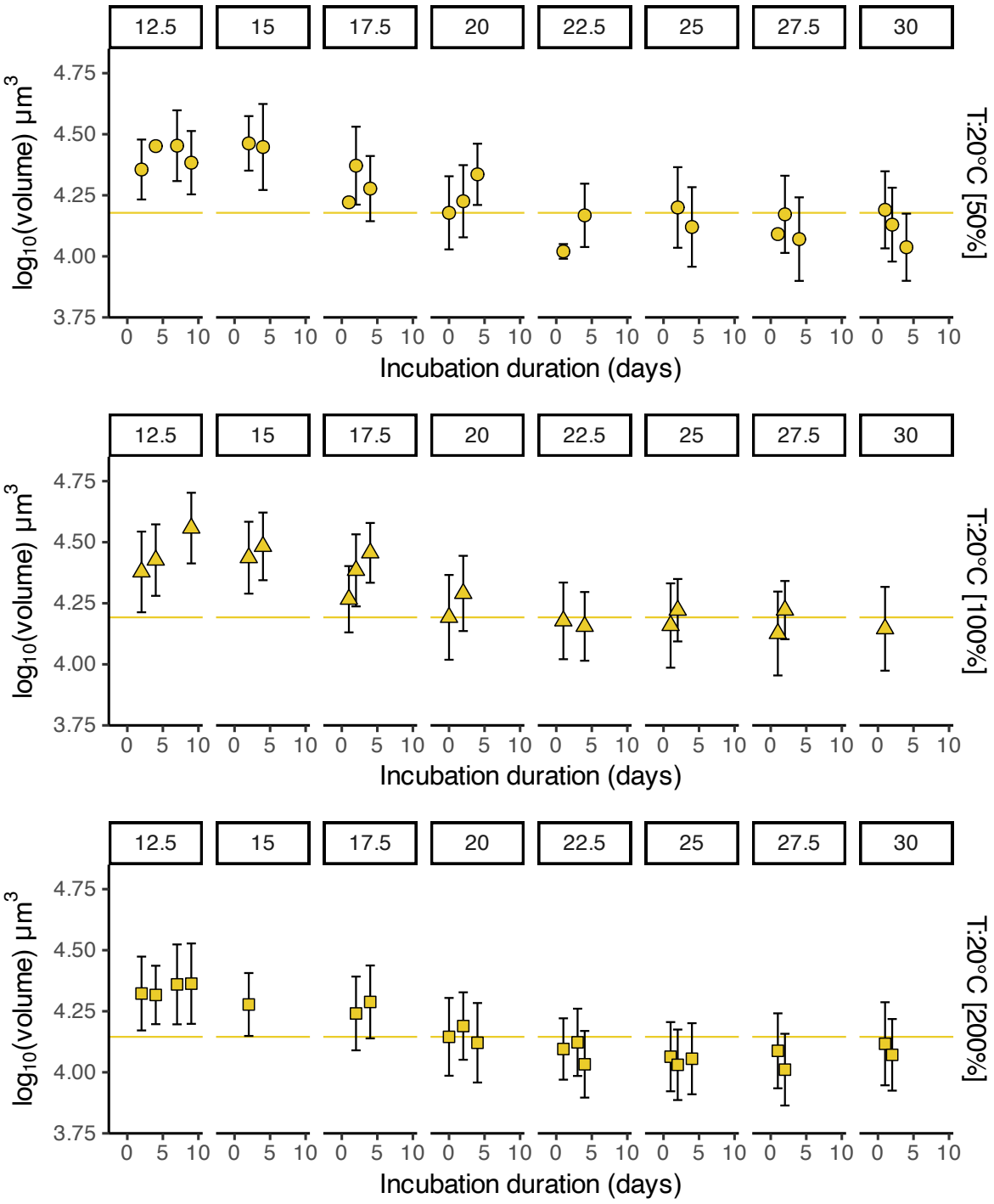

Figure S2.15: **Body size change over time – adaptation temperature 20 °C**. Rows correspond to different values of medium concentration; columns correspond to different test temperatures. Markers and errorbars indicate the mean ± standard deviation across all measurements on a given day of incubation; independent replicate lines were merged together. The yellow lines indicate the mean volume of the original cell lines.

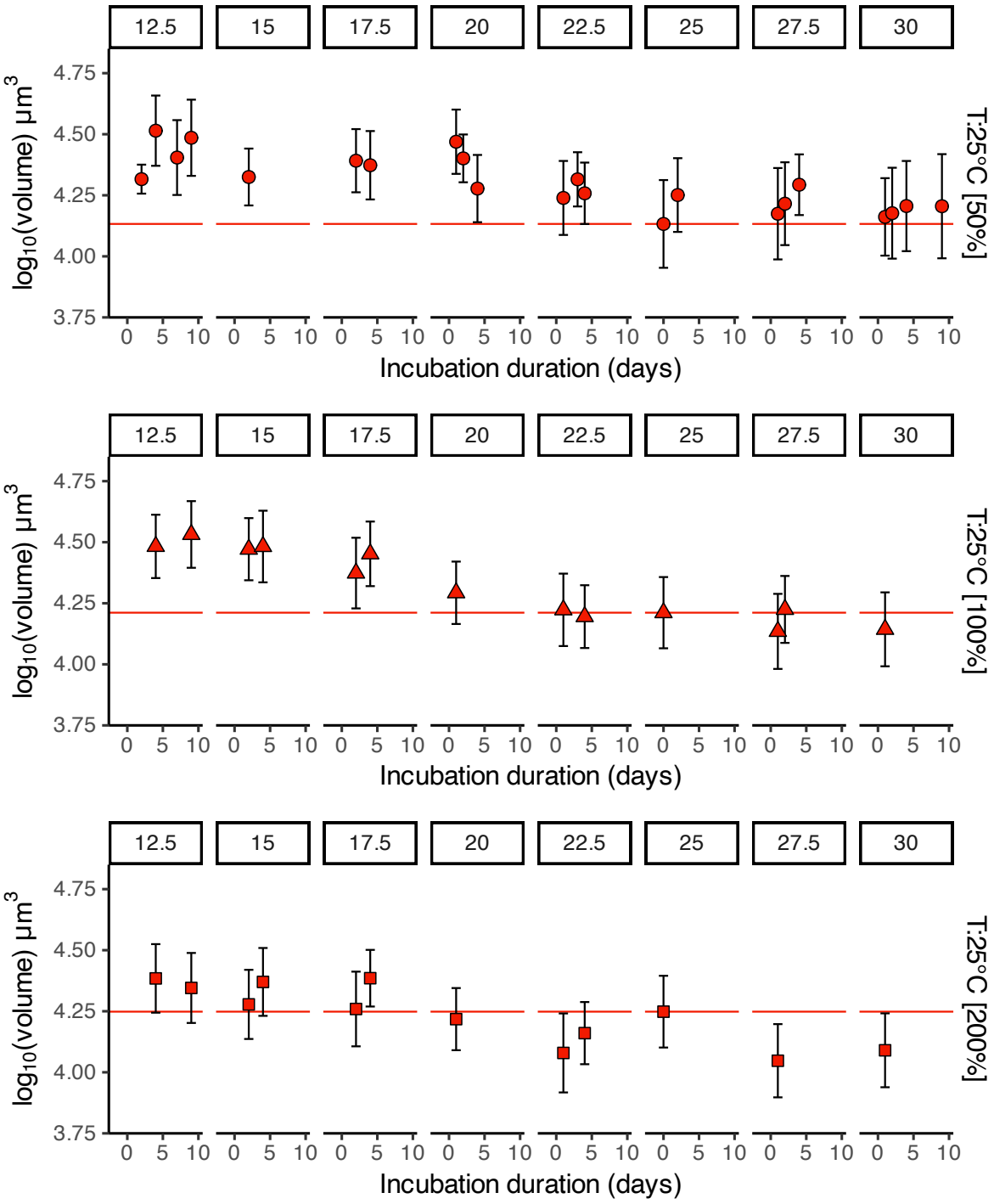

Figure S2.16: **Body size change over time – adaptation temperature 25 °C**. Rows correspond to different values of medium concentration; columns correspond to different test temperatures. Markers and errorbars indicate the mean ± standard deviation across all measurements on a given day of incubation; independent replicate lines were merged together. The red lines indicate the mean volume of the original cell lines.

Figures S2.14-S2.16 present a re-analysis of the data that describe the thermal response curve for cell volume (the curves presented in figure 4, right column, in the main document, and SI figure S2.10). To collect these data, cells from the nine adaptation conditions (3 × temperature and 3 × medium concentration) were moved to a different temperature condition (in the range 12.5 - 30°C). Cell volume was measured repeatedly on different days after the transfer to the new temperature, and the re-analysis presented here reports the mean and standard deviation of volumes measured on each day. The baselines indicated by flat horizontal lines mark the starting volume in each condition (the volume of cells in the adapted culture before they were transferred to the new temperature conditions).

In the figures we can see that the volume measured in each condition deviated from the baseline (with typically larger cells at low temperature and smaller cells at high temperature). However, measurements over different days were similar to each other, indicating that the change of volume from the baseline to the observed value was produced very rapidly, already before the first measurement at the new temperature was taken, and potentially already at the first cell division after exposure to the new temperature. In fact, we can anecdotally report that when we took cells cultured at low temperature (i.e. 10 - 15 °C) out of the incubator and left them at room temperature for various tests and observations, we frequently observed cells undergoing mitosis during the first few hours that followed the change of temperature (while dividing cells were rare when the cultures originated from a higher than room-temperature incubator). These observations suggest that cell size regulation might be triggered very soon after the change of temperature, and operate within the first few hours. Unfortunately, we did not characterise this phenomenon in detail, e.g. by measuring cell volume and the proportion of cells undergoing mitosis at short regular intervals after the change of temperature: this is something that could be explored in more detail in a future study.

2.11.B Speed changed rapidly after the transfer to the new temperature condition and remained stable afterwards

Figures S2.17-S2.19 present a re-analysis of the data that describe the thermal response curve for 'long-term' movement speed (the curves presented in figure 3, right column, in the main document, and SI figure S2.8). To collect these data, cells from the nine adaptation conditions (3 × temperature and 3 × medium concentration) were moved to a different temperature condition (in the range 12.5 - 30°C). Movement speed was measured repeatedly on different days after the transfer to the new temperature, and the re-analysis presented here reports the mean and standard deviation of speed measured on each day (note that, as in all other measurement of speed, the speed values that we report are those from the 20% fastest moving cells, to avoid counting cells that might have been stuck against the microscope slide). The baselines indicated by flat horizontal lines mark the speed value in the acute speed response (analogous to the speed that would have been measured at the beginning of this long-term speed response). Measurements of speed deviated from those recorded during the acute responses, but measurements taken on different days remained similar to each other, suggesting that speed changed rapidly, already before the first 'long-term' speed measurement at the new temperature was taken.

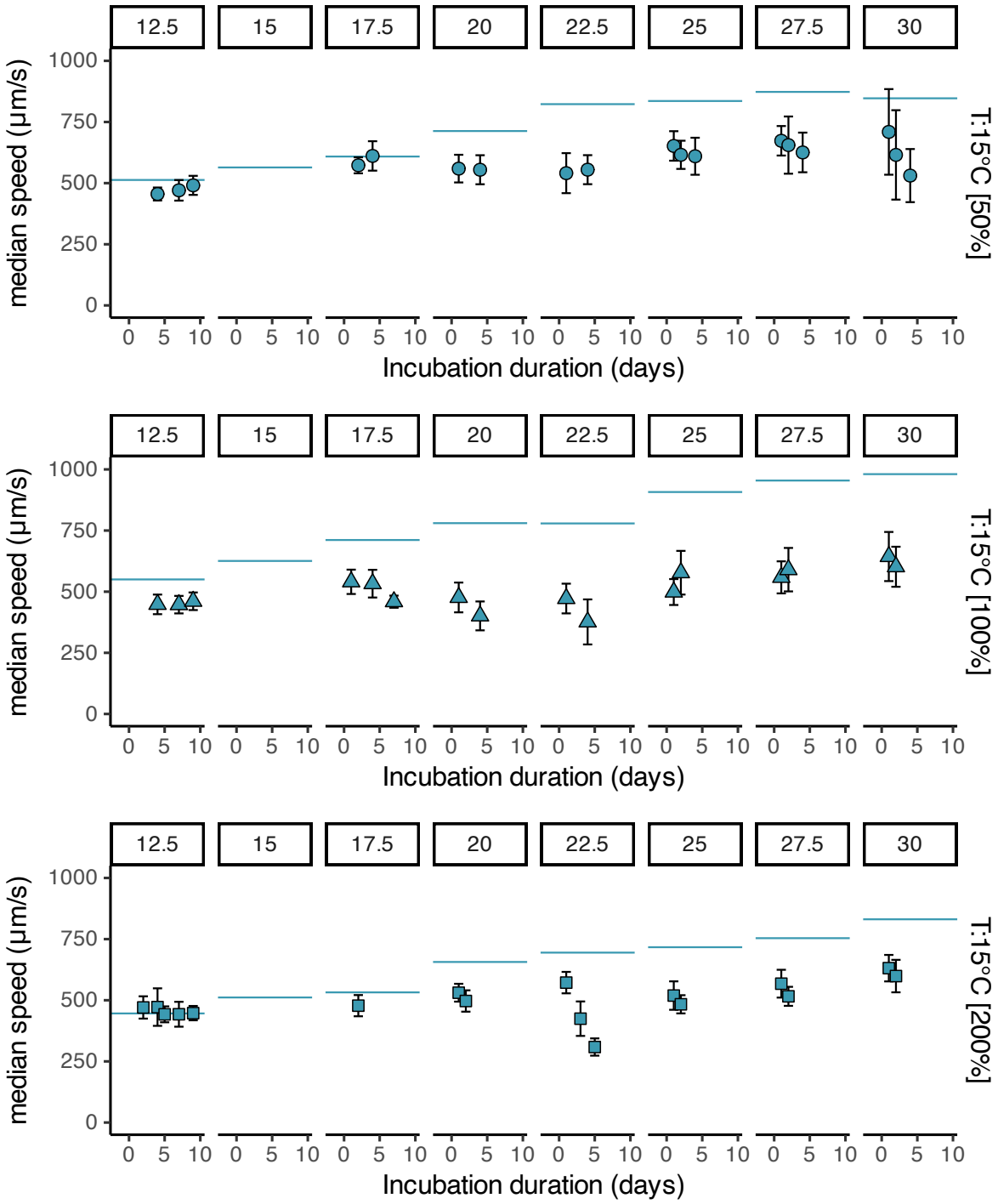

Figure S2.17: **Speed change over time – adaptation temperature 15 °C**. Rows correspond to different values of medium concentration; columns correspond to different test temperatures. Markers and errorbars indicate the mean ± standard deviation across all measurements on a given day of incubation; independent replicate lines were merged together. The blue lines indicate the mean speed value in the acute speed response (analogous to the speed that would have been measured at the beginning of this long-term speed response).

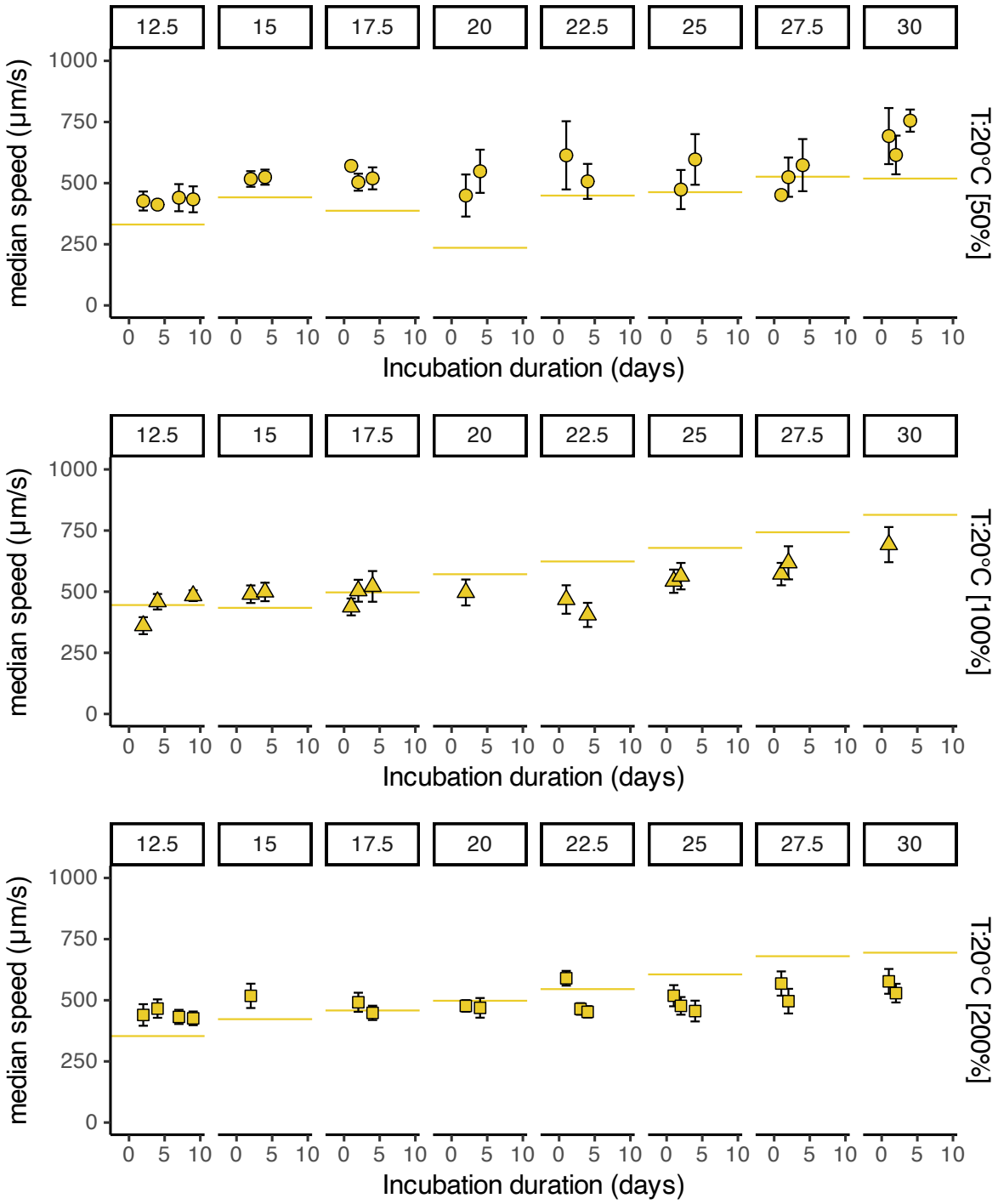

Figure S2.18: **Speed change over time – adaptation temperature 20 °C**. Rows correspond to different values of medium concentration; columns correspond to different test temperatures. Markers and errorbars indicate the mean ± standard deviation across all measurements on a given day of incubation; independent replicate lines were merged together. The yellow lines indicate the mean speed value in the acute speed response (analogous to the speed that would have been measured at the beginning of this long-term speed response).

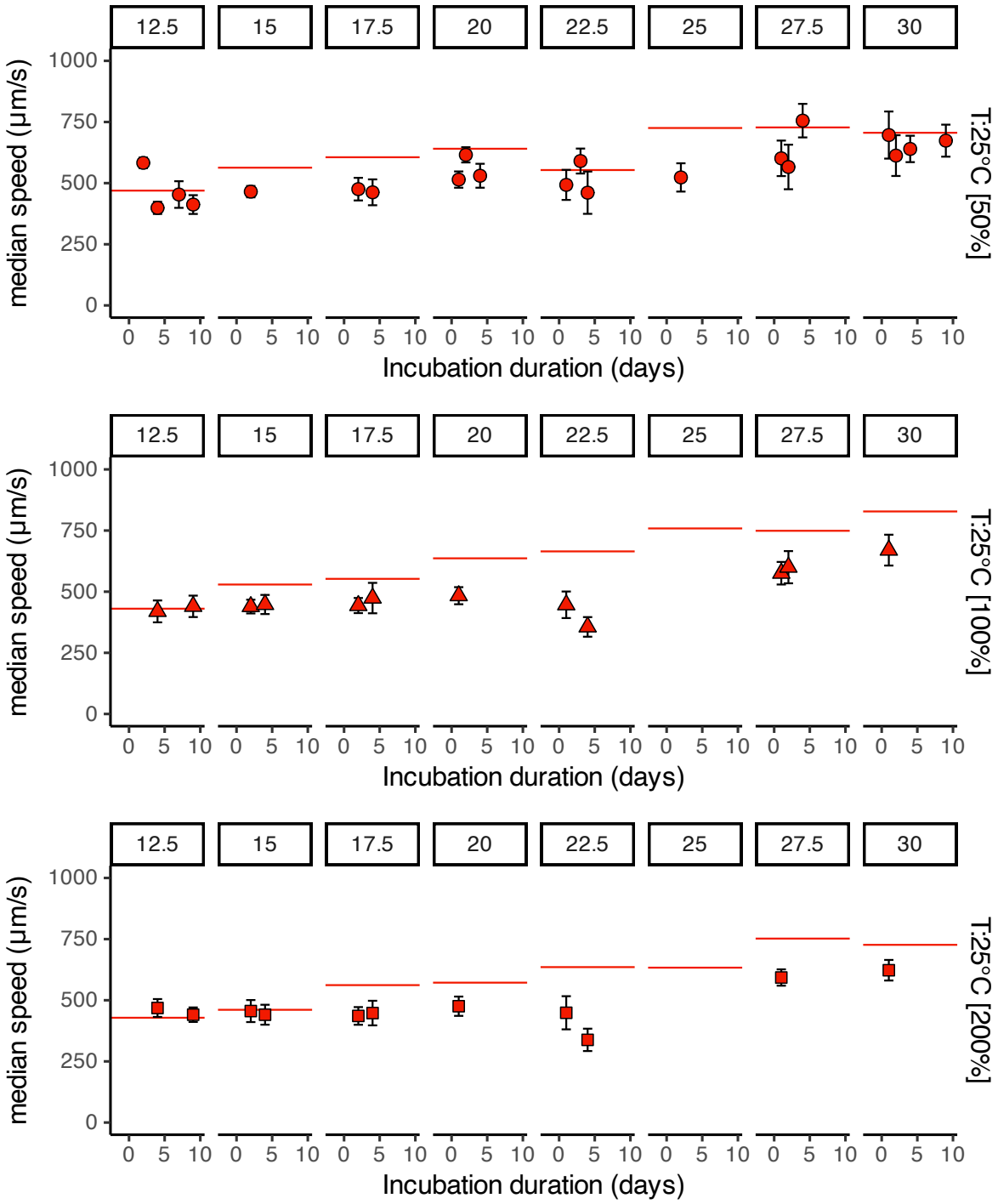

Figure S2.19: **Speed change over time – adaptation temperature 25 °C**. Rows correspond to different values of medium concentration; columns correspond to different test temperatures. Markers and errorbars indicate the mean ± standard deviation across all measurements on a given day of incubation; independent replicate lines were merged together. The red lines indicate the mean speed value in the acute speed response (analogous to the speed that would have been measured at the beginning of this long-term speed response).

2.11.C Effects of changes of temperature on population growth rates

Figures S2.20-S2.22 present a re-analysis of the data that describe the thermal response curve for population growth (the curves presented in figure 4, left column, in the main document, and SI figure S2.9). This analysis essentially breaks down the estimates of population growth rate presented in figure S2.9 by individual measurements of growth rate in-between pairs of population density counts.

Before we interpret these figures, we should make a few important caveats. Movement speed and cell volume can be measured independently for each cell, and the measurements can then be averaged over large numbers of cells. In addition, each measurement of speed and volume is collected on a single day, and it is largely unaffected by the measurements taken on the previous and following days. The same does not happen with measurements of population growth rates. Population growth rates are measured from multiple population-level counts taken on different days. For this reason, measurements of population growth rates are intrinsically noisier than measurements of speed and cell volume. This is because only one value of density is measured for each population (compared to the several independent measurements of movement speed for each cell in the population), and because two population counts need to be compared over time to produce a single estimate of population growth rate.

Growth rates measured at different times are not independent from each other: a higher (or lower) population count on one day would lead simultaneously to an overestimate (underestimate) of population growth in the previous time interval, and to an underestimate (overestimate) in the subsequent time interval. This is expected to amplify differences between data points, making them 'jump' up and down more when the value of population growth is measured from only two counts, rather than being fitted across several independent daily counts. Finally, the measurements of population growth are also not entirely independent across different temperature conditions because, for instance, the count of density of the starting population affects all the measurements of population growth for cultures originating from that experimental condition and subsequently tested across the entire range of temperature conditions.

Having acknowledged these limitations, we can attempt an interpretation of the results presented in figures S2.20-S2.22. The first data point in each time series corresponds to the growth between the start of the subculture at day 0, and the first population count in the new conditions, on the day indicated in the abscissa. In the cold-adapted lines (fig. S2.20) this first data point tends to be higher than subsequent recordings. If we consider this initial transient increase in *per capita* growth rate in the context of the analogous result on cell volume (fig. S2.14), which showed that cell volume of cold adapted cells decreased rapidly during this same time interval, we can conclude that this transient increase in cell division rate was associated with the reduction in individual cell volume, rather than with an increase in biomass production at the new temperature. Measurements of growth rate for cells initially adapted at higher temperature (20 and 25 °C, figs. S2.21 and S2.22) are noisy for the reasons explained above, but they are difficult to interpret in terms of a temporal variation in *per capita* growth rate.

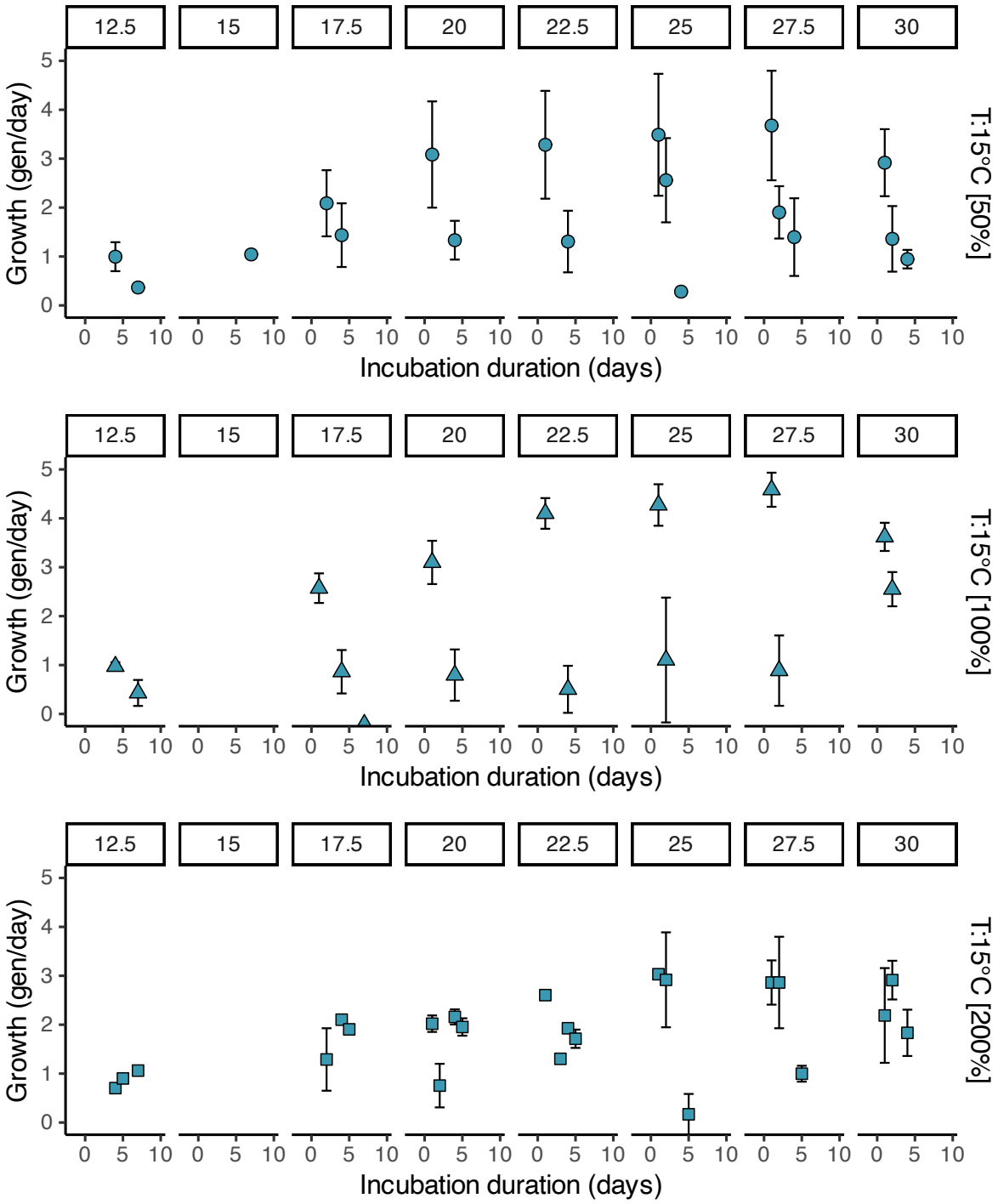

Figure S2.20: **Growth rate change over time – adaptation temperature 15 °C**. Estimated growth rate of cells adapted at 15°C and various nutrient concentrations during the first few days after they had been transferred to a different temperature (in the range 12.5 - 30°C). Markers represent the mean population growth rate across replicate lines, measured between the previous count and the time indicated the x axis, and errorbars represent the standard deviation across replicate lines (but note that the number of replicates is small, and errors are not independent).

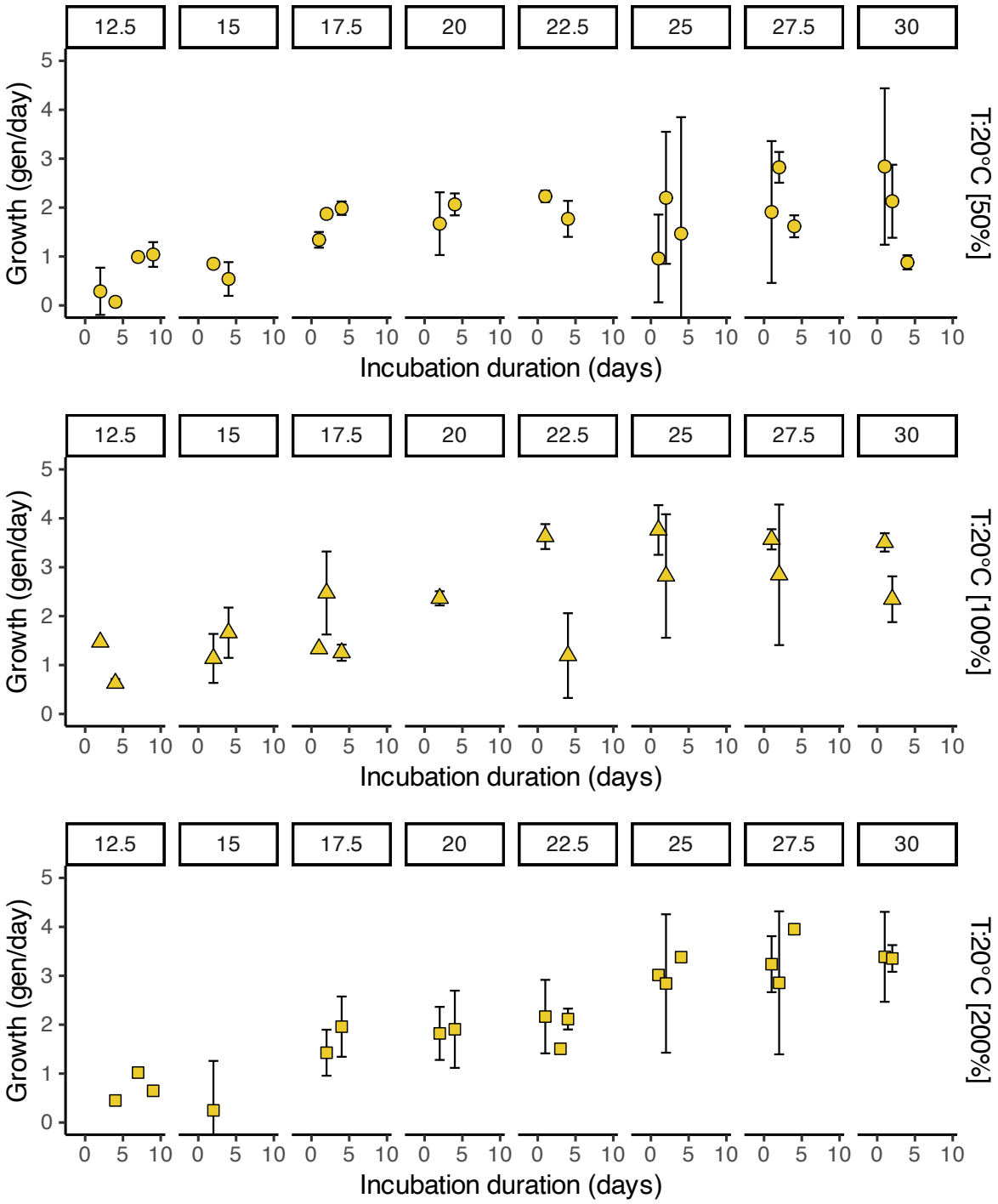

Figure S2.21: **Growth rate change over time – adaptation temperature 20 °C**. Estimated growth rate of cells adapted at 20°C and various nutrient concentrations during the first few days after they had been transferred to a different temperature (in the range 12.5 - 30°C). Markers represent the mean population growth rate across replicate lines, measured between the previous count and the time indicated the x axis, and errorbars represent the standard deviation across replicate lines (but note that the number of replicates is small, and errors are not independent).

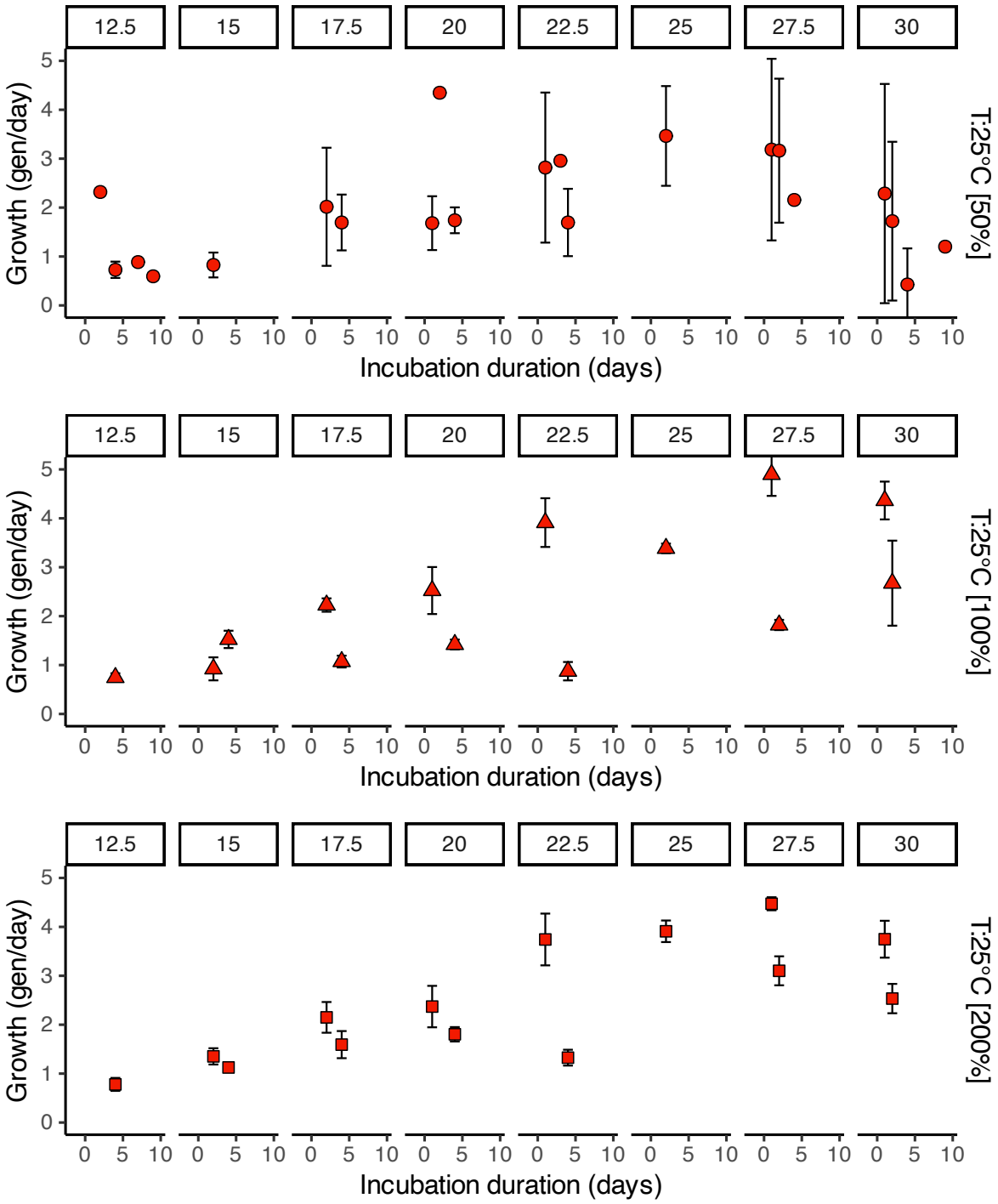

Figure S2.22: **Growth rate change over time – adaptation temperature 25 °C**. Estimated growth rate of cells adapted at 25°C and various nutrient concentrations during the first few days after they had been transferred to a different temperature (in the range 12.5 - 30°C). Markers represent the mean population growth rate across replicate lines, measured between the previous count and the time indicated the x axis, and errorbars represent the standard deviation across replicate lines (but note that the number of replicates is small, and errors are not independent).

2.12 Impact of cell volume on metabolic rate and speed

Larger organisms move typically faster than smaller ones. They also have a faster *per capita* metabolic rate, simply because they are bigger. The observation that, in our experiments, *Tetrahymena* cells changed their volume rapidly and substantially, depending on the experimental conditions, begs the question: to what extent do the observed changes in cell volume alone account for the other observed changes in metabolic rate and movement speed?

To understand the relation between cell volume and speed, we can consider the example of an isogeometric unicellular organism: its metabolic rate – and total available power – would scale as the volume of the cell, or as the third power of the linear dimension (assuming a linear scaling between metabolic rate and cell volume in unicellular eukaryotes [*S15*]), and this metabolic power would have a positive impact on speed; the viscous drag would scale as the linear dimension (having negative impact on speed; the mathematical formulas behind all these statements are given below, in section S3). If we further assume that this isogeometric organism is also allocating a constant proportion of its metabolic energy to fuel its movement, we have that speed U depends on the power P invested into movement as $P = sU^2$ (see SI equation S4), where P itself is proportional to the volume V of the cell ($P \propto V$), and s is proportional to the linear dimension ($s \propto V^{1/3}$). Based on this, we would predict that the movement speed U should scale as the linear dimension of the cell: $U \propto V^{\alpha}$ with $\alpha = 1/3$. (If, instead of assuming a linear scaling of metabolic rate with cell volume we assumed a 3/4 power scaling as in Kleiber's law, the same reasoning would lead to a predicted relationship between movement speed and cell volume as $U \propto V^{\alpha}$, with $\alpha = 5/24$).

Based on these scaling arguments, we could predict that a change by a factor 2 in the cell volume would translate into a factor $2^{1/3} \simeq 1.26$ in the change of speed (or $2^{5/24} \simeq 1.16$ if we assumed a 3/4 power scaling of metabolic rate with cell volume).

Inevitably, this isogeometric unicellular organism is only a very crude approximation of our *Tetrahymena*, and among its limitations we could mention that the beating cilia themselves responsible for cell propulsion cover the surface of the cell, and their number would scale as the square of the linear cell dimension, possibly affecting the fraction of metabolic energy allocated to movement. The assumption that a constant proportion of metabolic energy is spent for fuelling movement is probably also simplistic. Nevertheless, we believe that the scaling arguments presented above are a good starting point against which the empirical data can be compared, and more refined models could eventually be formulated. Hence, let's have a closer look at the scaling relations that we can observe empirically from our own data.

One way how we can test the relationship between movement speed and cell volume, excluding the effect of other variables, is by exploiting the intrinsic variability of cell sizes in our experimental populations: in each culture condition there were smaller and larger cells – partly related to their stage of growth in-between mitotic divisions – which were otherwise all exposed to identical culture conditions. To do this, we re-analyzed the data that are summarized in each data point of figure S2.6 by plotting the logarithm of movement speed as a function of the logarithm of cell volume. We excluded from this re-analysis data in which cells were tested in the deactivation part of their thermal performance curve (i.e. at 32.5 °C or higher temperature) because we were concerned about possible confounding interactions between cell size, shape, metabolic rate and speed (for example, we anecdotally observed that cells exposed to temperatures higher than 30 °C changed their shape as an acute response to temperature), and for even higher temperatures of 37.5 or 40 °C speed was not even constant over time (figure S1.2).

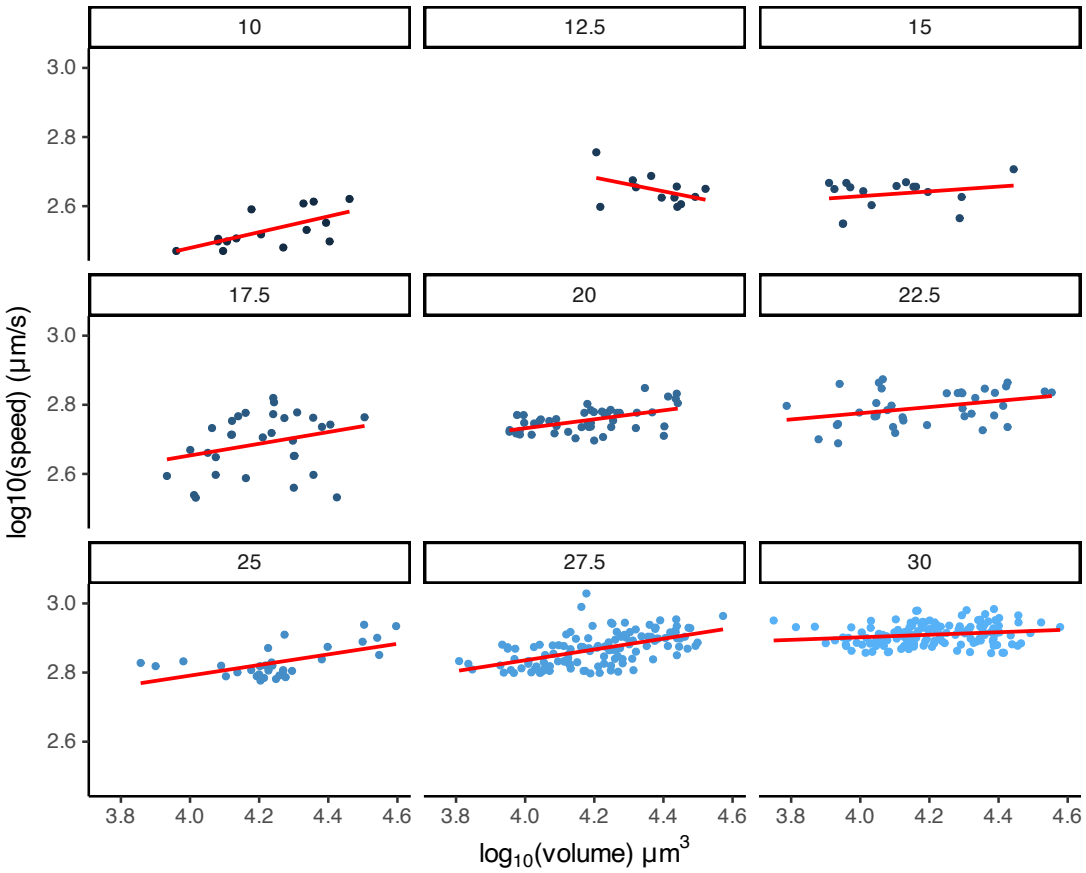

Figure S2.23: Cell speed as a function of cell volume for cells adapted at 20°C and 100% medium concentration.

Figure S2.23 presents an example of the plots resulting from this re-analysis, by showing the speed-volume relationship for cells adapted at 20 °C and 100% medium concentration, for each value of temperature at which they are tested (i.e. for the data in fig. S2.6, middle panel). The curves depict a generally positive trend of increasing speed with increasing cell volume. The slopes of $\log U = \alpha \log V + K$ fitted in a least squares sense across all the 81 conditions that correspond to the activation part of the *Tetrahymena* thermal response curve gave a value of $\alpha = 0.36 \pm 0.12$ (mean $\pm$ s.e.), not dissimilar from the theoretically predicted value $\alpha = 1/3$.

Given that cells in the nine adapted conditions differed in their typical cell volume (figure 2(c) in the main text), and also by their movement speed and metabolic rate when they were all tested at the same reference temperature of 20 °C (figure 3, middle row, left and central column, in the main text), it is interesting to verify to what extent the change of cell volume alone accounted for the observed changes in respiration, and in movement speed, based on a hypothesized increase of respiration linearly with cell volume $B \propto V$ and on a scaling of movement speed proportional to the linear cell dimension $U \propto V^{1/3}$. The relationships between respiration rate and cell volume, and between movement speed and cell volume are presented in figure S2.24.

The theoretically predicted relations (black lines in the figure) provide a reasonably good fit through most data points, showing that cell volume is a good explanatory variable also for res-

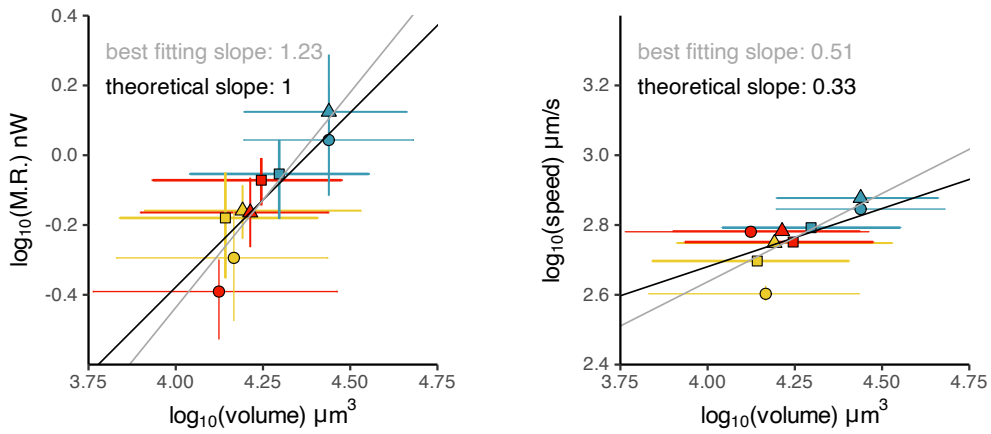

Figure S2.24: **Left:** Logarithm of metabolic rate measured at the reference temperature vs. logarithm of cell volume in the nine adapted *Tetrahymena* cell lines. If the changes in cell volume was the only way how cells adapted to their new environment, without any additional

piration rate and movement speed. However, the best fitting curves (grey lines in the figure) are steeper, indicating that volume alone does not account for all the variation in metabolic rate and movement speed. The fact that the best fitting curves are only fitted in a least square sense on the nine data points, ignoring the errors – which are especially pronounced along the x axis – does not change this conclusion: fitting techniques that account for regression dilution and for the measurement error in the variable on the x axis would lead to even steeper fitted slopes. The fact that we assumed metabolic rate to scale linearly with cell volume, rather than as volume to the power 3/4, also does not change this conclusion, as it would lead to the prediction of a shallower slope.

We can hence conclude that cell volume accounts to a large extent, but not completely, for the changes of metabolic rate and movement speed that we observe in our adapted populations. Other mechanisms than the simple regulation of cell volume contribute to the adaptation of temperature to its environment. For example, cells adapted at low temperature could also compensate for the slower metabolic rate induced by the low temperature by increasing their density of mitochondria and associated enzymes, or by regulating the number and chemical properties of other intracellular components (see e.g. [*S16*] for a review).

Section 3

Some theoretical considerations

3.1 The energetic balance of individual cells

Individual organisms are able to grow and to reproduce if the amount of energy that they obtain from feeding F is larger than the energy that they consume for body maintenance B (the basal metabolic rate) and for movement P (in natural populations, energy can also be lost to predation and to other causes of mortality, but we considered that these can be neglected in our axenic populations of *Tetrahymena* maintained in exponential growth). This means that we can imagine an equation for the *per capita* population growth rate which depends on the three components of the energy budget introduced above:

$$\frac{1}{N}\frac{dN}{dt} = \frac{1}{C_t}\Big(F - B - P\Big), \tag{S1}$$

where N is the population size (number of cells) or density (cells/ml), F, B, and P have units of power (e.g. nanoWatts) and C_t can be thought as the energy amount required to form a new cell.

The individual components of the energetic balance expressed in equation S1 can be expanded and progressively refined to make explicit the dependence on other parameters.

Basal metabolic rate

The basal metabolic rate B is known to depend both on temperature T and on cell size V (relative to a reference volume V_0):

$$B(V,T) = B_0 e^{-\frac{E}{k_B}\left(\frac{1}{T}-\frac{1}{T_0}\right)}\left(\frac{V}{V_0}\right)^{\beta} \tag{S2}$$

where B_0 is the value of metabolic rate measured as some reference temperature T_0. The dependence on temperature is described by the activation energy parameter E; k_B is the Boltzmann constant and T is the environmental temperature expressed in Kelvin degrees. The scaling of metabolism with volume V (here expressed as relative to a reference volume V_0) follows an allometric relation with exponent β [*S17*, *S18*]. Deviations from equation S2, particularly at extreme temperatures, can be captured by more complex equations. In particular, in our analyses we use a modified version of the Sharpe-Schoolfield equation [*S19*, *S20*]:

$$B_V(T) = B_{V0}\frac{e^{\frac{-E}{k_B}\left(\frac{1}{T}-\frac{1}{T_0}\right)}}{1+e^{\frac{E_d}{k_B}\left(\frac{1}{T_h}-\frac{1}{T}\right)}} \tag{S3}$$

where $B_V(T)$ is the metabolic rate (already accounting for body size) at a given temperature T, E_d is the deactivation energy, T_h is the temperature at which 50% of the units of a hypothetical rate-controlling enzyme become inactive. Like in the previous equations, E is the activation energy and k_B is the Boltzmann constant. B_{V0} is the rate at a reference temperature T_0. Equation S3 is similar to equation 7 in [*S20*], except that it does not include the dependence on temperature in the pre-exponential factor, as a way to facilitate the comparison with Arrhenius-type models.

Movement

Swimming entails an energetic cost, associated with overcoming the drag of the water (we neglect here other costs of swimming, such as a possibly increased risk of predation [*S21*]). For small organisms swimming at low Reynolds numbers, the power P required for swimming at speed U is

$$P(U) = sU^2, \tag{S4}$$

where the factor s accounts for the energy dissipation due to drag, and to the conversion of metabolic energy to movement, and it can be expanded as

$$s = \frac{C_D \mu}{\eta_c}. \tag{S5}$$

Here, C_D is the drag coefficient, μ is the dynamic viscosity of the culture medium, and η_c is the efficiency of conversion of metabolic energy into movement.

If we approximate *Tetrahymena* as a prolate spheroid moving along its long axis, the drag coefficient can be calculated as

$$C_D = \frac{8\pi r_s}{\sqrt{\tau^2 - 1}\left(\frac{(\tau^2+1)}{2} ln\left(\frac{\tau+1}{\tau-1}\right) - \tau\right)} \tag{S6}$$

[*S22*], where r_s is the short radius and r_l is the long radius, while $\tau = r_l/(r_l^2 - r_s^2)^{1/2}$, or, as a good approximate formula, the drag is given by

$$C_D = 1.2\pi r_s(4 + \frac{r_l}{r_s}), \tag{S7}$$

as reported for instance in [*S23*] ($\frac{r_l}{r_s}$ here is the elongation of the cell).

The parameter μ, which expresses the dynamic viscosity of water, is in the order of 10^{-3} Kg/(m s), but its value is also dependent on salinity, and on temperature (it decreases at high temperature). In our analyses we calculate viscosity with the following version of Andreade equation,

$$\mu(T) = A \exp\left[\frac{Q}{T} + CT + DT^2\right], \tag{S8}$$

where the parameters take values: $A = 1.856 \times 10^{-14}$ (Pa s), $Q = 4209$ K, $C = 0.04527$ K^{-1}, $D = -3.376 \times 10^{-5}$ K^{-2}.

Parameter η_c in equation S5 quantifies the efficiency of energy conversion in the cilia, and accounts for the fact that only a fraction of the mechanical power of ciliary beating results in propulsive power. Ciliary propulsion is not efficient and values of η_c calculated for paramecium are for instance of the order of 0.7%. We do not have a measure of η_c for *Tetrahymena*, but we can

estimate its approximate value relative to respiration energy consumption (which likely reflects both movement and basal metabolic rate) based on the typical values of relevant quantities that we measured in our experiments, e.g. by considering a respiration rate of $\sim 0.7\,\mathrm{nW}$, a movement speed of $\sim 500\,\mu\mathrm{m/s}$, a small radius $r_s = 12.5\,\mu\mathrm{m}$ and an elongation $r_l/r_s = 2$, and a viscosity $\mu = 0.001\,\mathrm{Kg/(m\ s)}$, leading to a value of η_c as small as 0.01%.

Feeding

All energy acquisition is associated with feeding. We assume a Holling type II functional response in which the encounter rate with food is proportional not just to food density, but also to the encountered volume of medium or, equivalently, to the movement speed of *Tetrahymena*. This is described by the following equation for the feeding rate $f(U)$:

$$F(U) = \frac{f^* U}{U + \eta \frac{d_0}{d}}. \tag{S9}$$

Here, U is the movement speed of *Tetrahymena*, η is the "half saturation speed" or the speed at which the feeding rate reaches half the maximum value, f^* is the maximum feeding rate (which in our system might be limited by digestion time more than by prey handling). Finally, d is the medium concentration relative to a standard medium with concentration d_0 (in our experiments, d_0 is the concentration of the 100% growth medium).

It should be noted that the functional forms of all the equations presented here, from S2 to S9, represent choices among multiple possible alternatives. For example, equation S9 assumes a direct encounter model for food – food encounters increase linearly with speed – while alternative models, e.g. based on diffusional deposition (see e.g. [*S24*]) might also be relevant in our system. Similarly, equation S5 assumes that the efficiency of conversion of metabolic energy to propulsion η_c is not itself dependent on temperature. Because of these and many other assumptions in the formulation of the model, and because of the uncertainty in many parameters (some that we did not measure directly in our experiments, such as the feeding rates, and some that change rapidly during the adaptation, such as cell size and shape, or the movement speed of *Tetrahymena*), we intend the modelling presented here as a tool to gain some insight into the contribution of different drivers of *Tetrahymena* adaptation, rather than as a rigorous quantitative model that can be fitted to the empirical data.

In the coming sections, we analyse the model focusing specifically on the question, how should swimming speed change with temperature if *Tetrahymena* were to simply allocate a constant proportion of metabolic energy to movement? And how should speed change as a function of temperature and nutrients in order for *Tetrahymena* to optimise its energy budget (its energy intake relative to energy expenditure)?

3.2 Predicted relationship between activation energies for respiration and movement speed

Here we aim at obtaining a prediction for the activation energy for movement of a microorganism swimming at low Reynolds numbers under the assumption that the organism does not change its shape or size when it is exposed to a different temperature, that it allocates a constant fraction of

its metabolic energy to movement, and that the efficiency of energy conversion is independent of temperature. This kind of reasoning has the double purpose:

1. Formulating an initial and general prediction for the scaling of movement speed with temperature in microscopic organisms. In this case, the prediction will be that the activation energy for speed should be substantially lower than the activation energy for respiration.

2. Providing a null hypothesis against which to compare the experimental data: deviations of data from the predicted values will be informative of additional factors that play a role in determining how *Tetrahymena* movement speed changes with temperature. For example, deviations from the expected values could indicate that one or more of the assumptions that we made above are violated (e.g. the fraction of metabolic energy allocated to movement might not be constant, or the efficiency of energy conversion might be dependent on temperature).

Our starting point are equations S4 and S5, which combined describe the relationship between power of swimming P and speed U, as a function of the drag coefficient C_D, the efficiency of conversion of metabolic energy into movement η_c, and the viscosity μ of the medium in which the microorganism moves:

$$P(U) = \frac{C_D \mu}{\eta_c} U^2. \tag{S10}$$

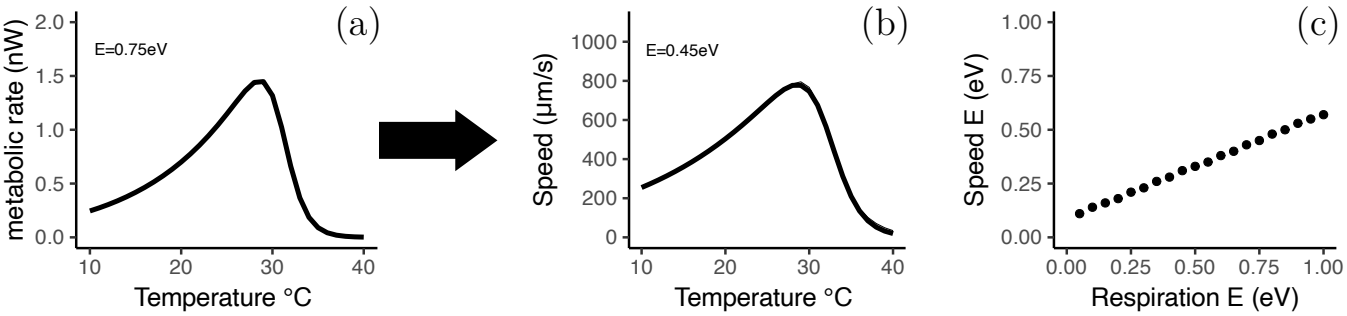

Figure S3.1: Modelled relationship between metabolic rate and speed in thermal response curves for short-term exposure. **(a)** Thermal response curve for metabolic rate simulated with a Sharpe-Schoolfield equation (eq. S3) with rate at reference temperature $B_{V0} = 0.7\,\mathrm{nW}$, activation energy E =0.75 eV, reference temperature T_0=293.15 K, deactivation energy E_d =7 eV, and high temperature T_h =304.15 K. The thermal response curve for metabolic rate in (a) translates into the thermal response curve in panel (b) for movement speed once accounting for the viscous drag of moving at low Reynolds numbers and of temperature-dependent changes in water viscosity. Curve in **(b)** based on the assumption that cells move at 500 μm/s when tested at the reference temperature of 293.15 K, and that the efficiency of conversion of metabolic energy into movement is $\eta_c = 1.0276 \times 10^{-4}$, independent of temperature. The best fitting value of activation energy is here E =0.45 eV, slightly larger than 0.75/2=0.375 eV because of the additional effect of temperature on water viscosity. **(c)** Predicted relation between activation energy for movement speed as a function of the activation energy for respiration based on the same parameters and assumptions as in the other figure panels.

The drag coefficient C_D only depends on cell size and shape, as in equation S6 or S7 (see also S34 below for another equivalent expression). The dependence of viscosity μ on temperature is expressed by equation S8.

Looking at equation S10 we can see that if μ, η_c and C_D were independent of temperature, and P represented a fixed proportion of the total metabolic power, independent of temperature, then we would simply have $P \simeq U^2$, and we would predict that the activation energy for speed U should be 1/2 the activation energy for metabolic rate. In practice, as water viscosity μ also changes with temperature, we can calculate the predicted dependence of speed on temperature also incorporating into equation S10 the calculated values for μ. For example, figure S3.1(a) shows a simulated thermal response curve for metabolic rate, and the corresponding modelled thermal response curve for movement speed (fig. S3.1(b)). A simulation across a range of values of activation energy gives the relationship in figure S3.1(c), which is well summarized by the equation $y = 0.0868 + 0.487x$, where y is the activation energy for movement speed and x is the activation energy for metabolic rate (respiration).

3.3 Optimisation of swimming speed

If instead of allocating a fixed proportion of metabolic energy to movement, an organism is free to change this allocation, e.g. to move at faster or slower speed, we could ask what is the swimming speed that maximizes energy accumulation and population growth. This is verified when the derivative of the energy balance with respect to speed is zero:

$$\frac{\partial\,(F - B - P)}{\partial U} = 0. \tag{S11}$$

If we consider that the basal metabolic rate does not depend on movement speed, then the energy intake associated with movement depends on feeding F and on the energetic cost P of movement itself, and the balance between the two reaches a maximum when:

$$\frac{\eta\frac{d_0}{d}f^*}{\left(U + \eta\frac{d_0}{d}\right)^2} - 2sU = 0, \tag{S12}$$

where the two terms of the equation are obtained by deriving equations S9 and S4, respectively. When solved for U, equation S12 gives the following expression for the optimal swimming speed U^*:

$$U^* = \sqrt[3]{\frac{\tilde{\eta}\sqrt{f^*\cdot(8\tilde{\eta}^2 s + 27f^*)}}{4\cdot 3^{\frac{3}{2}}s} + \frac{\frac{3f^*\tilde{\eta}}{2s} + 2\tilde{\eta}^3}{6} - \frac{8\tilde{\eta}^3}{27}} + \frac{\tilde{\eta}^2}{9\sqrt[3]{\frac{\tilde{\eta}\sqrt{f^*(8\tilde{\eta}^2 s+27f^*)}}{4\cdot 3^{\frac{3}{2}}s} + \frac{\frac{3f^*\tilde{\eta}}{2s}+2\tilde{\eta}^3}{6} - \frac{8\tilde{\eta}^3}{27}}} - \frac{2\tilde{\eta}}{3} \tag{S13}$$

where we substituted $\tilde{\eta} = \eta\frac{d_0}{d}$ to simplify the notation.

If we plot the optimal speed calculated in this way as a function of temperature and medium concentration, we obtain the two graphs in figure S3.2, where we used $\eta = 250\,\mu$m/s, $f^* = 6\,$nW,

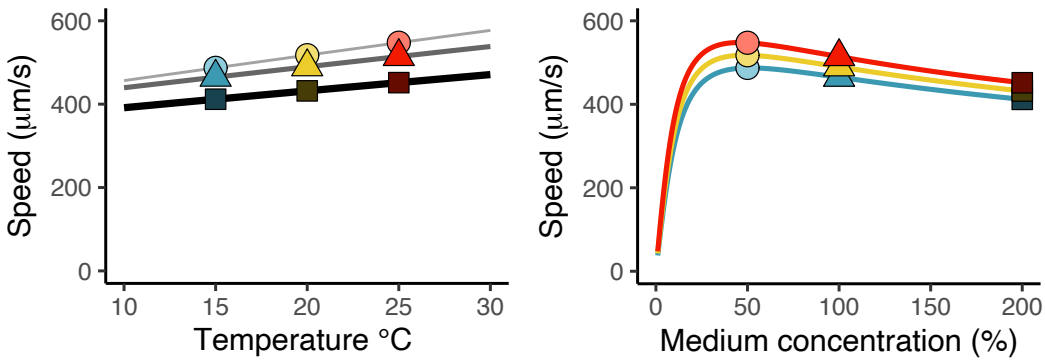

Figure S3.2: Estimated optimal speed as a function of medium concentration and temperature; model details are given in the text. The figure on the left would be equivalent to the bottom-right panel of figure 3 in the main document.

and s is calculated on the basis of a spheroidal cell of length 50 μm ($r_l = 25\mu$m), cell width 25 μm, and other parameters as described in the **Movement** subsection above.

We should point the attention to some important assumptions of this model. The first is that the maximum feeding rate f^* is independent of temperature. The maximum feeding rate can also be seen as the inverse of the digestion time, and one could argue that food digestion should be faster at higher temperature. However, measurements of metabolic rate in cell populations adapted at different temperature suggest that the metabolic rate is similar across cells adapted at different temperature (see fig. S2.5). Perhaps, then, we can imagine that cells kept at low temperature are able to process food at a similar rate as cells kept at larger temperature, possibly through a larger number of food vacuoles. Anecdotally, the number of food vacuoles seemed to be larger in larger cells, although we do not have a precise quantification of the number and turnover rate of food vacuoles in our experiments.

The model also assumes – for better clarity of illustration – a cell of fixed size, independently of temperature and growth medium concentration, while temperature-induced changes in cell size and shape can also mechanistically affect movement speed (section 2.12).

For another similar treatment of optimal swimming speed see also [*S21*].

One first observation made possible by the graphs in figure S3.2 is that optimal speed remains relatively constant with temperature (panel on the left in the figure). In the model, this is mainly a consequence of the fact that the maximum feeding rate does not change with temperature. In these conditions, the slightly reduced viscosity of water at high temperature induces a slight decrease of the cost of swimming with increasing temperature, and justifies the small increase of speed at higher temperature.

The right panel in figure S3.2 shows the speed predicted by the model as a function of medium concentration. The figure suggests that movement speed should be very slow when nutrients are scarce: under these conditions, the energy consumption associated with a fast movement is not compensated by feeding. Movement speed reaches a maximum for intermediate concentration of the culture medium, and then decreases again. In fact, when nutrients are abundant, a large amount of nutrients are encountered in a small volume, and feeding is limited by handling and digestion, rather than by food encounter rate: a higher speed would not bring any additional benefit!

These predicted graphs tentatively resemble observations in figure 3 in the main text, and SI figure S2.11, but future modelling work is needed in order to confirm these qualitative resemblances.

3.4 Oxygen availability to *Tetrahymena* cells

The reduced solubility of oxygen in water at high temperature has often been indicated as a possible factor underlying the temperature-size rule of ectotherms (the observation that many organisms tend to reach a smaller adult body size when they grow in a warmer environment)[*S11*, *S25*].

While we did not aim at studying specifically the role of oxygen in our experiments, it can still be interesting to consider briefly to what extent *Tetrahymena* growth could be limited by oxygen availability directly, rather than by the metabolic ability of cells to process oxygen and nutrients.

Oxygen solubility in water decreases with temperature, and is hence likely to become a limiting factor at high temperature. At 30 °C, O_2 concentration in a saturated water solution would be about 252 μM (see below, section 3.6, for details). Considering that, in our cultures, oxygen concentration was always very close to saturated values, could oxygen availability be directly limiting the growth of an organism the size of *Tetrahymena* in these conditions?

Without giving a complete answer to this question, we could consider a limiting case scenario, of a spherical cell of radius r_o that does not move – meaning that all the oxygen consumption required to fuel its metabolism has to be provided through diffusion alone – and yet, whose metabolic rate is the same as that of an active *Tetrahymena* cell. The current I of oxygen to a spherical, stationary cell of radius r_o can be calculated as described in section 3.5 below, and it is given by equation S25. We report the equation also here:

$$I(r_o) = 4\pi D(C_\infty - C_o)r_o. \tag{S14}$$

Here, C_∞ is the concentration of oxygen in the culture medium away from the cell, which at 30 °C would be approximately $C_\infty = 252\mu\text{M} = 0.252\text{mol/m}^3$. C_o is the concentration of oxygen required at the position of the cell membrane in order for the cell to be able to function normally. Mitochondria are not limited by oxygen availability if the local oxygen concentration is above 10 μM (based on [*S26*]). The diffusion coefficient (also at 30 degrees) for oxygen in water (see 3.7) is $D = 2.71 \times 10^{-9}\text{m}^2$ / s: If the cell diameter is 50 μm and, consequently, $r_o = 25\mu$m we can calculate the current into the cell as follows (making sure that all units of distance here are in metres):

$$\begin{aligned} I(r_o) = 4\pi 2.71 \times 10^{-9} \times (0.252 - 0.010) \times 25 \times 10^{-6} = \\ 2.06 \times 10^{-13}\text{mol/cell/s} = 12.36 \times 10^{-6}\mu\text{mol/cell/min}. \end{aligned} \tag{S15}$$

The fact that these values are one or two magnitude orders larger than the measured respiration rate of individual cells in our experiments, indicate it as unlikely that oxygen limitations played a major direct role in shaping *Tetrahymena* adaptation (also increasing the concentration of oxygen C_o required on the cell surface by one order of magnitude, to 100 μM does not change substantially this result).

The calculation above is intended to illustrate how we would estimate the supply of oxygen to a spherical cell for a specific value of temperature and of cell radius. The same calculations can be applied across the full range of temperature values used in our experiments and for a wide range of

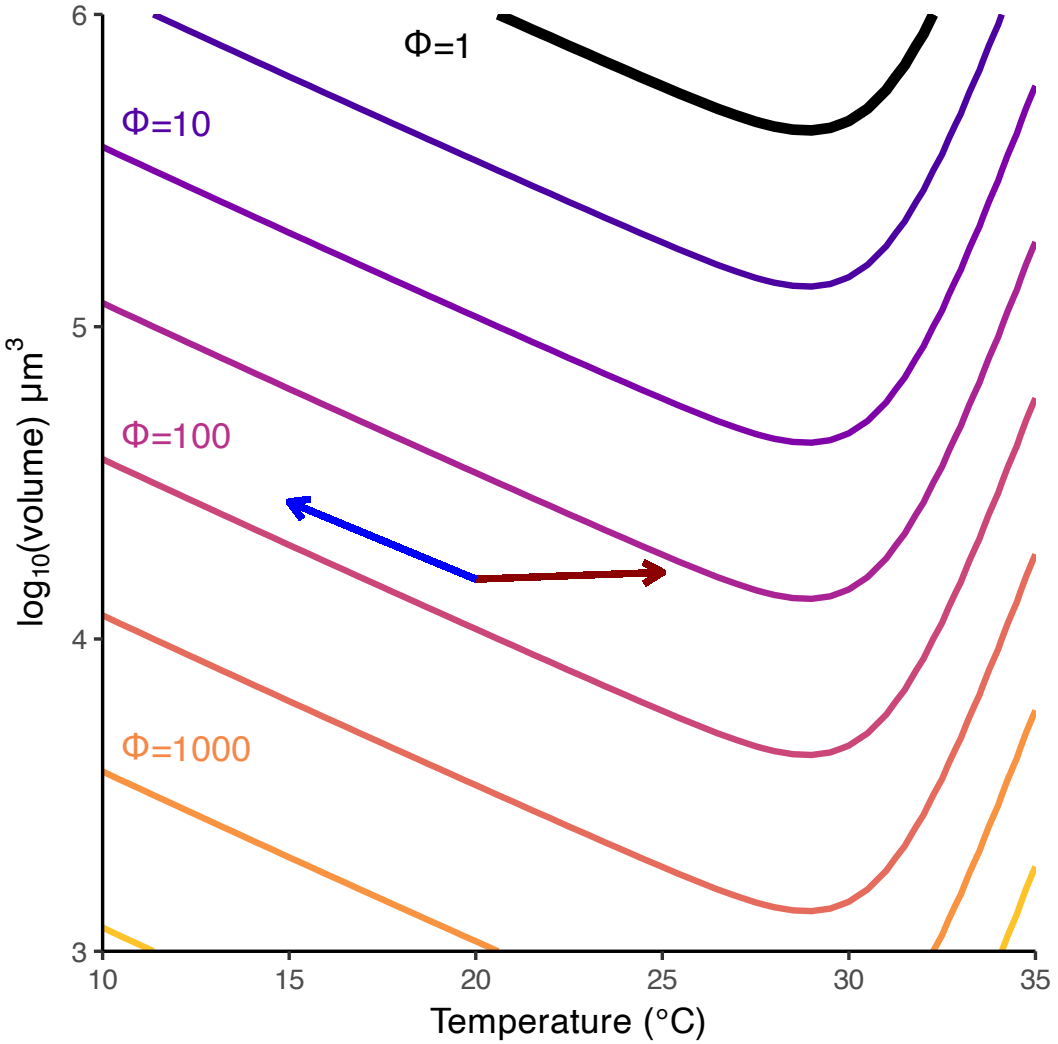

Figure S3.3: **Supply and demand of oxygen**. Demand of oxygen is calculated based on an activation energy of 0.89 eV and an oxygen/energy demand of 0.69 nW at 20°C. Oxygen supply is calculated based on the solubility and diffusion coefficients of oxygen in water, scaled with temperature, and assuming that the concentration required at the position of the cell membrane is 100 μM. The arrows correspond to the changes of volume of *Tetrahymena* cells between 20°C (base of the arrow) and the other two main temperature conditions of 15 and 25°C (tips of the arrows). The curves of Φ indicate different ratios between oxygen supply and oxygen demand as a function of temperature and cell volume (large values of Φ indicate that supply is in excess with respect to demand). The black curve indicates the critical value of $\Phi = 1$

cell volumes in order to model oxygen supply to cells of different sizes and at different temperatures. In parallel, we can also model oxygen demand as a function of cell size and temperature based on eq. S3. We can then calculate the ratio, which we indicate with the Greek letter Φ, between oxygen supply and demand predicted for each combination of parameters of cell size and temperature. The isolines of the supply/demand ratio Φ are presented in figure S3.3, in an analysis and visual representation inspired by [*S27*].

In the figure, the value of $\Phi = 1$ is marked by the thick black line near the top of the graph. For large cells, falling in the region above the thick black line, the supply of oxygen would be insufficient to meet the metabolic demand of the cell. Conversely, small cells, especially if they are cultured at low temperature (bottom-left part of the graph) are predicted to have an oxygen supply far in excess of metabolic demand. The volume of *Tetrahymena* cells in our experiments is marked by the two arrows in the figure, with the base of the arrows marking the volume of cells adapted at 20 °C (and growth medium concentration 100%) and the tips of the arrows marking the volume of cells adapted at 15 °C and 25 °C, respectively for the blue and for the red arrow (medium concentration 100%).

From the plot in figure S3.3 we can see that the change in cell volume observed for *Tetrahymena*, indicated by the arrows, is roughly aligned with the isolines of Φ. Other data on the volume change of *Tetrahymena* from our experiment, such as those at different medium concentrations (figure 2(c) in the main text), or those from the thermal response curves for volume change (e.g. fig. S2.10) would also present a similar alignment. The alignment of the cell-size changes of *Tetrahymena* with the isolines of Φ could suggest that cell volume changes are a mechanism that guarantees a constant oxygen supply-demand ratio to the cell. However, we should also note that the region of the graph that corresponds to the cell volume of *Tetrahymena* is very far from the thick black curve that marks the critical value of $\Phi = 1$: no matter how cells in this region of the graph change their volume or their metabolic rate, oxygen supply will always be far in excess of demand!

An alternative approach to the study of oxygen supply and demand

In the type of modelling that we just described above we made a number of assumptions, which we would like to review here before we introduce an alternative modelling approach that has been followed in the scientific literature:

1. We assumed that cells were not moving. In reality, the fast movement of *Tetrahymena* means that the concentration of oxygen at the cell membrane is likely to be much higher (C_o close to C_∞), as the cell constantly reaches into new fresh culture medium.

2. For simplicity, we assumed spherical cells. This is unlikely to affect the calculations significantly given the aspect ratio of *Tetrahymena*.

3. The assumption which certainly might have the biggest consequences is that oxygen is 'consumed' at the cell surface: we set C_o to take a fixed value at the position of the cell membrane. We could speculate that the diffusion of oxygen across the cell membrane and to the mitochondria is particularly inefficient and for this reason a very high concentration C_o is required (though in terms of diffusion across cellular membranes at least, this does not seem likely, see [*S28*]). We could also speculate that oxygen is utilised uniformly everywhere inside the cell.

This situation – in which oxygen is utilised uniformly everywhere inside the cell – can be modelled by considering that, inside the cell, both diffusion and oxygen consumption affect the availability of oxygen to the most internal parts of the cell. As we don't focus on oxygen in our study, we leave a detailed modelling of oxygen supply and consumption inside *Tetrahymena* cells to a future

study, but we just mention an analogous system, which was modelled by [*S29*]. These authors considered a model, in which the oxygen concentration at the cell membrane (though their model was not originally developed for cells, but for tumour spheroids) is essentially C_∞, and oxygen reaches the inner core of the cell (or tumour spheroid) if

$$C_\infty \geq \frac{B{r_o}^2}{6DV}, \tag{S16}$$

where C_∞ is the concentration of oxygen at the cell membrane, r_o is the cell radius, D is the diffusion coefficient, V is the cell volume, and B is the metabolic rate (expressed in units of molar oxygen consumption in order to match the units of oxygen concentration C_∞). Rearranging equation S16 we get that anoxic regions inside the cell are avoided if the cell radius is be $r_o \leq \sqrt{\frac{6DC_\infty V}{B}}$. We take $\frac{B}{V} = \frac{1.57\text{nW}}{16000\mu\text{m}^3}$, or $\frac{B}{V} = 98125W/m^3$, as the ratio between metabolic rate at 30 °C and cell volume, roughly matching the experimental data). The term $\frac{B}{V}$ represents a measure of metabolic rate per unit of biomass inside the cell, and can be converted to units of molar oxygen depletion by assuming the equivalence 1 mol O_2 = 478576 J, giving $\frac{B}{V} = 0.20\text{mol O}_2/\text{m}^3/\text{s}$. Hence, by this model, the maximum cell radius before cell size impacts diffusion-driven oxygen supply for a cell at 30 °C would be $r_{max} = \sqrt{\frac{6\times2.71\times10^{-9}\times0.252}{0.20} \times 10^-6} = 143\ \mu\text{m}$. In a sense, then, also this alternative set of arguments seems to suggest that oxygen availability only becomes a limiting factor for cells or organisms substantially larger than *Tetrahymena* when these are tested in our growth conditions.

Discussion

The calculations that we presented in this section all point to the fact that oxygen availability was not directly limiting the growth and metabolic activity of *Tetrahymena* in our culture conditions. Undoubtedly, there is ample room for refining these calculations, and it remains possible that by combining limitations of oxygen supply due to the diffusion from the growth medium to the cell membrane, and limitations due to the diffusion inside the cell we would find that oxygen availability becomes limiting already in the range of sizes of *Tetrahymena*.

However, the conclusion that oxygen is not a direct limiting factor for *Tetrahymena* in our experimental conditions is also supported by empirical evidence. This evidence includes the observation that *Tetrahymena* population growth remains in the exponential growth phase also for densities much larger than those used in our experiments, when it is more likely that oxygen becomes depleted to some extent from the culture medium (presented above in section S1.2). Oxygen consumption in the Sensor Dish Reader also remained stable throughout our measurements, with oxygen decreasing linearly in time also after it had reached low values below $100\mu M$, showing no evidence of altered metabolism within a wide range of oxygen concentrations. Finally, in our preliminary experiments in which we altered oxygen concentration directly (SI section S2.10) we did not observe changes of cell size or shape.

While not conclusive, all these different pieces of evidence suggest that if there are effects of oxygen availability on cell metabolism and population growth, these are only likely to be indirect.

We should note that while in our experimental conditions of axenic cultures kept at low population densities in well-aerated culture flasks, *Tetrahymena* might never encounter growth-limiting concentrations of oxygen, these conditions are far from being representative of the conditions that *Tetrahymena* is likely to experience in its natural environment, such as in a pond or in the groundwater, and even in laboratory cultures, as soon as cultures are left to grow and reach high cell

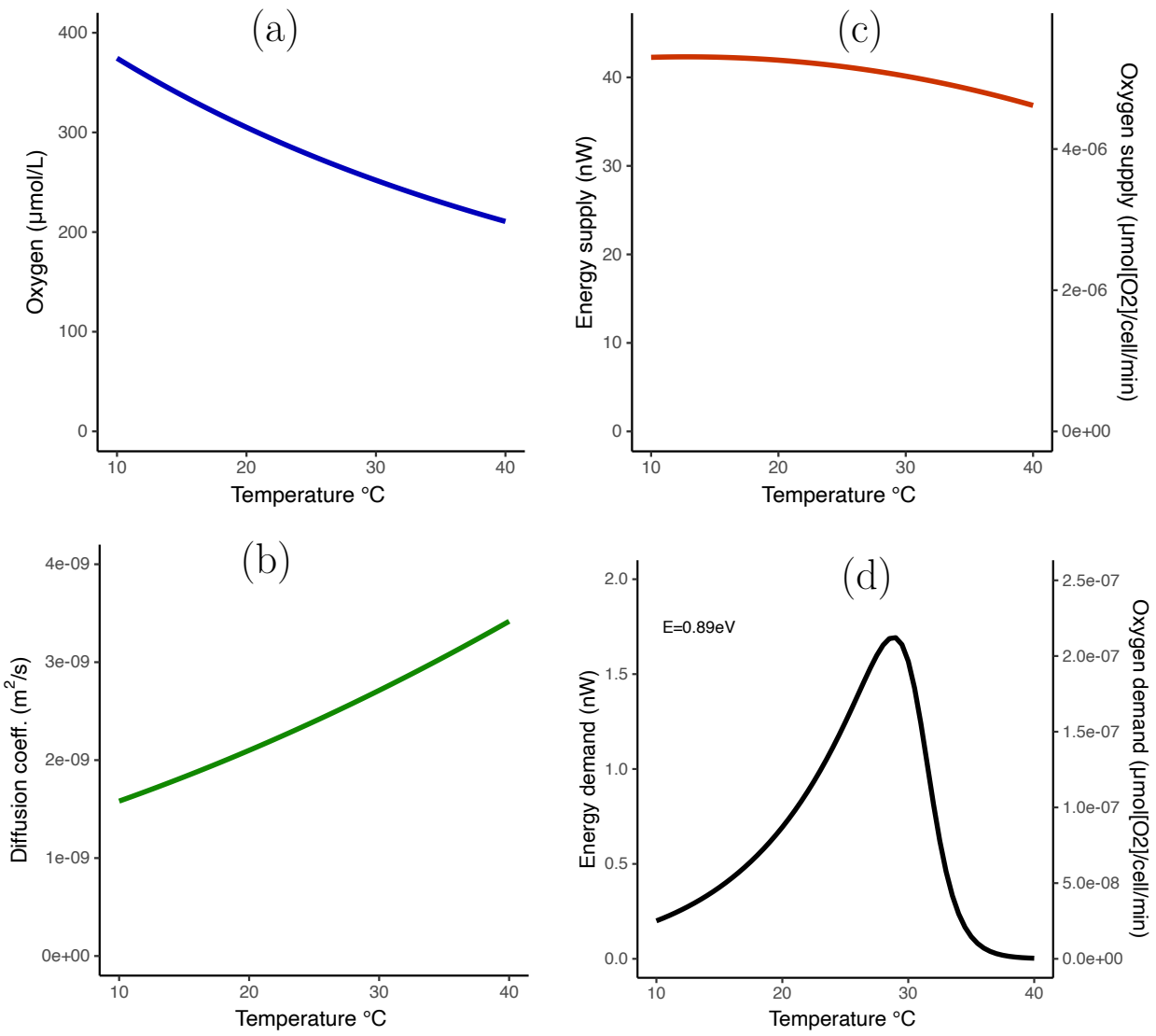

Figure S3.4: **Effects of temperature on oxygen concentration and diffusion. (a)** Effects of temperature on oxygen concentration at fully saturated equilibrium. **(b)** Effects of temperature on the diffusion coefficient of oxygen in water. (c) Estimated oxygen supply to a spherical cell of volume $10^{4.5}\mu m^3$ assuming that the cell absorbs oxygen up to a concentration 100 μM on the cell surface. **(d)** For comparison, estimated energy and oxygen demand for a cell with the same volume ($10^{4.5}\mu m^3$) based on plausible parameter values obtained experimentally from our experiments.

densities beyond the exponential growth phase. Our *Tetrahymena* cells might have evolved reaction norms that decrease body size when temperature increases, due to previous selection when growing conditions with respect to oxygen were less favourable (reviewed in [*S11*]). In this case, some of the phenotypic changes – such as the changes in cell volume – that we observe when we expose *Tetrahymena* to a different temperature would represent adaptive norms of reaction that provide a selective advantage for coping with limiting oxygen supply/demand ratios, except that these phenotypic changes would not be directly beneficial in our culture conditions, and they would

be triggered not by oxygen directly, but by other environmental cues (for instance, by temperature itself). This would be the reason why we observe them also in our experimental conditions in which oxygen, most likely, was not limiting.

To conclude this section, we should also mention one final observation: within the range of parameters that we used in our calculations the curves that describe the ratio between supply and demand Φ (fig. S3.3) are almost entirely determined by changes in oxygen demand (through the temperature- and body-size-dependence of metabolic rate). The modelled oxygen supply to the cells only showed little variation across the entire temperature range (figure S3.4(c), calculated on the basis of eq. S14). Oxygen supply is little affected by temperature changes because while an increasing temperature reduces the solubility of oxygen (decreasing C_∞, S3.4(a); see below, section S3.6 for details of the calculations), it also increases the diffusion coefficient D that also contributes to oxygen supply in eq. S14 (fig. S3.4(b)). The estimated rates of oxygen supply also depend on the parameter C_o in eq. S14, but it remains generally true that oxygen demand, rather than supply, is likely to be the main determinant of the supply/demand ratio (see also [*S10*]).

The importance of metabolic demand, relative to supply, limits the explanatory power of the type of supply/demand curves presented in figure S3.3, because supply-demand curves for other nutrients and resources different from oxygen, or for the removal of catabolic products would likely be similar, as long as their shape is mostly determined by the cellular metabolism rather than by the specific nature of the molecules considered. Experiments in which oxygen concentrations are directly manipulated would be required in order to fully disentangle the role of oxygen availability from other factors.

3.5 Diffusion around a sphere

For the convenience of our readers, here we provide a derivation of equation S14, that we used above to model the diffusive supply of oxygen to an individual cell. The problem considered is that of a small spherical unicellular organism of radius r that lives in a non-turbulent medium and obtains oxygen through diffusion. The concentration of oxygen at an infinite distance from the cell is C_∞, while the concentration on the surface of the cell is C_o. The extreme when $C_0 = 0$ corresponds to the assumption of a perfectly absorbing cell surface (any molecule that touches the surface of the cell is immediately taken). Based on these boundary conditions for the diffusion equation, we can estimate the gradient of oxygen concentration around the cell, and the total flow or current of oxygen into the cell per unit time. This topic is covered for instance in the book by Berg [*S30*].

We start by writing the diffusion equation in spherical coordinates, assuming radial symmetry (i.e. neglecting cell elongation for the purpose of our approximate calculations):

$$\frac{\partial C}{\partial t} = D\frac{1}{r^2}\frac{\partial}{\partial r}\left(r^2\frac{\partial C}{\partial r}\right). \tag{S17}$$

At the steady state $\frac{\partial C}{\partial t} = 0$. This means that we must have:

$$\frac{\partial}{\partial r}\left(r^2\frac{\partial C}{\partial r}\right) = 0. \tag{S18}$$

If the left side is equal to zero, then its integral with respect to r is equal to a constant that we indicate here as K_1:

$$r^2 \frac{\partial C}{\partial r} = K_1. \tag{S19}$$

We can further rearrange and integrate to get

$$C(r) = -\frac{1}{r} K_1 + K_2. \tag{S20}$$

Now we can get the values of K_1 and K_2 from the boundary conditions. At $r = \infty$ we have $C(r) = K_2 = C_\infty$. At $r = r_o$ we have $C(r_o) = C_o$.

This leads to the following expression when $C_o = 0$:

$$C(r) = C_\infty \left[1 - \frac{r_o}{r}\right]. \tag{S21}$$

For $C_o \neq 0$ we have instead

$$C(r) = C_\infty - \frac{r_o \left(C_\infty - C_o\right)}{r}. \tag{S22}$$

One important observation from eq. S22 is that the concentration at any given point does not depend on the diffusion coefficient, but only on the radius of the cell and on the two concentrations C_o and C_∞.

Now that we know the gradient, we can calculate the flux if we remember that

$$J(r) = -D \frac{\partial C}{\partial r}. \tag{S23}$$

In fact, we obtain

$$J(r_o) = -D \frac{C_\infty - C_o}{r_o} \tag{S24}$$

for the flux at the position of the cell membrane. In this case the flux does depend on the diffusion coefficient. In general the relevant quantity is not the flux at the position of the cell membrane, but the total rate of nutrients arriving to the cell, which is flux times area. Let's call this the current or the flow of oxygen into the cell, and indicate it with the letter I. This is easily calculated if we remember that the surface area of a sphere is $4\pi r_o^2$:

$$I(r_o) = 4\pi D (C_\infty - C_o) r_o \tag{S25}$$

The main result of these calculations is that the current into the cell scales with the radius of the cell. This means that for large cells it might becomes soon insufficient to supply enough molecules (oxygen, nutrients) to the entire cell volume (which scales instead as r_o^3).

3.6 Temperature dependence of oxygen concentration in fully saturated water

At equilibrium, the amount of oxygen (or another gas) dissolved in water is proportional to the partial pressure of the gas above the water. The proportionality constant is called Henry solubility

constant. For oxygen at 25 °C we have $H^{cp} = 0.001321528 \frac{\text{mol}}{\text{L atm}}$. This means for instance that at one atmosphere, with a partial pressure of oxygen of 0.20948 atmospheres we have a concentration in water of 277μmol/L or 8.86mg/L. In practice, the presence of solutes in water also affects the solubility of oxygen so that we should have a different constant for each level of salinity.

When the temperature increases or decreases, the Henry solubility constant also changes and this change is well described by Van't Hoff equation:

$$H(T) = H \exp\left[K_v \left(\frac{1}{T} - \frac{1}{T*}\right)\right], \tag{S26}$$

where

$$K_v = \frac{-\Delta_{sol} H}{R}. \tag{S27}$$

As a worked example, let's calculate the concentration of oxygen at equilibrium at a temperature of 30 degrees Celsius.
The partial pressure of oxygen at one atmosphere is $p_{O_2} = 0.21atm$. In order to know how much of this oxygen is dissolved in water we need to know the Henry solubility constant. The Henry solubility constant at 25 °C (298.15 K) is $H^{cp} = 0.00132$mol/L/atm.

The Van't Hoff parameter K_v for O_2 is 1700. We can then calculate the Henry solubility constant at 30 °C (303.15 K) as

$$H^{cp}(T = 30\text{deg}) = 0.00132 \exp\left[1700\left(\frac{1}{303.15} - \frac{1}{298.15}\right)\right] = 0.0012. \tag{S28}$$

Oxygen concentration is then calculated by multiplying $[O_2] = 0.21 \times 0.0012$ mol/L, that is, $[O_2] = 252$ μM. The conversion to mg/L is easily obtained by considering the molecular weight of $\text{MW}(O_2) = 32$ g/mol: 252μmol/L $\times 10^{-3}$ mmol/μmol $\times$ 32 mg/mmol = 8 mg/L.

3.7 Diffusion of molecules in water

The diffusion coefficient in liquids is described by the Stokes-Einstein equation. In the special case of spherical particles moving through a liquid with low Reynolds number we have

$$D = \frac{k_B T}{6\pi\mu r}. \tag{S29}$$

Where D is the diffusion coefficient, k_B is the Boltzmann constant, T is the absolute temperature, μ is the dynamic viscosity of water and r is the radius of the particle. Note that the denominator is similar to the drag coefficient for a sphere.

Given this dependence on temperature we have that

$$\frac{D_{T1}}{D_{T2}} = \frac{T1}{T2}\frac{\mu_{T2}}{\mu_{T1}}. \tag{S30}$$

At 20 degrees Celsius, the diffusion coefficient of oxygen in water is about $2.10 \times 10^{-9}\text{m}^2/\text{s}$; the diffusion coefficient of CO_2 in water is $1.77 \times 10^{-9}\text{m}^2/\text{s}$. The diffusion coefficient of many other small molecules is in the same order of magnitude.

We can then estimate the diffusion coefficient for oxygen in water at 30 °C as $2.71 \times 10^{-9}\text{m}^2/\text{s}$

3.8 Implications of cell shape for swimming

In our experiments, cells increased size mainly through becoming more elongated, which mainly happened at low temperature and high nutrient concentrations (see fig. S2.3). One might ask about the possible implications of different cell shapes for swimming. For example, what shape a cell should have in order to minimise the drag when swimming at low Reynolds numbers. This problem was addressed for instance by Cooper and Denny [*S31*], who calculated the passive drag of a prolate spheroid moving in a viscous medium. The spheroid had constant volume and variable elongation, so that they could analytically find the value of elongation that minimized the drag. As the approximated equation used in the original article is only valid for extremely elongated spheroids and would lead to incorrect predictions, we re-derive it here.

Consider a prolate spheroid with a volume V:

$$V = \frac{4}{3}\pi r_s^2 r_l, \tag{S31}$$

where V is fixed, and the only thing that can vary are the small and large radius r_s and r_l, under the constraint of maintaining the same cell volume. We can define the elongation ψ of the spheroid as $\psi = \frac{r_l}{r_s}$. Once we have done this, we can rewrite the formula for the volume as

$$V = \frac{4}{3}\pi r_s^2 r_l = \frac{4}{3}\pi r_s^3 \psi = \frac{4}{3}\pi r_l^3 \left(\frac{1}{\psi}\right)^2. \tag{S32}$$

From this, we get an equation for r_s as a function of volume and elongation

$$r_s = \sqrt[3]{\frac{3}{4}\frac{V}{\pi}}\sqrt[3]{\frac{1}{\psi}} = r_E\sqrt[3]{\frac{1}{\psi}}, \tag{S33}$$

where r_E is an equivalent radius (the radius of a sphere with the same volume).

Clift, table 4.1 [*S23*] gives exact formulas for the drag coefficient of a spheroid.

$$C_D = \frac{8\pi r_s\left(\psi^2 - 1\right)}{\left(\frac{(2\psi^2-1)\ln\left(\sqrt{\psi^2-1}+\psi\right)}{\sqrt{\psi^2-1}} - \psi\right)}, \tag{S34}$$

as well as an approximate formula:

$$C_D = 1.2\pi r_s(4 + \psi). \tag{S35}$$

It is easy to replace r_s with the expression that we had above in terms of equivalent radius r_E and elongation ψ. For instance, if we do this in the approximate expression we obtain:

$$C_D = \frac{1.2\pi r_E\left(\psi + 4\right)}{\sqrt[3]{\psi}}. \tag{S36}$$

We then derive with respect to the elongation ψ, and we get

$$\frac{dC_D}{d\psi} = \frac{4\pi r\left(\psi - 2\right)}{5\psi^{\frac{4}{3}}}. \tag{S37}$$

The derivative indicates that the minimum drag is for an optimal value of elongation $\psi^* = 2$. Using the complete equation rather than the approximate one does not make a huge difference, giving an optimal elongation $\psi^* \simeq 1.95$. One important take-home message is that the shape that minimizes drag based on these calculations always has an aspect ratio of approximately 2:1 (length:width). We should however remember that these calculations are based on formulas for the passive drag, while *Tetrahymena* are active swimmers. It is possible that the more elongated shape of *Tetrahymena* cells adapted at low temperature might allow for a more powerful, albeit less efficient, swimming, due to an increase in the number of cilia oriented perpendicularly relative to the direction of movement, or to other similar factors. Alternatively, the change of elongation which we observe depending on temperature should be attributed to other internal constraints on cell size and shape, rather than to adaptive phenotypic responses related to the efficiency and power of swimming.

Bibliography

[S1] Hofmann E, Cleffmann G. 1981 External factors limiting the multiplication potential of *Tetrahymena*. Journal of cell science **50**, 407–418.

[S2] Mogami Y, Yamane A, Gino A, Baba SA. 2004 Bioconvective pattern formation of *Tetrahymena* under altered gravity. Journal of experimental biology **207**, 3349–3359.

[S3] DeLong JP, Hanson DT. 2009 Metabolic rate links density to demography in *Tetrahymena pyriformis*. The ISME Journal **3**, 1396–1401.

[S4] Dupont L, Thierry M, Zinger L, Legrand D, Jacob S. 2024 Beyond reaction norms: the temporal dynamics of phenotypic plasticity. Trends in Ecology & Evolution **39**, 41–51.

[S5] Beveridge OS, Petchey OL, Humphries S. 2010 Mechanisms of temperature-dependent swimming: the importance of physics, physiology and body size in determining protist swimming speed. Journal of Experimental Biology **213**, 4223–4231.

[S6] Rohr JR, Civitello DJ, Cohen JM, Roznik EA, Sinervo B, Dell AI. 2018 The complex drivers of thermal acclimation and breadth in ectotherms. Ecology Letters **21**, 1425–1439. (https://doi.org/10.1111/ele.13107)

[S7] Rubalcaba JG, Verberk WC, Hendriks AJ, Saris B, Woods HA. 2020 Oxygen limitation may affect the temperature and size dependence of metabolism in aquatic ectotherms. Proceedings of the National Academy of Sciences **117**, 31963–31968.

[S8] Frazier MR, Woods HA, Harrison JF. 2001 Interactive effects of rearing temperature and oxygen on the development of Drosophila melanogaster. Physiological and Biochemical Zoology **74**, 641–650.

[S9] Hoefnagel KN, Verberk WC. 2015 Is the temperature-size rule mediated by oxygen in aquatic ectotherms?. Journal of thermal biology **54**, 56–65.

[S10] Verberk WC, Bilton DT, Calosi P, Spicer JI. 2011 Oxygen supply in aquatic ectotherms: partial pressure and solubility together explain biodiversity and size patterns. Ecology **92**, 1565–1572.

[S11] Verberk WC, Atkinson D, Hoefnagel KN, Hirst AG, Horne CR, Siepel H. 2021 Shrinking body sizes in response to warming: explanations for the temperature–size rule with special emphasis on the role of oxygen. Biological Reviews **96**, 247–268.

[S12] Carroll SP, Hendry AP, Reznick DN, Fox CW. 2007 Evolution on ecological time-scales. .

[S13] Plum K, Tarkington J, Zufall RA. 2022 Experimental evolution in *Tetrahymena*. Microorganisms **10**, 414.

[S14] Elliott AM. 1959 Biology of *Tetrahymena*. Annual Reviews in Microbiology **13**, 79–96.

[S15] DeLong JP, Okie JG, Moses ME, Sibly RM, Brown JH. 2010 Shifts in metabolic scaling, production, and efficiency across major evolutionary transitions of life. Proceedings of the National Academy of Sciences **107**, 12941–12945.

[S16] Angilletta MJ. 2009 Thermal adaptation: a theoretical and empirical synthesis. .

[S17] Gillooly JF, Brown JH, West GB, Savage VM, Charnov EL. 2001 Effects of size and temperature on metabolic rate. Science **293**, 2248–2251.

[S18] Brown JH, Gillooly JF, Allen AP, Savage VM, West GB. 2004 Toward a metabolic theory of ecology. Ecology **85**, 1771–1789.

[S19] Sharpe PJ, DeMichele DW. 1977 Reaction kinetics of poikilotherm development. Journal of Theoretical Biology **64**, 649–670.

[S20] Schoolfield RM, Sharpe P, Magnuson CE. 1981 Non-linear regression of biological temperature-dependent rate models based on absolute reaction-rate theory. Journal of Theoretical Biology **88**, 719–731.

[S21] Visser AW. 2007 Motility of zooplankton: fitness, foraging and predation. Journal of Plankton Research **29**, 447–461.

[S22] Katsu-Kimura Y, Nakaya F, Baba SA, Mogami Y. 2009 Substantial energy expenditure for locomotion in ciliates verified by means of simultaneous measurement of oxygen consumption rate and swimming speed. Journal of Experimental Biology **212**, 1819–1824.

[S23] Clift R, Grace JR, Weber ME. 2005 Bubbles, drops, and particles. Mineola, NY. Dover Publications, Inc.

[S24] Karp-Boss L, Boss E, Jumars P et al.. 1996 Nutrient fluxes to planktonic osmotrophs in the presence of fluid motion. Oceanography and Marine Biology **34**, 71–108.

[S25] Forster J, Hirst AG, Atkinson D. 2012 Warming-induced reductions in body size are greater in aquatic than terrestrial species. Proceedings of the National Academy of Sciences **109**, 19310–19314.

[S26] Wilson DF, Rumsey W, Green TJ, Vanderkooi J. 1988 The oxygen dependence of mitochondrial oxidative phosphorylation measured by a new optical method for measuring oxygen concentration.. Journal of Biological Chemistry **263**, 2712–2718.

[S27] Deutsch C, Penn JL, Verberk WC, Inomura K, Endress MG, Payne JL. 2022 Impact of warming on aquatic body sizes explained by metabolic scaling from microbes to macrofauna. Proceedings of the National Academy of Sciences **119**, e2201345119.

[S28] Subczynski WK, Hyde JS, Kusumi A. 1989 Oxygen permeability of phosphatidylcholine–cholesterol membranes.. Proceedings of the National Academy of Sciences **86**, 4474–4478.

[S29] Grimes DR, Kelly C, Bloch K, Partridge M. 2014 A method for estimating the oxygen consumption rate in multicellular tumour spheroids. Journal of The Royal Society Interface **11**, 20131124.

[S30] Berg HC. 1993 Random walks in biology. Princeton University Press.

[S31] Cooper S, Denny MW. 1997 A conjecture on the relationship of bacterial shape to motility in rod-shaped bacteria. FEMS Microbiology Letters **148**, 227–231. (10.1111/j.1574-6968.1997.tb10293.x)